

This item was submitted to [Loughborough's Research Repository](#) by the author.
Items in Figshare are protected by copyright, with all rights reserved, unless otherwise indicated.

Reconfigurable frequency selective surfaces

PLEASE CITE THE PUBLISHED VERSION

PUBLISHER

© Colin M. Moore

LICENCE

CC BY-NC-ND 4.0

REPOSITORY RECORD

Moore, Colin M.. 2019. "Reconfigurable Frequency Selective Surfaces". figshare.
<https://hdl.handle.net/2134/11890>.

This item was submitted to Loughborough University as an MPhil thesis by the author and is made available in the Institutional Repository (<https://dspace.lboro.ac.uk/>) under the following Creative Commons Licence conditions.



For the full text of this licence, please go to:
<http://creativecommons.org/licenses/by-nc-nd/2.5/>

LOUGHBOROUGH
UNIVERSITY OF TECHNOLOGY
LIBRARY

AUTHOR/FILING TITLE

Moore, C.M.

ACCESSION/COPY NO.

040101509

VOL. NO.

CLASS MARK

6 JUN 1997

Loan copy

26 JUN 1998

0401015092



BADMINTON PRESS
18 THE HALFCROFT
SYSTON
LEICESTER LE7 8LD
ENGLAND
TEL: 0533 602917

Reconfigurable Frequency Selective Surfaces

by

Colin M. Moore

A Master's Thesis submitted in partial fulfilment of the
requirements for the award of Master of Philosophy of the
Loughborough University of Technology

March 1994

© by Colin M. Moore 1994

Loughborough University of Technology Library	
Date	Jan 95
Class	
Acc. No.	060167529

V8911072

I am responsible for the work submitted in this Thesis, the original work is my own except as specified in references and acknowledgements.

Colin M. Moore

ABSTRACT

Reconfigurable Frequency Selective Surfaces

Colin Moore

Keywords:

Antennas, Electromagnetism, Frequency Selective Surfaces, Microwave Filters, Piezoelectricity, Polyvinylidene fluoride.

Synopsis:

Frequency Selective Surfaces (FSSs) consist of two dimensional arrays of conductive elements mounted on a dielectric substrate. FSSs act as passive filters to microwave radiation. The frequency response of the filter is primarily controlled by the dimensions and shape of the elements. The frequency selective property of a conventional FSS cannot be altered once it is installed.

By positioning two FSSs so they are parallel and closely coupled to each other a double layer FSS is created. If one FSS is moved across the plane of the other the frequency response of the double layer FSS alters. A method of moving the FSS using piezoelectric materials has been investigated. This allows the frequency response of the double layer FSS to be altered, or reconfigured, after it has been installed.

Suitable piezoelectric materials were studied and methods of utilising them in a Reconfigurable FSS (RFSS) were considered. Computer models and frequency response measurements of conventional FSSs were used to establish the design criteria necessary to maximise the variation in frequency response of the RFSS.

RFSSs were designed, modelled, and manufactured. Their frequency responses were then measured. The results of the computer models and measurements were compared and used along with knowledge of manufacturing problems to reiterate the design criteria and produce an RFSS with greater reconfigurability.

CONTENTS

	Synopsis	i
	Contents	ii
	Abbreviations	iv
1	Introduction	1
2	Frequency Selective Surfaces	2
3	Piezoelectricity	7
4	The RFSS Design	21
4.1	The RFSS Design Criteria	22
4.2	Implementation of Piezoelectric Materials in an RFSS	28
4.2.1	Implementing PZT in the RFSS	28
4.2.1.1	Stacked PZT between FSSs	34
4.2.2	Implementing PVDF in the RFSS	41
4.3	Piezoelectric Actuators	45
4.3.1	Bimorphs	45
4.3.2	Flexure Hinges	45
4.3.3	Cyclic Mechanisms	45
4.4	Piezoelectric Frequency Selective Surfaces	49
4.4.1	Experiments with PVDF	54
4.4.2	The Manufacture of FSSs	57
5	Experimental and Modelled Results	62
5.1	The effect of dipole length on resonant frequency	63
5.1.1	Double Layer FSS Models	63
5.1.2	Single Layer FSS Models	68
5.2	Modelling FSSs with arrays of slots	70
5.2.1	Experimental proof of Booker's extension to Babinet's Principle	70
5.3	The RFSS as a microwave shutter	73
5.3.1	Shuttering the RFSS	81
5.4	The suitability of PVDF in the manufacture of FSSs	83
5.4.1	Comparisons between PVDF and Copper-Polyester FSSs	84
5.4.1.1	Modelled PVDF and Copper-Polyester FSSs	84

5.4.1.2	Measurements of PVDF and Copper -Polyester FSSs	86
5.4.1.3	Comparisons between modelled and measured results	88
5.5	Methods of mounting the RFSSs	89
5.5.1	The Sliding Frame	89
5.5.2	A PTFE Frame	93
5.5.2.1	The Transmission Response of PTFE	93
5.6	The effect of the FSS geometry on the resonant frequency	98
5.6.1	Square Loops	98
5.6.1.1	The Frequency Response of Square Loops	102
5.6.1.2	The effect of the perspex frame on the square loops	109
5.6.2	Different Length Slots	114
5.7	PVDF FSSs	118
5.7.1	PFSSs in the PTFE Frame	118
5.7.2	PFSSs in the Perspex Frame	122
5.7.2.1	Shuttering the PFSSs	122
5.7.2.2	Shuttering the PFSSs in the Perspex Frame	127
5.8	The effect of the gap, S , between the FSSs	136
5.9	The effect of varying the slot length	137
5.9.1	Variation in slot length of FSSs in the perspex frame	137
5.10	The effect of varying the PVDF substrate thickness	145
5.11	The effect of varying the width of the slots	148
5.12	Energisation of the PFSSs	151
6	Conclusions	162
Appendix		
	References	A1

ABBREVIATIONS

The following abbreviations are used throughout this thesis:

DS	The relative shift between two FSSs in a double layer FSS structure (defined in Figure 4.1)
FSS	Frequency Selective Surface
pcb	printed circuit board
PFSS	Piezoelectric Frequency Selective Surface
PVDF	Polyvinylidene Fluoride
PZT	Lead (Pb) Zirconate Titanate
PZT5H	A PZT material
RAM	Radar Absorbent Material
RFSS	Reconfigurable Frequency Selective Surface
RPFSS	Reconfigurable Piezoelectric Frequency Selective Surface
S	The distance between two FSSs in a double layer FSS structure (defined in Figure 4.1)

The abbreviations FSS, PFSS, RFSS, and RPFSS are not synonymous. They are used to refer to the following structures.

- FSS Frequency Selective Surface; refers to a single conductive sheet etched with a doubly periodic array of elements. The conductive sheet may be mounted on a dielectric substrate. The frequency response of an FSS is fixed, i.e. it cannot be altered after manufacture.
- PFSS Piezoelectric Frequency Selective Surface; refers to a single PVDF sheet with electrodes on both sides. Identical doubly periodic arrays of elements are etched in both electrodes. The frequency response of a PFSS is considered to be fixed, i.e. it cannot be altered (significantly) after manufacture.
- RFSS Reconfigurable Frequency Selective Surface; refers to two conductive sheets, both etched with doubly periodic arrays of elements. The conductive sheets may be mounted on dielectric substrates. (An RFSS is actually

two FSSs). The two FSSs are positioned close to each other and are considered to act as a single RFSS. The frequency response of an RFSS can be altered after it is in position.

RPFSS Reconfigurable Piezoelectric Frequency Selective Surface; refers to two piezoelectric sheets with doubly periodic arrays of elements etched in the electrodes (i.e. two PFSSs). The two PFSSs are positioned close to each other and are considered to act as a single RPFSS. The frequency response of a RPFSS can be altered after it is in position by applying a suitable voltage to the electrodes.

1 INTRODUCTION

The purpose of this study was to investigate the practical feasibility of manufacturing an electrically adjustable microwave filter.

Microwave filters known as *Frequency Selective Surfaces* (FSS) have been widely studied^[1]. The FSS is positioned in front of a microwave antenna (e.g. a horn or microstrip patch) where it acts as a filter permitting some frequencies to pass through (passband frequencies, where the FSS is described as being transparent), whilst reflecting at other frequencies (where the FSS is described as being opaque). Once the FSS has been positioned its frequency response cannot be altered. The physical structure and frequency selective properties of FSSs are described in Chapter 2.

This study involved developing a concept, which was patented by the University^[2], to the working prototype stage. The concept was for a Reconfigurable Frequency Selective Surface (RFSS) which would permit the frequency response of the FSS to be altered, after installation, by electronic control. Primarily the research was experimentally based but it also involved modelling the frequency response of FSSs using computer software.

The Patent suggested the reconfigurability could be achieved using piezoelectric materials. These materials alter their physical dimensions when subjected to an electric field. Piezoelectric materials and the nomenclature used to describe their piezoelectric properties are described in Chapter 3.

Chapter 4 describes preliminary experiments with piezoelectric materials. This chapter then lists the design criteria for the RFSS and details the development of techniques which use piezoelectric materials to meet these criteria. Some of the designs were modelled and manufactured. Extensive transmission response measurements were made of the manufactured RFSSs in an anechoic chamber. Chapter 5 compares these measured responses with those produced from computer modelling.

Chapter 6 lists conclusions made from the measurements and models along with suggestions for further research into the RFSS.

2 FREQUENCY SELECTIVE SURFACES

This chapter describes the structure and functions of Frequency Selective Surfaces (FSSs). Complementary FSSs are explained and their frequency responses are shown. Different shape elements which have been used in FSS designs are listed as well as examples of applications where FSSs are utilised. The Chapter concludes by describing methods of modelling the frequency response of FSSs using computer software.

FSSs, also known as dichroic surfaces, usually consist of thin sheets of low permittivity dielectric material supporting a two dimensional periodic array of conductive elements. FSSs without the low permittivity dielectric supporting material take the form of perforated metal plates^[3] and wire meshes^[4,5].

FSSs, which can be manufactured using an etching process similar to that used for manufacturing printed circuit boards, have frequency dependent reflection and transmission characteristics. An FSS is transparent to electromagnetic waves at one frequency but reflective (opaque) at other frequencies^[6]. Potential applications of FSSs include microwave filters^[7,8], bandpass antenna radomes^[7,8], dual frequency reflector antennas^[6], and telemetry and communication systems^[9,10].

The frequency response of the FSS is dependent on the geometry of the elements which form the two dimensional arrays. Computer models can be used to predict the frequency response of an FSS. One method involves using simple equivalent electronic circuits to model the arrays^[12], this method has led to the definition of two types of FSS, *capacitive* and *inductive*. The names capacitive and inductive indicate the equivalent circuit components used in the computer model. Capacitive FSSs consist of conductive elements positioned on the dielectric substrate, the elements would typically be dipoles^[1] as shown in Figure 2.1

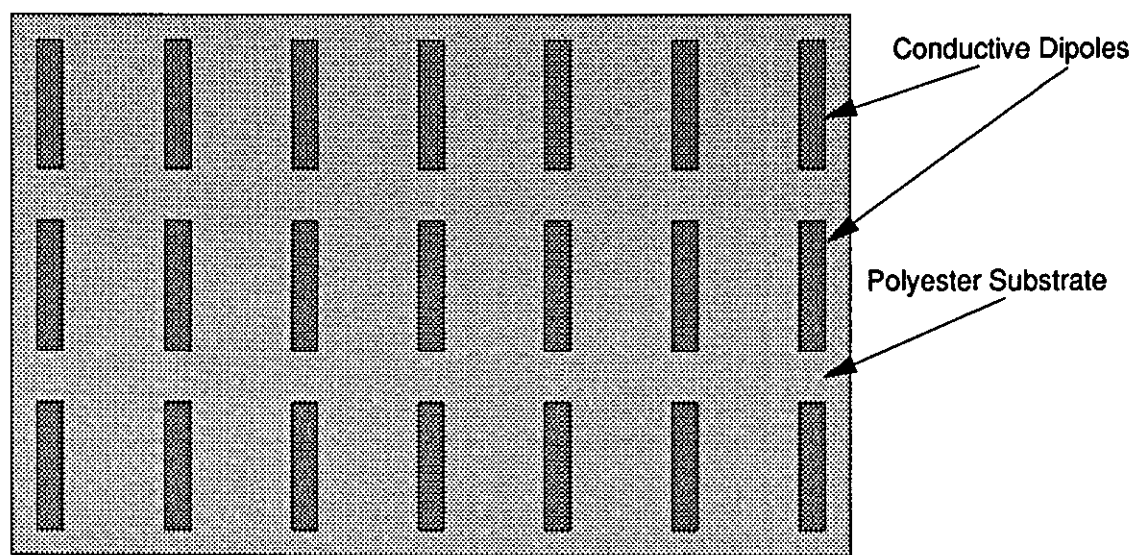


Fig.2.1: A section of a Capacitive FSS

An inductive FSS consists of slots cut, or etched, in a conductive sheet. A typical element for an inductive FSS would be a circular aperture^[3]. An inductive FSS is shown in Figure 2.2.

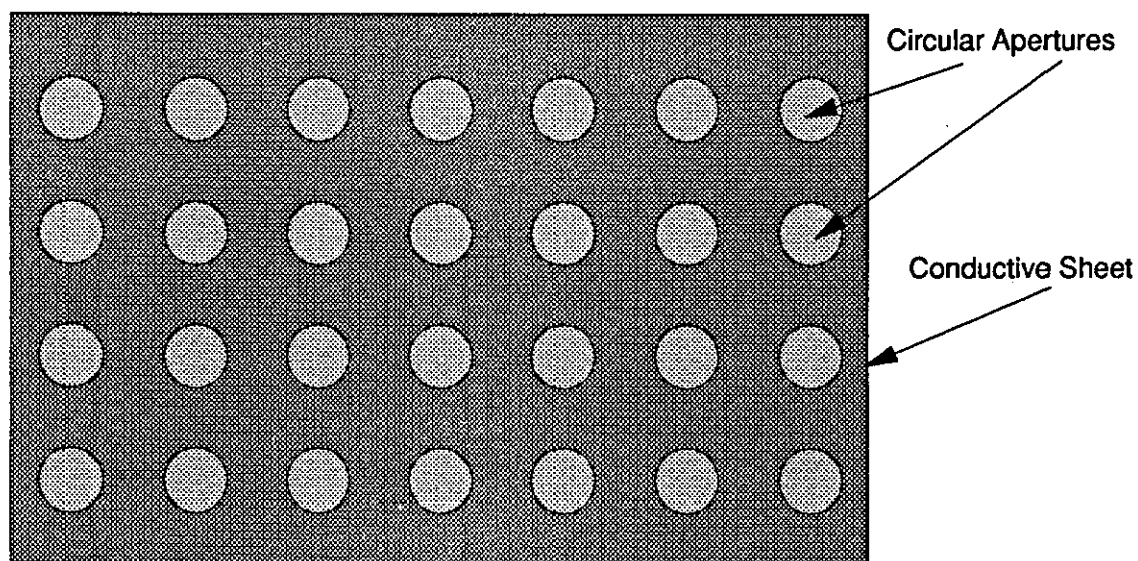


Fig.2.2: A section of an Inductive FSS

If the elements on an inductive and capacitive FSS are the same size and shape, e.g. the slots on the capacitive FSS are the same size as the dipoles on the inductive FSS, the two FSSs are said to be complementary. Typical transmission response curves for inductive and capacitive FSSs are shown in Figure 2.3.

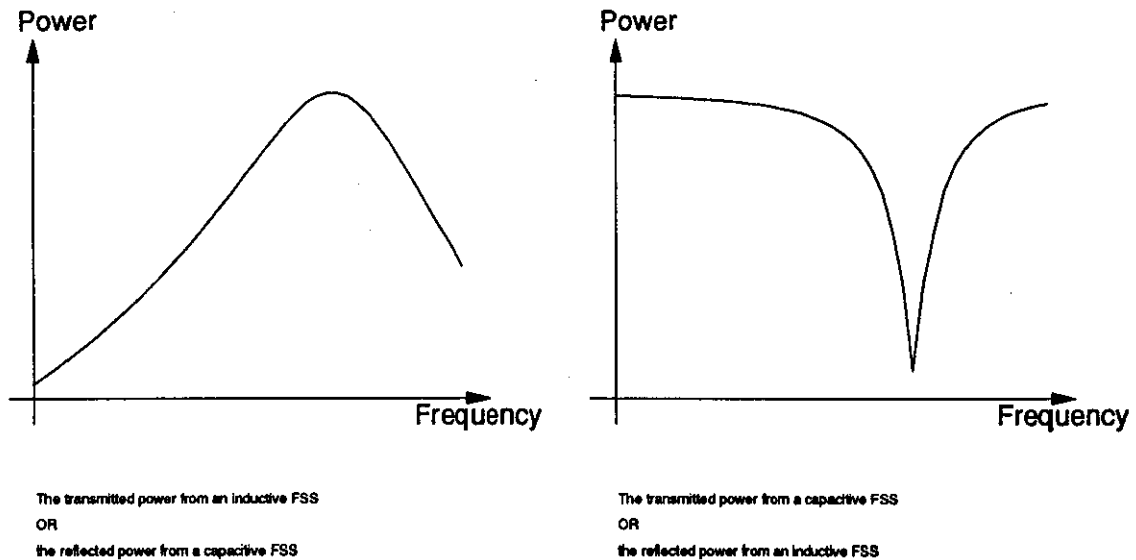


Fig.2.3: The frequency responses of capacitive and inductive FSSs

As well as dipoles and circular apertures, FSSs with other shape elements have been studied. These include square^[12], rectangular^[13], and elliptical patches^[13], crossed dipoles^[6], square^[10], rectangular^[7], and circular apertures^[11], concentric rings^[14], rings^[15], square loops^[16,17], tripoles^[18], and Jerusalem crosses^[19,20].

FSSs have also been studied in cascade, i.e. positioned behind each other. Methods of computer modelling cascaded FSSs are the Modal Analysis Method^[21], an iterative method^[23], and the Coupled Integral Equation Method^[22].

This chapter has described the physical structure and frequency responses of FSSs. Methods of modelling the frequency response using computer software were listed. The Chapter also listed different shape elements which have been used in FSS designs and applications which use FSSs.

3 PIEZOELECTRICITY

This chapter describes the piezoelectric properties exhibited by natural and synthetic materials. Examples of materials which exhibit these properties are cited and their relative merits are discussed. The manufacturing process of polyvinylidene fluoride, a piezoelectric polymer is described.

The study of piezoelectricity has its own nomenclature which is used to describe the properties and operational modes of piezoelectric materials. This nomenclature is explained. The Chapter is concluded by matching the properties of the piezoelectric materials available with the requirements of the Reconfigurable FSS.

Piezoelectricity is the property of a material to change shape when exposed to an electric field. Alternatively, when mechanical pressure is applied to the piezoelectric material a potential difference is generated across it. Piezoelectric material is used as a transducer to convert mechanical pressure to electrical potential in applications including impact sensors^[24] and strain gauges^[25 p.22]. An early application of ceramic piezoelectric materials was converting the vibrations in the stylus of a gramophone into electrical signals^[26].

Applications which use piezoelectric materials to convert electrical potential to mechanical displacement include audio frequency headphones and tweeters^[27 p.1602] and an inchworm motor^[28].

Piezoelectric polymers which absorb infrared radiation have been used in applications including intrusion detectors^[27 p.1606]. These devices sense the infrared radiation emitted by the human body and trigger an alarm signal.

3.1 Piezoelectric Nomenclature

The nomenclature for describing piezoelectric properties centralises around the piezoelectric strain constant, d , and the piezoelectric stress constant, g . For electromechanical transducers (i.e. applied electrical energy converted to mechanical energy) the piezoelectric strain constant, d , is defined as:

$$d = \frac{\text{Strain}}{\text{Applied Field}} = \frac{\epsilon}{E} \quad (\text{m/V})$$

(eqn.3.1)

where

$$\epsilon = \frac{\text{Length Extension}}{\text{Original Length}} = \frac{\delta l}{l} \quad (\text{no units})$$

(eqn.3.2a)

or

$$\epsilon = \frac{\text{Thickness Expansion}}{\text{Original Thickness}} = \frac{\delta t}{t} \quad (\text{no units})$$

(eqn.3.2b)

depending on the mode being considered.

Strain has no units whilst the applied electric field has units of volts per metre, this leads to the units of piezoelectric strain constant of metres per volt (m/V) as shown in equation 3.1. The piezoelectric strain constant is also measured in units of $10^{-12} \text{C/N}^{[24]}$. These units are derived from an alternative definition of the piezoelectric strain constant:

$$d = \frac{\text{Electrical Charge Density Developed}}{\text{Applied Mechanical Stress}}$$

$$= \frac{D}{T} \left(\frac{\text{C/m}^2}{\text{N/m}^2} = \text{C/N} \right)$$

(eqn.3.3)^[25 p.43]

The piezoelectric stress constant, g , is defined for use when the material is used as a mechanical-electrical transducer (i.e. applied mechanical force is converted to electrical potential). Like the strain constants there are two definitions for stress constant^[25 p.43]:

$$g = \frac{\text{Electric Field Developed}}{\text{Applied Mechanical Stress}} = \frac{E}{T} \quad (\text{Vm/N})$$

(eqn.3.4)

and

$$g = \frac{\text{Strain Developed}}{\text{Applied Charge Density}} = \frac{S}{D} \quad (\text{m}^2/\text{C})$$

(eqn.3.5)

The reconfigurable frequency selective surfaces described implement the piezoelectric materials as electromechanical transducers. The strain constant is applicable to piezoelectric materials used in this fashion. This strain constant, d , as opposed to the piezoelectric stress constant, g , will be used to describe the piezoelectric properties of materials in this thesis.

Two subscripts are positioned after the piezoelectric constants to indicate the directions of the applied or generated field, stress, and strain. The directions are denoted by the numbers 1 to 6 and are related to the orthogonal axes as described in Table 3.1 and shown in Figure 3.1. The direction of shear is defined as being clockwise around the appropriate axis looking towards the origin.

Subscript Number	Direction
1	Positive x Direction
2	Positive y Direction
3	Positive z Direction
4	Shear Form Around x-axis
5	Shear Form Around y-axis
6	Shear Form Around z-axis

Table 3.1: The relationship between the x-y-z axis and the subscripts appended to the piezoelectric constants

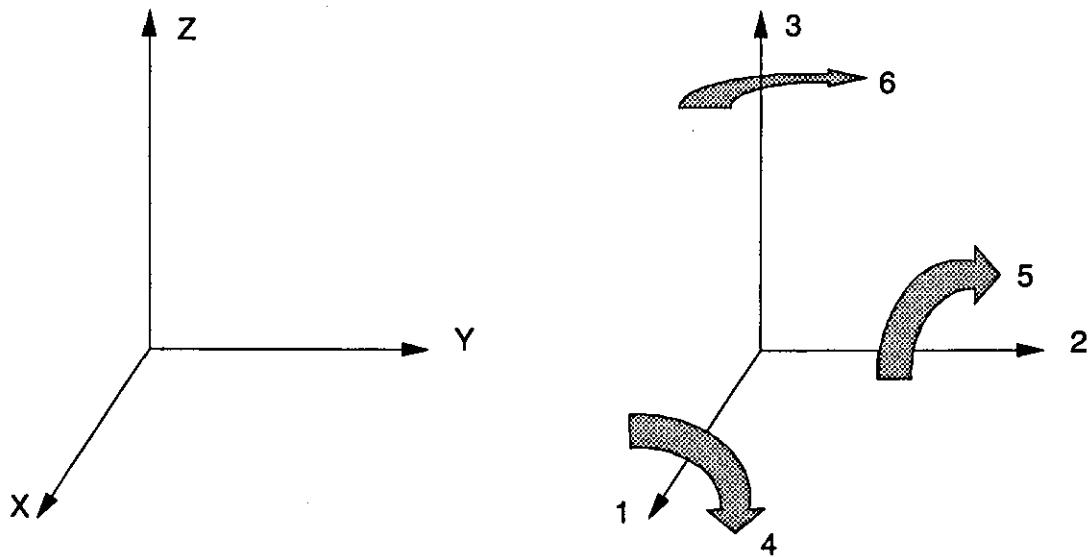


Figure 3.1: The relationship between the x-y-z axis and the subscripts appended to the piezoelectric constants

The first subscript associated with the piezoelectric constants describes the axis which the electrodes are perpendicular to. This is the direction of the applied or generated electric field, i.e. the electric field axis. The second subscript denotes the direction of the applied or induced stress or strain, i.e. the mechanical stress or strain axis. Tensile stress or strain is defined as positive mechanical action or reaction, while compressive stress or strain is defined as negative ^[25 p.31].

When used as an electromechanical transducer the piezoelectric material can operate in one of four modes:

- (a) Length (Transverse) Expansion d_{31}
- (b) Thickness Expansion d_{33}
- (c) Face Shear d_{14} ^[31 p.1]
- (d) Thickness Shear d_{15}

These modes are shown in figures 3.2(a) to (d).

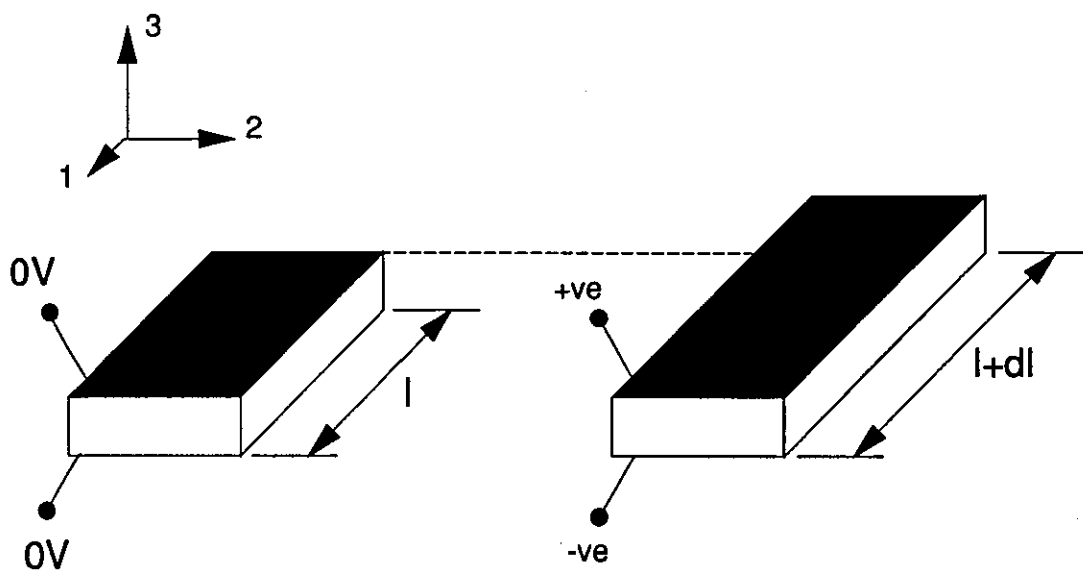


Fig.3.2(a): Length Expansion Mode (d_{31})

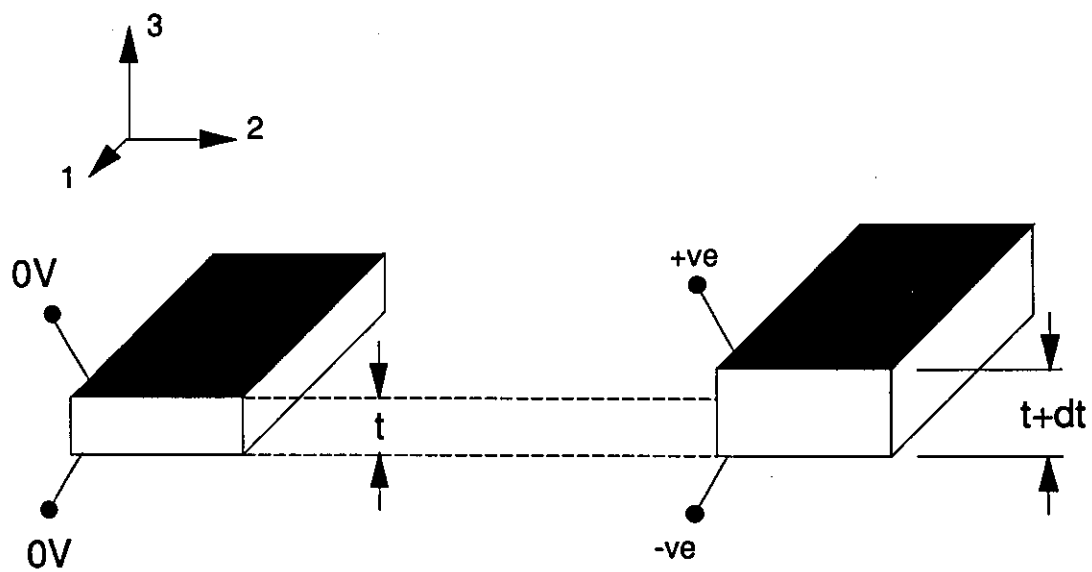


Fig.3.2(b): Thickness Expansion Mode (d_{33})

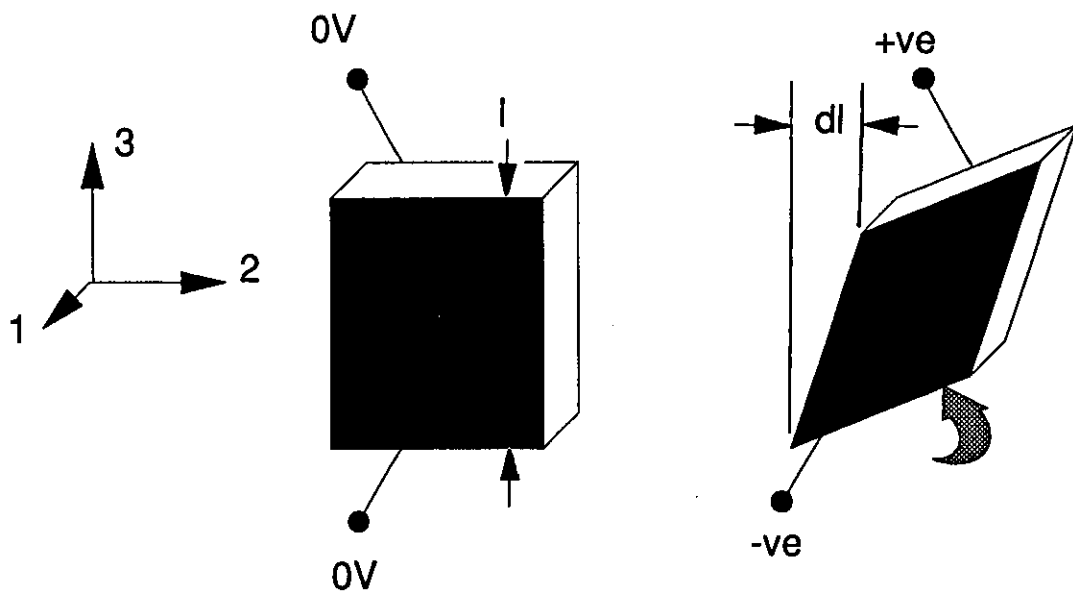


Fig.3.2(c): Face Shear Mode (d_{14})

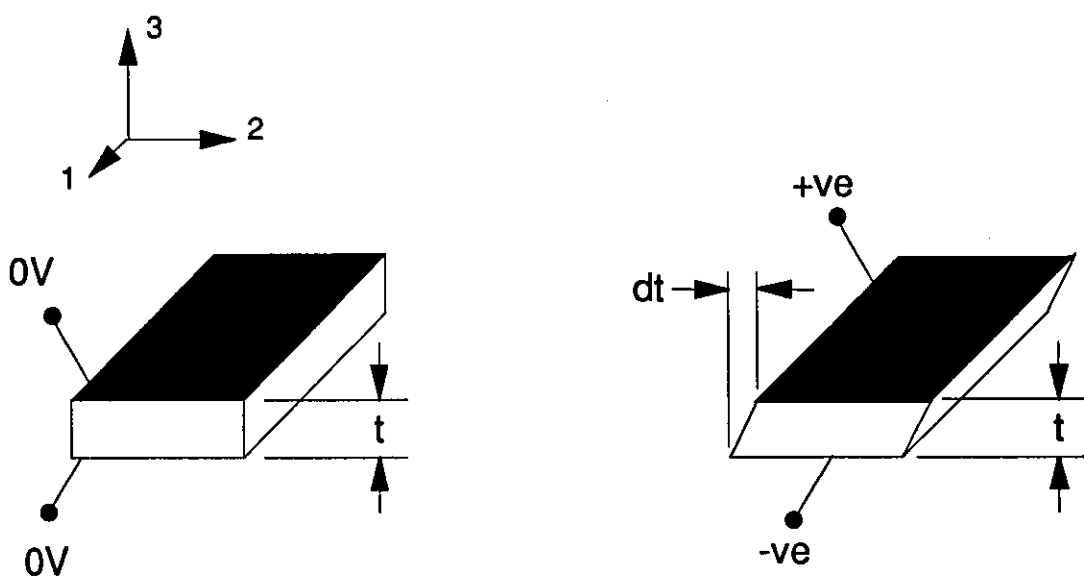


Fig.3.2(d): Thickness Shear Mode (d_{15})

For shear modes the displacement denoted δ occurs perpendicular to the length (face shear), or thickness (thickness shear) ^[29 p.63] of the material.

e.g. For thickness shear,

$$\text{Strain} = \frac{\text{Displacement}}{\text{Original Thickness}}$$

(eqn.3.6)

from figure 3.2(d),

$$\epsilon = \frac{\delta t}{t} \quad (\text{no units})$$

(eqn.3.7)

When operating in the electromechanical mode some piezoelectric materials (e.g. ceramics) exhibit an effect dependent on the polarity of the electric field applied. An electric field in one direction causes expansion and in the opposite direction it causes contraction ^[30 p.4].

Usually two or more of the piezoelectric modes are present when the piezoelectric material is energised. If one mode is operating in expansion and the other is operating in contraction there may be no overall change in the volume of the material. This is not always the case. In some materials there is a change in volume when the material is energised.

3.2 Piezoelectric Materials

Materials which exhibit the piezoelectric properties can be split into three groups:

- (a) Naturally occurring materials; minerals and crystals, these include quartz and Rochelle salt^[32].
- (b) Ceramics; these include Lead Zirconate Titanate (PZT) and Lead Titanate^[31 p.1].
- (c) Polymers; Polytrifluoroethylene (PVF₃)^[33] and Polyvinylidene Fluoride (PVDF)^[27 p.1].

3.2.1 Naturally Occurring Piezoelectric Materials

Two commonly used piezoelectric crystals are quartz (Silicon Oxide) and Rochelle salt (Sodium Potassium Tartrate Tetrahydrate)^[32]. Rochelle salt is a water soluble crystal which exhibits changes in its crystalline structure at temperatures of +24°C and -19°C. Other piezoelectric crystals include Tourmaline^[28 p.3] (an aluminosilicate), Potassium Tartrate, and Ethylenediamine Tartrate^[32 p.107].

3.2.2 Ceramic Piezoelectric Materials

Piezoelectric ceramics consist of small crystallites sintered at high temperatures. Ceramics must undergo a poling process before they exhibit the piezoelectric property. This is necessary because, unlike the piezoelectric crystals described above, the properties of each individual crystallite are not arranged in an ordered fashion^[32 p.109].

3.2.2.1 Poling

The piezoelectric ceramic is heated above its characteristic 'Curie Temperature'. A strong electric field is applied to the heated material and the crystallites become aligned in the direction of this field. This direction is parallel to the *poling axis*. The material is now cooled below the Curie Temperature and the electric field is removed, the crystallites will remain partially aligned^[28 p.3].

A direct analogy can be drawn between poling a piezoelectric ceramic and magnetising a ferroelectric material, such as soft iron. Soft iron can be magnetised by heating in a magnetic field.

Once poled, a smaller electric field can be applied to the ceramic to produce an expansion or contraction along the poling axis.

The Curie Temperature is quoted in piezoelectric material suppliers data because it is the maximum temperature the ceramic may be exposed to without losing its piezoelectric property^[30 p.6].

3.2.3 Piezoelectric Polymers

Polytrifluoroethylene (PVF₂) and Polyvinylidene Fluoride (PVDF) are piezoelectric polymers^[33]. Like ceramics, PVDF, which has the largest piezoelectric properties of any polymers, has to be poled before it exhibits the piezoelectric behaviour. Unlike ceramics, which are brittle and difficult to manufacture in large pieces, PVDF is flexible and is manufactured in sheets. The rigidity of ceramics is an advantage in converting electrical energy to mechanical energy. Conversely, PVDF is a better transformer of mechanical energy to electrical energy^[25 p.9].

PVDF is 50% crystalline and 50% amorphous. Its structure is a head-to-tail arrangement of CH₂-CF₂ molecules^[24]. Four forms of PVDF exist, these are denoted β , α , γ , and α_p (or sometimes δ). These four forms differ in their crystalline structure which gives rise to different physical and electrical properties^[27]. e.g. β form PVDF has a relative permittivity (ϵ_r) of 14 whereas α form PVDF has a relative permittivity of 10. The relative permittivity of PVDF is dependent on temperature and the frequency of the electromagnetic (EM) field the material is situated in^[25 p.55]. The values of ϵ_r quoted above apply to PVDF at room temperature positioned in an EM field with a frequency of 1kHz.

The α and β forms are the most commonly used. The β form has the largest piezoelectric action because the hydrogen and fluoride atoms are arranged in a CH₂-CF₂ molecular structure which provides the maximum movement per molecule.

β -phase piezoelectric film is manufactured in four steps ^[24]:

- (a) Extrusion: α -phase PVDF is extruded from the molten PVDF material.
- (b) Stretching: the extruded material is stretched along one axis (i.e. uniaxially) until it is three to five times its original length. This stretching is performed at a temperature of between +60°C and +65°C. The material re-crystallises in its β -form and is annealed at +120°C to heal the damage caused by stretching ^[27].
- (c) Metallisation: electrodes are evaporated onto the PVDF film ^[24]. If the material is poled by the corona poling method (step (d) described below) the metallisation is not performed until after the poling process ^[27].
- (d) Poling: this process installs the piezoelectric property in the material and can be performed by a thermal or corona procedure.

Thermal Poling ^[27]

The material is metallised (step (c) above) and has an electric field of 80kV/mm applied to the electrodes whilst heated to a temperature of between +90°C and +110°C for between 40 minutes and an hour. This process causes the CH₂-CF₂ molecules to align in the direction of the field. The applied field is maintained during cooling, this causes the molecular alignment to stabilise resulting in permanent polarisation.

If the material is poled for long enough (at least 40 minutes) the polarisation is only proportional to the size of the applied field (an electric field of 200kV/mm produces the maximum polarisation of 2 μ C/cm²). The poling temperature determines the rate at which polarisation occurs.

Corona Poling

The PVDF is positioned a few centimetres from a needle electrode which produces a corona discharge. The charge builds up on the PVDF which causes a large field across the material and aligns the $\text{CH}_2\text{-CF}_2$ chains. This poling method can be performed at room temperature but only produces a small polarisation if the field across the material is less than 100 kV/mm. If the field is greater than this the polarisation increases suddenly up to $12\mu\text{C}/\text{cm}^2$ ^[27].

The piezoelectric materials described in this section are listed in Table 3.2 along with their piezoelectric strain constants, temperature dependence, poling voltages, and the dimensions of typical pieces of each of the materials.

Property	Quartz ^[32 pp.105-6]	Rochelle Salt ^[32 p.107]	Ceramic PZT5H ^[30 p.10]	PVDF ^[24]
Temperature Dependence	Exists as α quartz up to +573°C, then transforms to β quartz	Changes in crystalline structure occur at -19°C and +24°C	Curie Temperature +195°C	Curie Temperature +80°C
Strain Constants ($\times 10^{-12}$ C/m):				
d_{11} mode	2.31 (α quartz)	275 ^[25 p.52]	N/A ⁽¹⁾	N/A ⁽¹⁾
d_{14} mode	0.73 (α quartz) 1.82 (β quartz)	2300 (at +25°C)	N/A ⁽¹⁾	N/A ⁽¹⁾
d_{31} mode	N/A ⁽¹⁾	N/A ⁽¹⁾	274	23
d_{33} mode	N/A ⁽¹⁾	N/A ⁽¹⁾	593	33
d_{15} mode	N/A ⁽¹⁾	N/A ⁽¹⁾	741	N/A ⁽¹⁾
Poling Voltage	N/A ⁽²⁾	N/A ⁽²⁾	>500- 1000V/mm ^[30 p.14]	50-80kV/mm ^[27]
Dimensions:				
Thickness	Varies with cut of crystal	40mm	200 μ m min.	9, 28, 52, 110, 500 μ m
Length and Width		250 x 40mm	90 x 40mm (typical)	8m x 300mm

⁽¹⁾ The piezoelectric strain coefficients of the listed materials are too small to provide significant electromechanical transduction in some modes.

⁽²⁾ Quartz and Rochelle salt do not have to be poled to exhibit the piezoelectric property.

Table 3.2: The Properties of Piezoelectric Materials

The Table shows the piezoelectric property exists in different modes for the natural piezoelectric materials compared with the ceramics and polymers.

Rochelle salt has the largest piezoelectric coefficients but it undergoes changes in state at -19°C and $+24^{\circ}\text{C}$. This renders the material impractical for use in the reconfigurable FSS.

Quartz has the lowest piezoelectric constants which indicate it is suitable as a mechanical-electrical transducer. A small amount of stress or strain results in a large induced voltage. If operated as an electromechanical transducer quartz produces insignificant mechanical movement. The low piezoelectric constant makes quartz unsuitable in the reconfigurable FSS.

The electrical properties of the ceramic PZT5H and polymer PVDF are listed in Table 3.3. The listed properties include the loss tangent and relative permittivity of the materials which affect the operational characteristics of FSSs.

Property	PVDF ^[24]	PZT5H
ϵ_r	12-13 (at 10^4Hz ^[25 p.56])	3400 ^[31 p.33] (operated in the d_{33} mode at 10^3Hz)
$\tan\delta$	0.015 (at 10Hz) 0.02 (at 10^4Hz)	0.02 (at 10^3Hz) ^[31 p.33]
Maximum Operating Voltage	30V/ μm	500-1000V/mm (breakdown voltage)
Breakdown Voltage	100V/ μm	500-1000V/mm ^[30 p.14]

Table 3.3: The Electrical Properties of Ceramic and Polymer Piezoelectric Materials

Disadvantages of PZT in an RFSS application are the high relative permittivity and the brittle nature of the material, which means it is only available in relatively small, thick, pieces (Table 3.2).

A distinctive advantage of polyvinylidene fluoride (PVDF) in the RFSS application is its availability in sheets with thicknesses varying between 9 μm and 500 μm . Sheets of piezoelectric material can be easily utilised in the RFSS designs, which will be described in Chapter 4. The disadvantages of PVDF include its small piezoelectric strain constants, compared with PZT, and larger energisation voltages.

This Chapter has described the piezoelectric property which exists in some materials. Examples of both naturally occurring and synthetic materials were listed along with their piezoelectric, electric, and physical properties. The nomenclature used for describing piezoelectricity was explained and equations relating the piezoelectric properties were listed. Synthetic piezoelectric materials require 'poling' before they exhibit their piezoelectric property. This poling process was described as well as the manufacturing process of polyvinylidene fluoride. The Chapter was concluded by comparing the properties of the different piezoelectric materials with the requirements of the Reconfigurable FSS (RFSS) and disregarding quartz and Rochelle salt as materials suitable for use in the RFSS.

4 THE RFSS DESIGN

This chapter explains how a Reconfigurable FSS (RFSS) can be created from two single or double layer FSSs. The FSSs are positioned parallel and close enough to be electromagnetically coupled to each other.

Moving one FSS across the plane of the second causes the frequency response of the structure to alter, i.e. the RFSS is *reconfigured*. The effect of the relative movement between the two FSSs and the space between them is assessed by computer modelling. The computer models are also used to determine the effect of varying the angle of incidence between the electromagnetic (EM) waves and the RFSS.

Methods of using piezoelectric materials to produce the planar FSS shift and methods of minimising the energisation voltage required to achieve this shift are considered. Initial experiments to assess the extension of PVDF sheets were performed.

The Chapter concludes with an explanation of how conventional FSSs are manufactured and explains the difficulties of manufacturing FSSs from piezoelectric materials.

4.1 The RFSS Design Criteria

The Patent^[2] cited an example of two FSSs consisting of arrays of dipoles. The dipoles were positioned in 6mm square lattices and had lengths of 4.3mm (FSS1) and 3.25mm (FSS2). The dipoles on both FSSs were 0.4mm wide. The FSSs were manufactured from laminated copper and polyester sheets using printed circuit board (pcb) etching techniques. The etching process leaves 24 μ m thick copper dipoles on the 37 μ m thick polyester substrate. The material properties of the laminate sheets are listed in Table 4.1^[34].

Copper:	
Thickness	24 μ m ⁽¹⁾
Resistivity	0.0036 Ω .g/m ²
Polyester:	
Thickness	37 μ m
Tolerance	$\pm 10\%$
Permittivity (at +23°C)	3.25
Loss Tangent (at +23°C))	0.005

⁽¹⁾ This value was obtained by measuring the copper and polyester laminate and subtracting the thickness of the polyester quoted in reference 34. Measurements were made using a 0-25mm micrometer with vernier scale graduations of 0.001mm.

Table 4.1: Properties of polyester based flexible electrical laminates

Figure 4.1 shows how the two FSSs were positioned behind each other with a space, S , between them. The distance labelled DS in the Figure is the relative planar movement between the two FSSs.

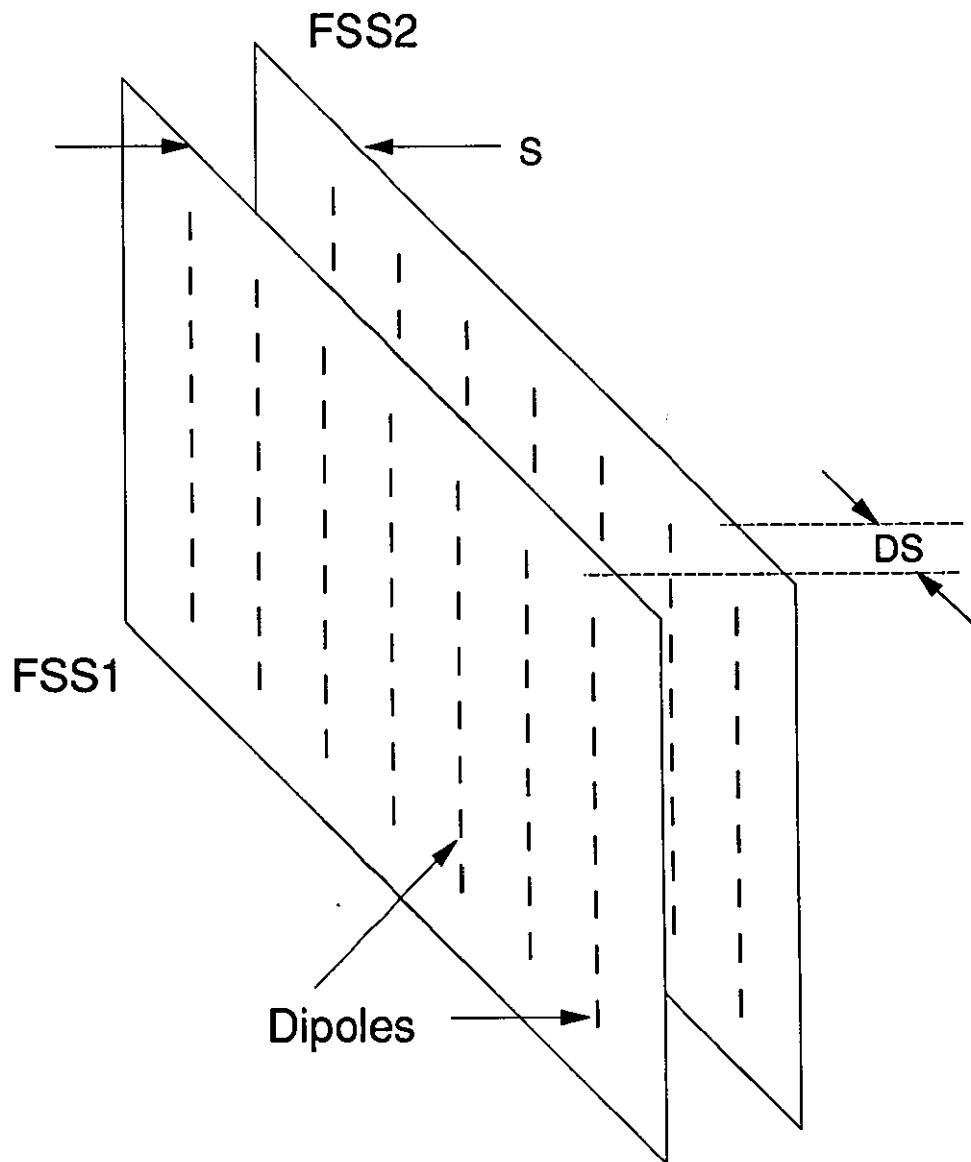


Fig.4.1: Two FSSs positioned to form a double layer FSS

The Patent^[2] explained this double layer FSS was modelled using modal^[21] and iterative^[35] analysis methods to predict the transmission response of the FSSs.

During the first stages of this investigation the FSSs were modelled, using software owned by the University which implemented the modal analysis technique, with different values of S and DS .

A side view of the double layer FSS structure is shown in Figure 4.2. FSS2 in the Figure was modelled with its copper dipoles facing the rear (polyester substrate) of FSS1. This was to enable the total distance between the two FSSs to be reduced to one substrate thickness. The FSSs were modelled at normal and TE45 incidence angles with gaps, S , of 0.025mm and 0.225mm. These gaps make the total distance between the *copper dipoles* 0.062mm and 0.262mm respectively when the thickness of the polyester sheet is added to the gap.

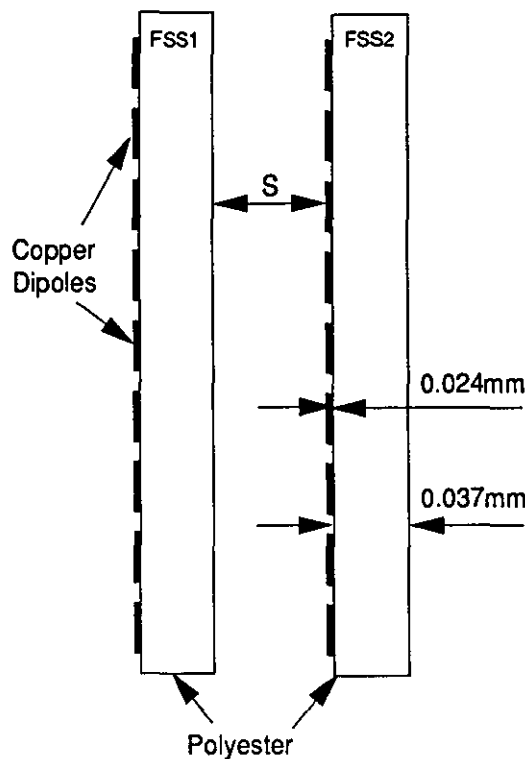


Fig.4.2: Side view of the Double Layer FSS Structure

NOTE:

Having the copper elements of both FSSs on the inside of the structure, i.e. facing each other, would enable the distance, S , to be minimised to zero. This would mean the copper elements would be shorting against each other, a situation which the computer program cannot model.

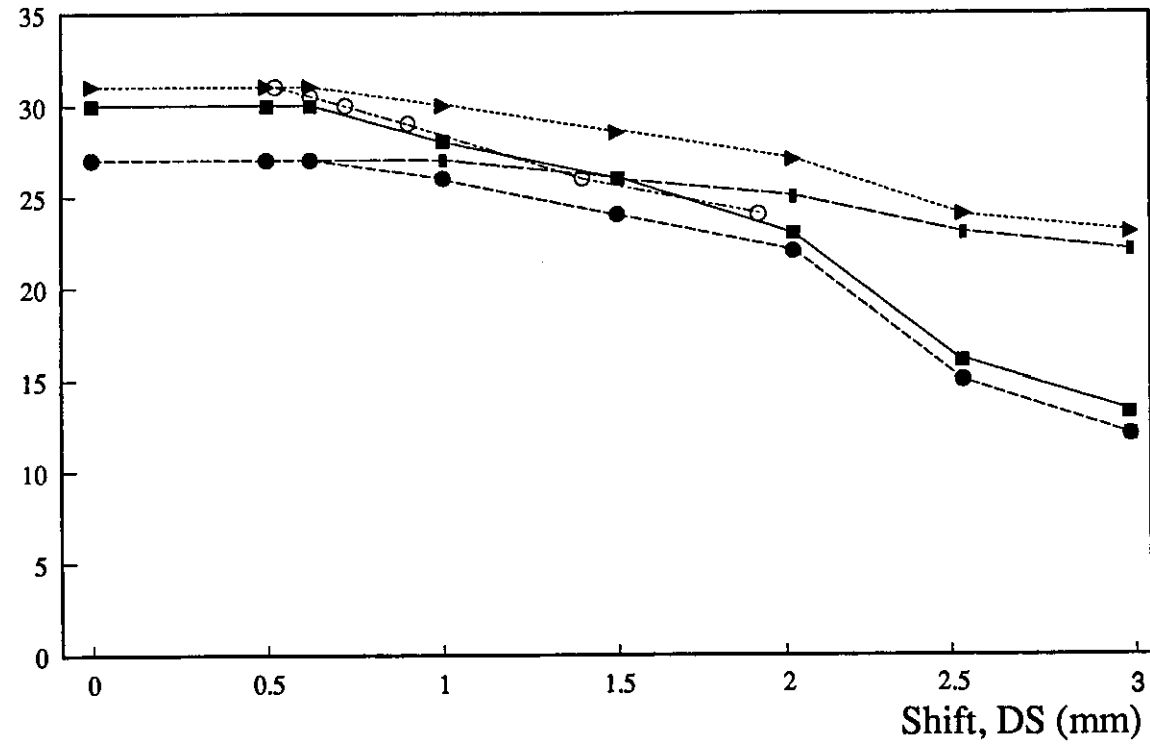
The planar displacement of one FSS with respect to the other was varied between 0 and 3mm. The results of the modelling are shown in Graph 4.1. For comparison a single FSS with dipole lengths varying between 4.3 and 5.7mm was modelled using the modal analysis technique. The Graph shows the importance of keeping the space between the two FSSs, S , to a minimum in order to maximise the frequency shift which can be obtained from a given planar displacement, DS .

At normal incidence, with a gap, S , between the FSSs of 0.025mm a shift in resonant frequency of 12GHz is obtained when the rear FSS is moved from an offset, DS , of 1.0mm to 2.5mm. When the space between the FSSs was increased to 0.225mm this resonant frequency shift was halved to just 6GHz. These predictions were used to establish the fundamental design criteria of the RFSS: to minimise the space, S , and maximise the displacement, DS .

The models also predicted a smaller frequency shift would be obtained if angles of incident microwaves other than normal incidence, 0° , were used.

The curve showing the effect of varying the length of the dipoles on a single FSS indicates the 0.025mm gap between the two FSSs in an RFSS will not cause a significant reduction in the resonant frequency shift. Varying the lengths of the dipoles on this single layer FSS between 4.3mm and 5.7mm (see Note 2 after Graph 4.1) produced the same frequency shift, 7GHz, as the double layer FSS with a gap S of 0.025mm produced when its effective dipole length was increased from 4.3mm to 5.7mm.

Frequency (GHz)



Graph 4.1: Computer models of a double layer FSS structure
(See notes 1 and 2 overleaf.)

NOTE:

1. The Graph shows no resonant frequency shift of the double layer FSS until DS is greater than 0.525mm. This is because the shorter dipoles (3.25mm) on the rear FSS are completely obscured by the longer dipoles (4.3mm) on the front FSS until the displacement, DS, is at least 0.525mm. The dipoles on the double layer structure are said to have an effective length of 4.3mm until the displacement is greater than 0.525mm. The effective length increases with DS for values of DS greater than 0.525mm.

(4.3mm - 3.25mm = 1.15mm; half of this, 0.525mm, is the length the ends of the longer dipoles on the front FSS overlap the ends of the shorter dipoles on the rear FSS when the centres of the dipoles on the two FSSs are aligned.)

2. The resonant frequency of the single layer FSS with dipoles 4.3mm long is plotted on the graph at DS = 0.525mm. Increases in the length of the dipoles on this single layer FSS are added to 0.525mm. e.g. With dipoles 4.775mm the resonant frequency is plotted on the graph at the abscissa 1.0mm (4.775mm - 4.3mm = 0.475mm; 0.475mm + 0.525mm = 1.0mm). This positioning of the plot of the resonant frequency of the single layer FSS allows a direct comparison with the resonant frequency plot of the double layer FSS with the same effective dipole length.

Having established the importance of maximising the displacement, DS, and minimising the gap, S, other design criteria which needed to be considered were established. These included trying to minimise both the energisation voltage and the effect of temperature variation, and maximising the rigidity and mechanical robustness of the RFSS.

4.2 Implementation of Piezoelectric Materials in an RFSS

Methods of utilising the piezoelectric materials PVDF and PZT, discussed in Chapter 3, to design an RFSS to the established criteria were now investigated.

4.2.1 Implementing PZT in the RFSS

Considering the structure of the RFSS the ideal solution to the design problem would be to position a sheet of piezoelectric material between the two FSSs. Energising the material to generate a shear movement would result in the relative position of the two FSSs changing and the resonant frequency of the structure altering. This is shown in Figure 4.3.

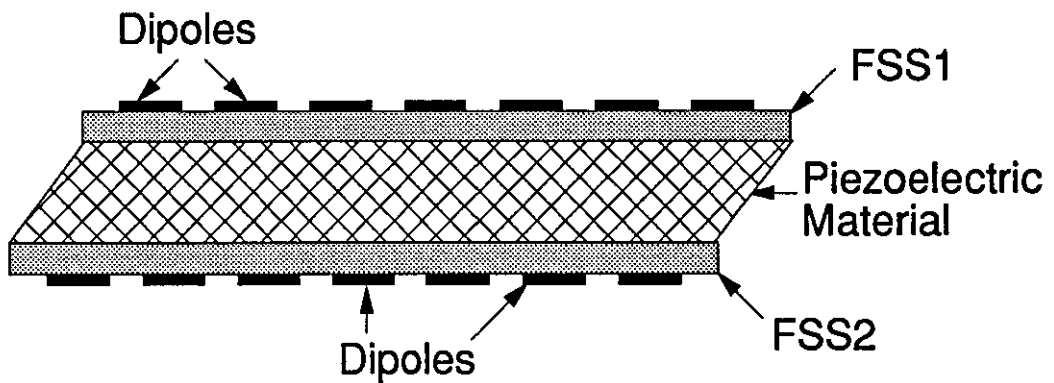


Fig.4.3: The effect of a shear displacement on the double layer FSS structure

Table 3.2 listed the physical properties of piezoelectric materials. This table showed PZT had the largest piezoelectric strain coefficient d_{15} suggesting it would be most suitable in this application.

Slotted FSSs have an area occupied mainly by copper. The PZT material could be positioned behind the copper area to try and reduce any undesired effects which it might have on the frequency response of the RFSS. This design is shown in Figure 4.4.

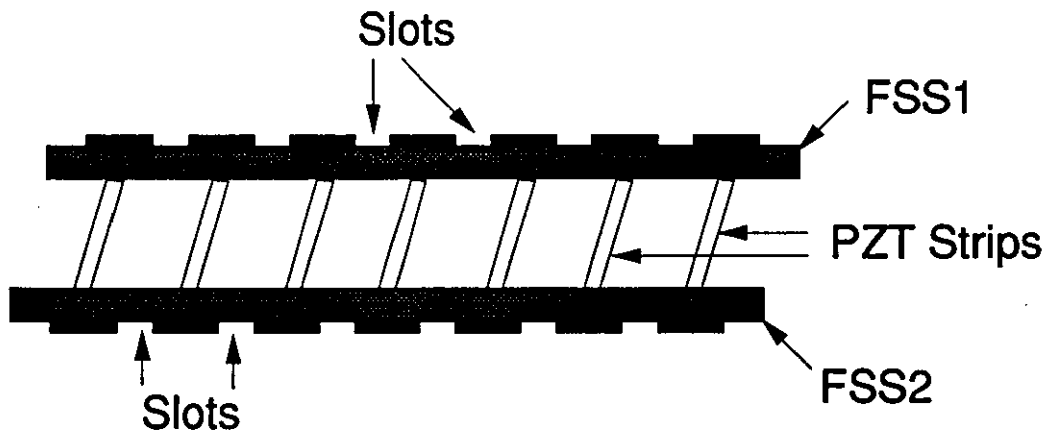


Fig.4.4: A slotted RFSS with "hidden" PZT strips

The minimum thickness of PZT is 200 μ m (Table 3.2). Once an adhesive has been used to secure the PZT to the two copper FSSs it was estimated the gap, S , between the FSSs would be close to the 225 μ m modelled in Graph 4.1.

The Graph was produced by modelling dipoles on a polyester substrate with no material positioned between the FSSs, i.e. $\epsilon_{rs}=1.0$ and $\tan\delta_s=0$. Software to model slotted FSSs is not available. However an approximation of the plane wave *transmission* response can be obtained by modelling FSSs with dipoles the same length as the slots and considering the *reflection* coefficients of these FSSs to be the *transmission* coefficients of the FSSs with slots. Likewise, the *transmission* coefficients of the FSS with dipoles is considered an approximation to the *reflection* coefficients of the FSS with slots^[37p.496].

Similarly, for double layer FSSs with the slots on the two FSSs aligned, the model of the complementary double layer dipole FSS, with the dipoles aligned, can be used to provide a good approximation for the transmission and reflection coefficients. When one FSS is shifted, i.e. $DS>0$, the slots will no longer be aligned and the approximation is **not** valid.

Shifting one FSS in the direction of the length of the slots will reduce the *effective* length of the slots on the double layer FSS. A reduction in slot length causes the double layer FSS to resonate at a higher frequency. Figure 4.5 shows a section of a double layer FSS with a relative shift between the FSSs of distance DS causing a reduction in slot length.

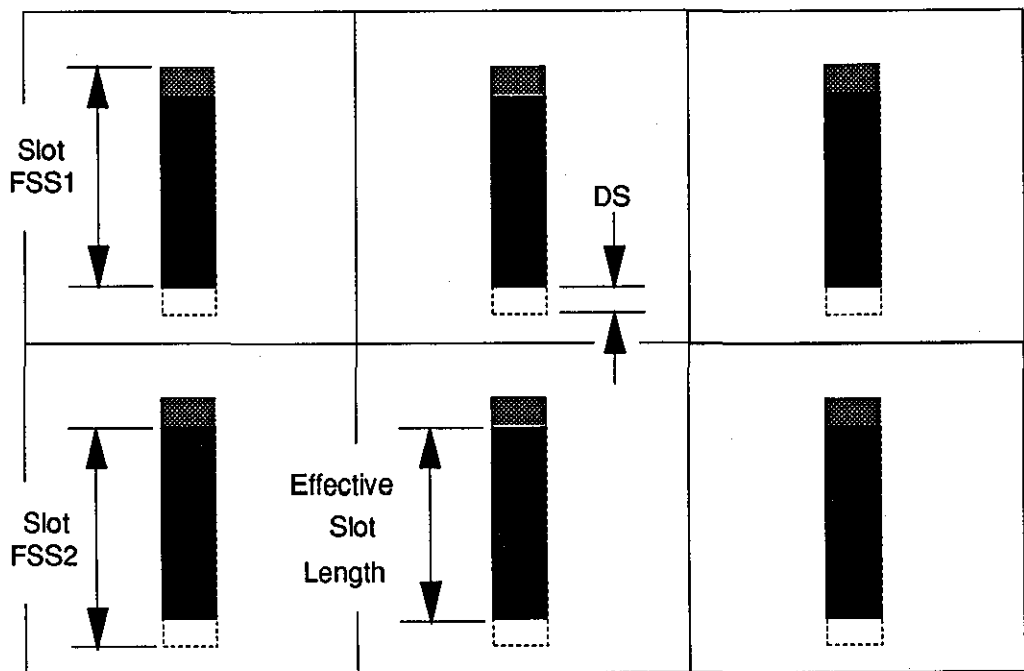


Fig.4.5: A section of a double layer slotted FSS with a relative displacement, DS , between the two component FSSs

Conversely, the effect of increasing the relative displacement, DS , in the direction of the length of the dipoles on a double layer FSS, (formed from two single layer FSSs with dipoles), is to increase the *effective* length of the dipoles on the double layer structure. This increase in dipole length causes the resonant frequency of the

double layer structure to reduce. Figure 4.6 shows a section of a double layer FSS with a relative shift between the FSSs of distance DS causing an increase in dipole length.

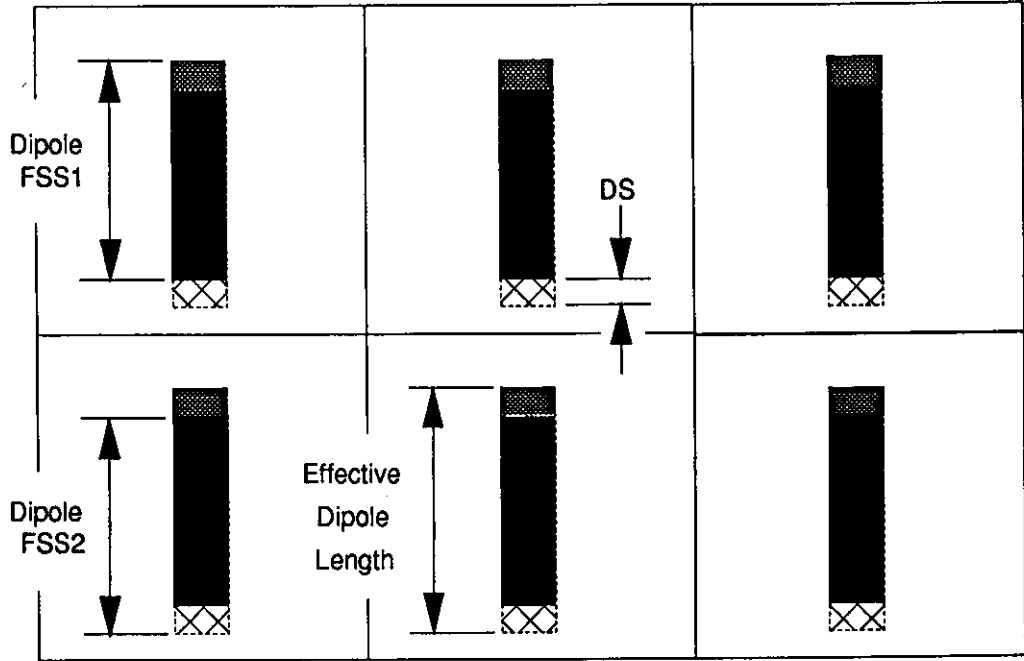


Fig.4.6: A section of a double layer dipole FSS with a relative displacement, DS , between the two component FSSs

Despite the differences in the effect of displacing slotted and dipole FSSs Graph 4.1 was still used to establish an *estimate* of the displacement, DS , needed to achieve a desired frequency shift. (Although the frequency shift will be an increase for slots and a decrease for dipoles.)

Using the piezoelectric strain equations 3.1, 3.6, and 3.7 discussed in Chapter 3, relabelled equations 4.1 and 4.2 here, the shear movement can be calculated:

$$d = \frac{\text{Strain}}{\text{Applied Field}} = \frac{\epsilon}{E} \left(\frac{m}{V} \right)$$

(eqn.4.1)

and

$$\text{Strain } (\epsilon) = \frac{\text{Displacement}}{\text{Original Thickness}} = \frac{\delta t}{t} \text{ (no units)}$$

(eqn.4.2)

Transposing Equation 4.1 and considering the piezoelectric thickness shear mode of operation produces:

$$\text{Strain } (\epsilon) = \text{Applied Field } (E) \times d_{15}$$

(eqn.4.3)

From Table 3.2 the piezoelectric strain constant d_{15} for PZT5H is $741 \times 10^{-12} \text{ m/V}$, and from Table 3.3 the maximum field which can be applied to PZT5H is 1000 V/mm . These figures are used to calculate a maximum strain of 741×10^{-6} .

$$(\text{Strain } (\epsilon) = 1 \times 10^6 \text{ V/m} \times 741 \times 10^{-12} \text{ m/V} = 741 \times 10^{-6})$$

Equation 4.2 transposed provides:

$$\text{Displacement } (\delta t) = \text{Original Thickness } (t) \times \text{Strain } (\epsilon)$$

(eqn.4.4)

Using the calculated value of strain (741×10^{-6}) and $200 \mu\text{m}$ as the original thickness of the PZT5H material the displacement can be calculated:

$$\begin{aligned} \text{Displacement } (\delta t) &= 200 \times 10^{-6} \text{ m} \times 741 \times 10^{-6} \\ &= 0.148 \mu\text{m} \end{aligned}$$

Clearly a displacement, DS , capable of producing a significant frequency shift cannot be generated using $200 \mu\text{m}$ thick pieces of PZT operating in their shear mode. The piezoelectric strain constant and the maximum electric field which can be applied without the material breaking down are constant for PZT. The only factor which can be altered to increase the shear displacement is the thickness of the material. This has to be increased for the shear displacement to increase. Increasing the thickness of the PZT material means the voltage applied to the electrodes to generate the same (maximum) electric field, which is necessary to

produce the maximum shear displacement, has to be increased. One of the design criteria established above was to minimise the applied voltage required to produce the desired displacement.

4.2.1.1 Stacked PZT between FSSs

Stacking pieces of 200 μm thick PZT on top of each other and then sandwiching the stack between the FSSs would allow the total shear displacement to be increased with no increase in applied voltage. This design incorporated between the two FSSs is shown in Figure 4.7. Each piece of PZT in the stack structure has to have the energisation voltage applied directly to its electrode faces. i.e. The voltage cannot be applied to the electrodes on the two outside pieces of PZT only.

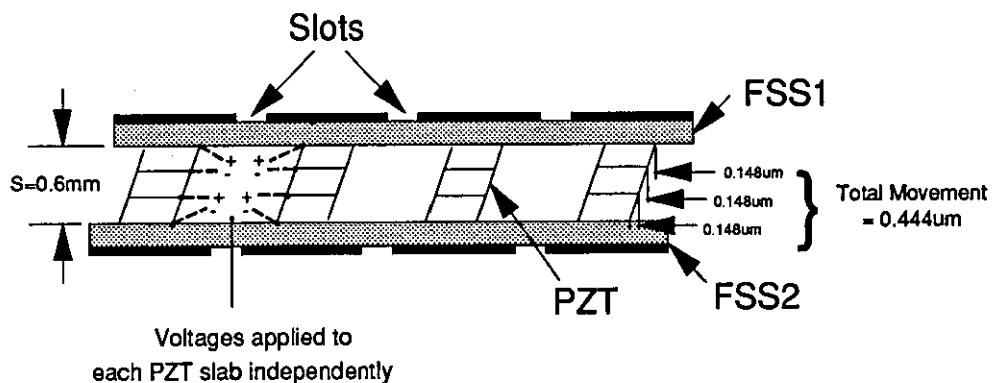


Fig.4.7: A stacked, shear mode, piezoelectrically controlled RFSS

Graph 4.1 demonstrated the importance of minimising the gap, S , and maximising the displacement, DS , to achieve a large resonant frequency shift. Using the technique depicted in Figure 4.7 the shear displacement can only be increased at the expense of increasing the gap, S , which in turn reduces the resonant frequency shift achieved from the displacement, DS . This increase in S necessary to produce the required increase in shift, DS , means this method cannot be implemented to produce a significant resonant frequency shift.

An alternative to stacking the ceramics vertically is to position them horizontally, i.e. "side by side", between the FSSs. Each PZT slab, when energised in its shear mode, pushes the adjacent slab, which is also energised to

deform in its shear mode. This slab in turn pushes the slab next to it. This process of each slab pushing the adjacent slab could be repeated until the desired movement was produced. This idea was called the *Stacked Horizontal Shear Method* and is shown in Figure 4.8.

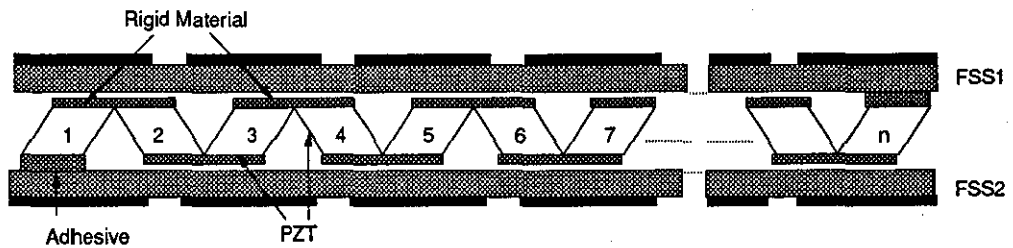


Fig.4.8: The Stacked Horizontal Shear Method

The first slab (labelled 1 in Figure 4.8) is secured along one face to FSS2. The other face of the slab is secured via a thin strip of rigid material to the adjacent slab (labelled 2). This slab is then secured via a further rigid strip of material along its other face to slab 3. This chain continues until the total displacement, due to the shear movement of all the slabs, is the FSS displacement required.

To utilise this design the minimum $200\mu\text{m}$ thick pieces of PZT would have to be used, thicker material would result in the gap, S , between the FSSs being too large. The brittle nature of PZT means thin pieces of the material can only be manufactured with small planar dimensions. In this application the planar dimensions of the material should be minimised anyway so they occupy the minimum area between the FSSs. This is necessary because the PZT must be hidden behind the copper parts of the FSSs to prevent it from interfering with the microwaves passing through the slots.

The maximum size FSS which can be manufactured by the University using the pcb manufacturing techniques is 400mm x 300mm. The 200 μ m thick PZT slabs will produce a maximum shear movement of 0.148 μ m. To achieve 1mm of movement would require 6757 slabs of PZT. To fit these slabs between FSSs with dimensions 400mm x 300mm would mean each could only be a maximum of 60 μ m long.

$$\left(\frac{400\text{mm Maximum FSS Length}}{6757, \text{ Number Of Slabs}} = 60\mu\text{m} \right)$$

Positioning electrodes along the 60 μ m length of PZT and connecting the energisation voltage source to these edges is a difficult manufacturing problem. Added to the other manufacturing difficulty of securing the slabs together renders this technique unfeasible.

The idea of stacking pieces of piezoelectric material to obtain a large movement could be adopted with the piezoelectric material operating in its length extension or thickness expansion mode.

Table 3.2, (Section 3) shows the PZT ceramic material has larger piezoelectric strain constants d_{31} and d_{33} (274×10^{-12} C/m and 593×10^{-12} C/m respectively) than PVDF (d_{31} and d_{33} have values of 23×10^{-12} C/m and 33×10^{-12} C/m respectively). This instigated an investigation into using PZT in its length extension and thickness expansion modes.

To achieve a significant resonant frequency shift the thinnest piece of PZT (200 μ m) must be used to minimise the gap S between the FSSs. The manufacturing difficulties of connecting to an electrode 200 μ m wide prevent the PZT material from being operated in its thickness expansion mode. Instead the material must be operated in its length extension mode (d_{31}) which has a smaller strain coefficient. The two modes and their extensions/expansions are shown in Figure 4.9.

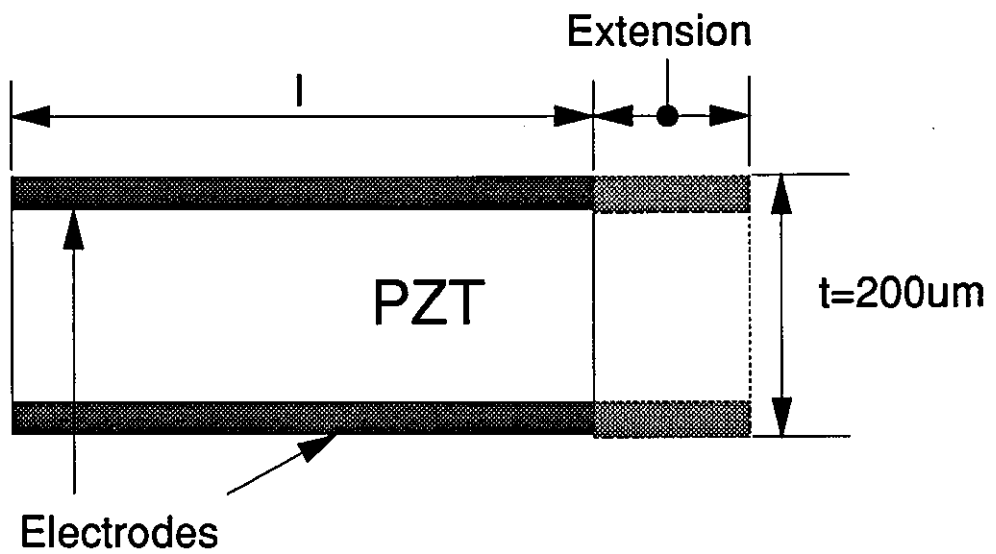


Fig.4.9(a): Operation in piezoelectric length extension mode

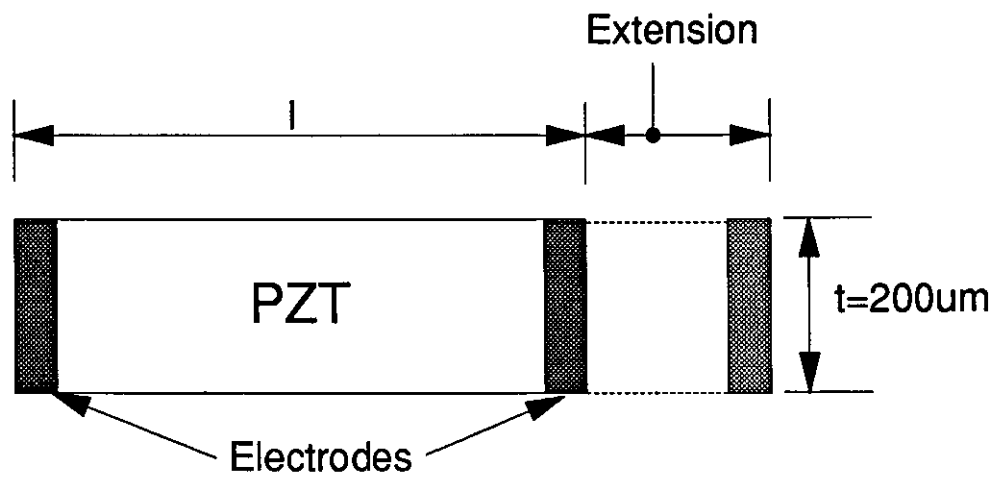


Fig.4.9(b): Operation in piezoelectric thickness expansion mode

Another problem with operating PZT in its thickness expansion mode is the high energisation voltage needed to achieve the required electric field. Figure 4.9(b) shows the electrodes at the ends of the PZT. To achieve the maximum electric field of 1000V/mm (Table 3.3) necessary to maximise the expansion of the material, a high voltage has to be applied.

$$V = E \times l$$

and l , in this instance, is large.

If l is made smaller the extension which can be obtained from the material is reduced since this extension is proportional to l (equation 3.2a).

The maximum strain which can be obtained from PZT is, using $E=1000\text{V/mm}$ and $d_{31}=274 \times 10^{-12}\text{C/m}$ (Table 3.2) and equation 4.1:

$$d_{31} = \frac{\text{Strain}}{\text{Applied Field}}$$

$$\begin{aligned} \text{Strain } (\epsilon) &= d_{31} \times \text{Applied Field } (E) \\ &= 274 \times 10^{-12} \text{C/m} \times 1000 \text{V/mm} \\ &= 274 \times 10^{-6} \end{aligned}$$

The maximum length of PZT is restricted by its brittle nature. At thicknesses of 200 μm this maximum length is 90mm (Table 3.2). Discussions with material suppliers revealed longer pieces of PZT can be manufactured, at a considerable financial premium. These long pieces of PZT are prone to breaking.

Using equation 3.2a, rewritten here as equation 4.5:

$$\text{Strain } (\epsilon) = \frac{\text{Length Extension } (\delta l)}{\text{Original Length } (l)}$$

(eqn.4.5)

$$\begin{aligned}
 \delta l &= l \times \epsilon \\
 &= 90\text{mm} \times 274 \times 10^{-6} \text{ m/V} \\
 &= 24.6\mu\text{m}
 \end{aligned}$$

Stacking pieces of PZT material operated in the length extension mode, as shown in Figure 4.10, will result in a total extension of $N \times 24.6\mu\text{m}$, where N is the number of pieces of PZT.

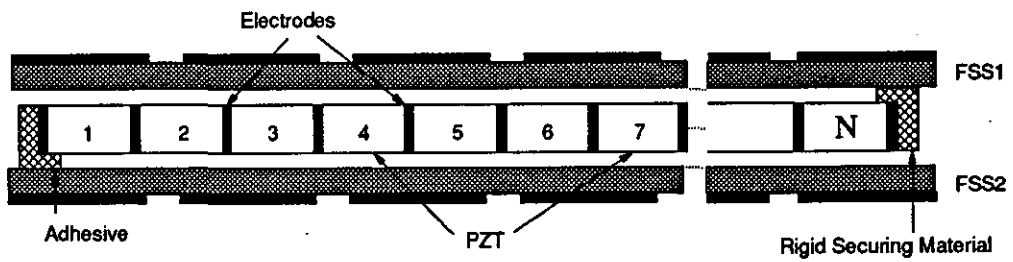


Fig. 4.10: The Stacked Horizontal Method operating in the length extension mode

To achieve 1mm of movement 41 pieces of PZT are needed, i.e. $N=41$. Each piece is 90mm long (90.0246mm when energised). To fit 41 of these pieces of PZT between the FSSs requires a length of 3.69m. This is much greater than the maximum FSS length of 400mm.

Instead of positioning all of the PZT pieces in a single 3.69m long line, they could be arranged in shorter lengths which fit between the FSSs. PZT will contract if its energisation voltage is reversed. By allowing one length of the pieces of PZT to expand and the adjacent lengths, to which it is connected, to contract, the 3.69m length could be incorporated between the FSSs as shown in Figure 4.11.

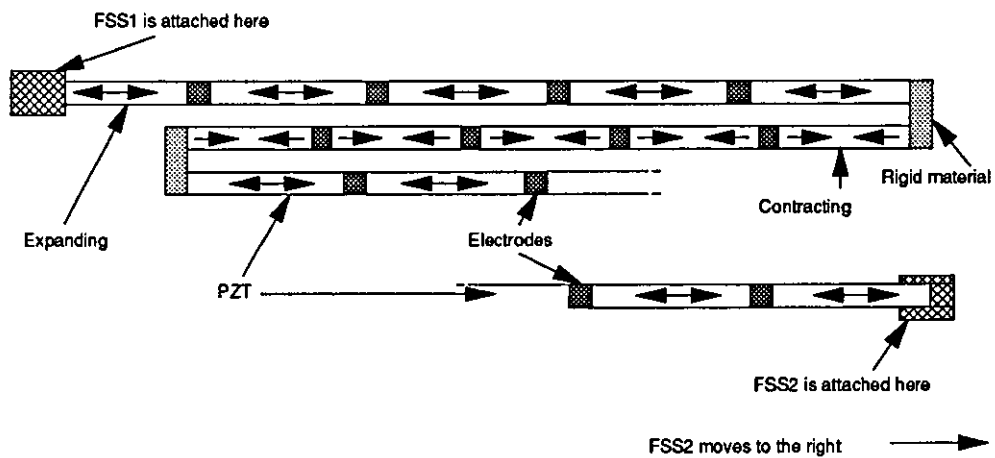


Fig.4.11: Configuration of the PZT length in the confined space between the FSSs

The planar surfaces of the PZT are electroded and must be positioned behind the copper areas of the FSSs, as opposed to the slotted areas, to avoid the electrodes interfering with the microwaves.

Splitting the 3.69m length of PZT pieces into ten, 0.369m, lengths would allow it to fit between the FSSs. A disadvantage of this technique is the PZT will occupy a considerable area between the FSSs. e.g. If the PZT pieces are 10mm wide, ten lengths will occupy an area 0.1m wide and 0.369m long. It will be hard to "hide" this amount of PZT behind the copper areas of the FSSs.

4.2.2 Implementing PVDF in the RFSS

The piezoelectric strain constants of Polyvinylidene Fluoride (PVDF) are not as large as those for PZT (Table 3.2 shows them to differ by a factor of at least ten). However an advantage of PVDF over PZT in the RFSS application is it is manufactured in sheets. The minimum thickness being $9\mu\text{m}^{[24]}$. This makes PVDF unsuitable for use in the thickness expansion or shear modes where the displacement is proportional to the thickness but does allow the length extension mode to be utilised with the electrodes close together. This means only a relatively small voltage is needed to energise the PVDF with its maximum electric field.

The piezoelectric strain equations, 4.1 and 4.5, can be used to calculate the length extension which could be obtained by energising a 400mm length of $9\mu\text{m}$ thick PVDF with a voltage which produces the maximum electric field within the material.

From Tables 3.2 and 3.3:

$$d_{31} = 23 \times 10^{-12} \text{ m/V}$$
$$E_{\text{max}} = 30 \text{ V}/\mu\text{m}$$

These values can be substituted into equation 4.1 rearranged to allow calculation of the strain:

$$\begin{aligned} \text{Strain } (\epsilon) &= d_{31} \times E \\ &= 23 \times 10^{-12} \text{ m/V} \times 30 \times 10^6 \text{ V/m} \\ &= 690 \times 10^{-6} \end{aligned}$$

This value of strain can be substituted into equation 4.5, rearranged, to allow the length extension to be calculated.

$$\begin{aligned} \text{Length Extension } (\delta l) &= \text{Strain } (\epsilon) \times \text{Original Length } (l) \\ &= 690 \times 10^{-6} \times 400 \times 10^{-3} \text{ m} \\ &= 0.276 \text{ mm} \end{aligned}$$

To achieve an electric field of $30\text{V}/\mu\text{m}$ a voltage of 270V must be applied across the electrodes.

$$(V = E \times t = 30\text{V}/\mu\text{m} \times 9\mu\text{m} = 270\text{V})$$

This is greater than the 200V source needed to energise the thicker, 200 μ m thick, PZT because the maximum electric field which can be applied to PVDF (30V/ μ m) is much greater than the maximum electric field which can be applied to PZT (1000V/mm). The maximum electric field is always considered because this maximises the expansion available from the piezoelectric material.

The thinner PVDF sheets can be stacked vertically between the two FSSs without increasing the gap between the FSSs, S , to a value which prevents the structure from producing a significant resonant frequency shift when the FSSs are shifted. This was not possible with the PZT material because it was not available in such thin pieces.

Four strips of PVDF, 400mm long, could be positioned between the FSSs and would, theoretically, produce a cumulative length extension of greater than 1mm if they were energised to operate with the maximum electric field.

Unlike PZT, PVDF will not contract if its energisation voltage is reversed. To obtain a net extension from strips of PVDF secured at opposite ends a method of producing an effective contraction is required. This can be achieved by only energising alternate strips at any one time. Figure 4.12a shows the PVDF stack with the slots in the two FSSs aligned. In this diagram strips 2 and 4 are energised and have expanded to the same length as the un-energised strips, 1 and 3. To move FSS2 strips 1 and 3 are energised and the energisation voltage is removed from strips 2 and 4. This causes strips 1 and 3 to expand and 2 and 4 to contract producing the arrangement shown in Figure 4.12b where FSS2 has moved, relative to FSS1.

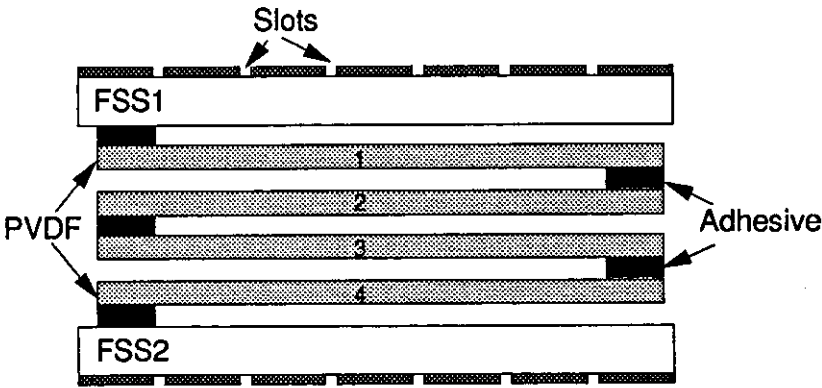


Fig.4.12(a): A double layer FSS with the slots on the two FSSs aligned

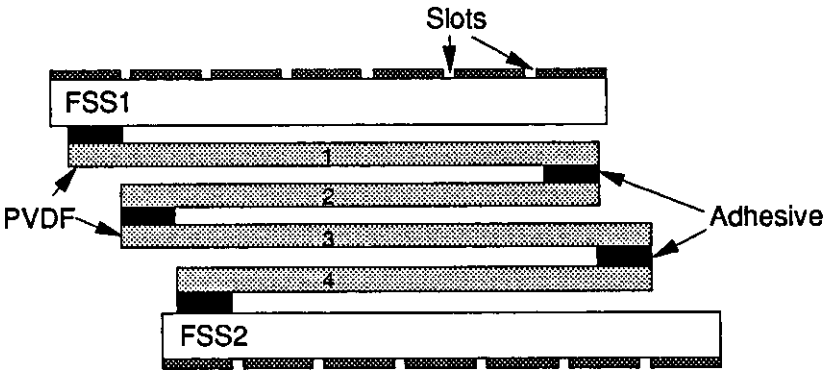


Fig.4.12(b): A double layer FSS with the slots on the two FSSs misaligned

By positioning more strips between the FSSs the displacement could be increased to the values modelled, and shown in Graph 4.1, which are necessary to achieve a significant resonant frequency shift. The problems with implementing this method arise from the manufacturing difficulties of accurately securing and clamping thin strips of PVDF; the facilities for achieving this accuracy in manufacture are not available at the University and so make a practical investigation into this method impossible.

4.3 Piezoelectric Actuators

Methods of increasing the displacement obtainable from piezoelectric materials have been developed for other applications and the possibility of implementing these in a Reconfigurable FSS were considered. These methods are now described.

4.3.1 Bimorphs^[25 p.16]

These structures consist of two strips of PZT secured along their length. A voltage is applied to the strips causing one strip to expand and the other to contract. This causes the bimorph to bend and the unsecured end to deflect. This is analogous to the action of a bimetallic strip. The bimetallic strip consists of two strips, or laminates, of different material. The two materials have different coefficients of thermal expansion. This causes one laminate to expand more than the other when the bimetallic strip is heated.

Bimorphs can produce a displacement of the order of 0.1mm and have been stacked to produce displacements of greater than 1mm^[28 p.9]. The large physical dimensions of bimorphs mean they cannot be positioned in the small space *S* between the FSSs and so could not be implemented in the RFSS application.

4.3.2 Flexure Hinges^[26]

The displacement available from these devices, which are essentially pieces of PZT shaped so as to amplify their small movement, is not large (typically less than 20µm). The advantages of using a flexure hinge to achieve this relatively small movement were considered to be outweighed by the complexities of incorporating them into the RFSS.

4.3.3 Cyclic Mechanisms

A rotary motor has been manufactured from piezoelectric materials by the Matsushita Electric Industrial Company^[26]. This device involves energising a loop of piezoelectric ceramics so they expand in a desired sequence. The energised ceramics distort an elastic material which pushes a 'rotor' around the loop. Although the rotary motor could not be utilised directly to displace the FSSs,

because it produces rotation as opposed to a linear motion, the concept of using the piezoelectric material cyclically to achieve this motion could be considered. e.g. Each piece of the piezoelectric material is used several times to achieve the required displacement.

Burleigh Instruments developed the 'Inchworm'^[28 p.10]. This device is capable of linear movements of up to 200mm. It uses a cyclic mechanism as described above for Matsushita's rotary motor. The Inchworm, shown in Figure 4.13, consists of three tubular piezoelectric ceramic elements which are positioned around a shaft. When these tubes are energised their inside diameter contracts. The first tube is energised and its contraction is used to clamp the shaft. The second tube has a larger inside diameter and when it is energised it does not clamp the shaft but exhibits an increase in length which pushes the third tube along the shaft. The third tube is now energised to clamp the shaft, the first and second tubes are un-energised and they un-clamp from the shaft and contract respectively. This has the effect of moving the tubes along the length of the shaft. The sequence is now repeated with the first tube clamping the shaft at its new position.

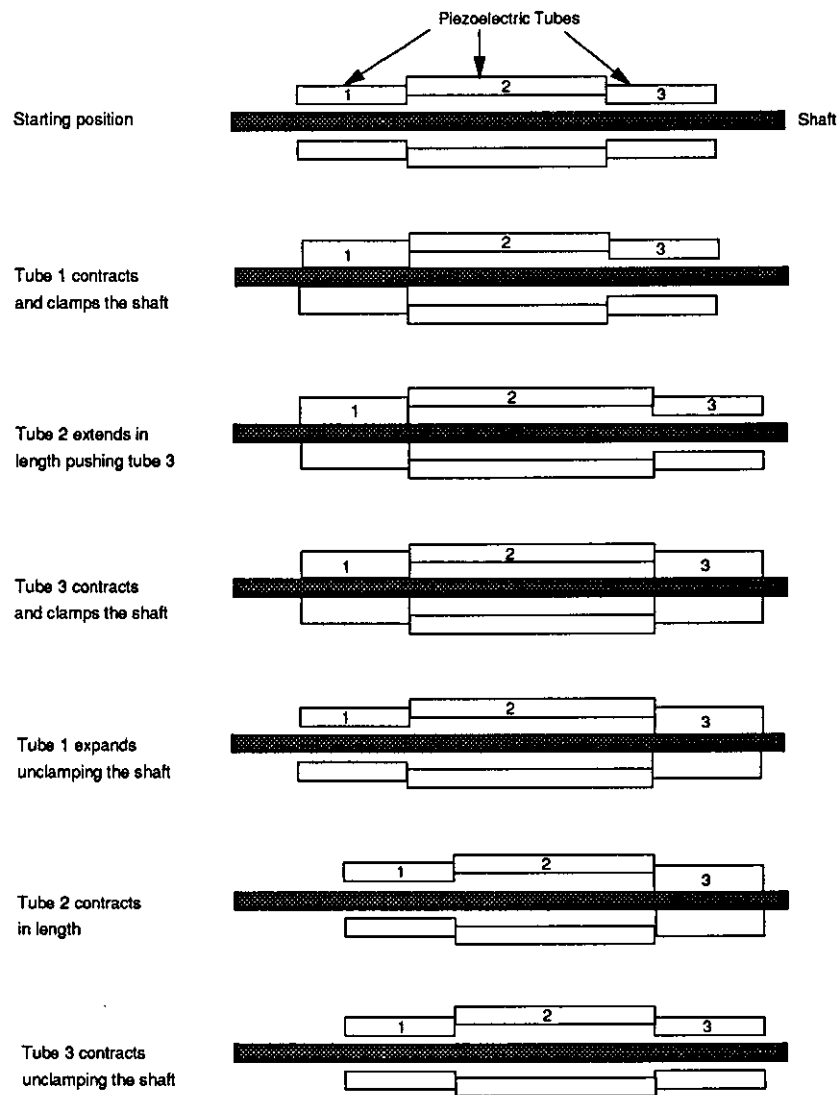


Fig.4.13: The operation of the Inchworm motor
(From Burleigh Instrument's *The Piezo Book*^[28])

The piezoelectric Inchworm would be suitable for use in the RFSS if it could be made small enough to fit between the FSSs. The Inchworm made by Burleigh Instruments is too large; designing a device with the dimensions required would be a difficult and expensive task.

The disadvantage of cyclic mechanisms is their slow speed. The Inchworm is only capable of 2mm/second. Ideally a speed greater than this is required for the RFSS.

4.4 Piezoelectric Frequency Selective Surfaces

Conventionally FSSs are manufactured from sheets of copper adhered to a polyester substrate. The copper has a high conductivity which exhibits little resistance to the currents induced by the incident microwaves. The polyester substrate acts as a supporting structure. Ideally no supporting material would be used but for arrays of dipoles, which are not interconnected, the polyester substrate is necessary to hold the dipoles in position on the FSS. The supporting substrate should have a relative permittivity and a loss tangent as close as possible to the values for free space, one and zero respectively.

PVDF is available in sheet form making it a suitable material for the construction of FSSs. The conductive electrodes which can be made from copper, nickel, or silver, act as a suitable material for conducting the induced currents whilst the PVDF substrate holds the FSS together. Table 3.3 lists PVDF with a higher relative permittivity (ϵ_{rPVDF} 12-13) and loss tangent ($\tan\delta_{PVDF}$ 0.02 at 10^4 Hz) than the polyester substrate used in conventional FSSs ($\epsilon_{rPolyester}$ 3.25 at 1MHz and $\tan\delta_{Polyester}$ 0.005 at 1kHz^[34]). This could have an effect on the frequency response of the FSS.

The PVDF material is electroded on both sides. If a FSS is etched onto it the etched slots must be identical on both sides. This creates a double layer FSS, separated by a gap, S , filled by the PVDF substrate.

If a Piezoelectric FSS (PFSS) consisting of arrays of dipoles was energised the length of the dipoles would increase. This expansion would be very small; calculations in Section 4.2.2 showed an extension of 0.276mm could be achieved from a 400mm length of PVDF. This can be calculated as a percentage of the length (0.069%) and, because the extension is directly proportional to the length, this *percentage length extension value* can be used to calculate the absolute extension of any length of PVDF.

e.g. The dipoles on a PFSS which has a resonant frequency of 20GHz are approximately 7.5mm long. If the PFSS is energised the dipoles will extend to 7.505mm.

$$7.5 + (7.5 \times 0.00069) = 7.505mm$$

Graph 4.1 shows this extension will have no significant effect on the resonant frequency of the PFSS, i.e. There would be no noticeable frequency shift.

The calculation shown above assumes the maximum electric field is applied across the entire PVDF. The material will only expand when it is subjected to an electric field, this is achieved by applying a voltage to the electrodes. Where the electrodes have been etched away around the dipoles, or, in the case of a slotted FSS, the electrodes are etched away to produce the slots, the electric field cannot be applied and so extension of the material will not occur. (It is expected some fringing of the electric field will occur around the dipole or in the slots producing a reduced extension, proportional to the reduced electric field, in this area - Figure 4.14.)

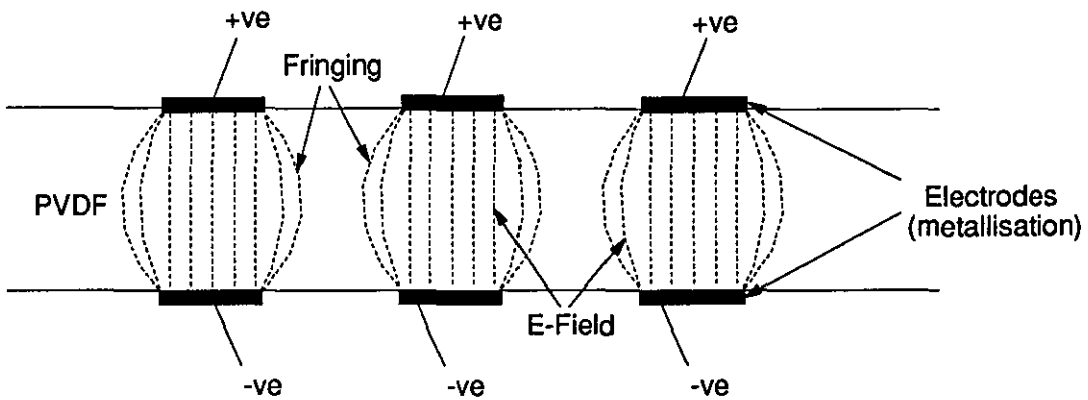


Fig.4.14: The fringing E-field in the slots of a PFSS

By ensuring the electrodes occupy the maximum possible area on the PVDF surface the electric field will be applied to the maximum volume of PVDF and the expansion will be maximised.

Etching dipoles on the PVDF means the individual dipoles must be connected together to enable a voltage to be applied. A PFSS consisting of slotted elements has electrical continuity across its electroded area allowing easy connection of the voltage

source. Also the electroded area of a PFSS with arrays of slots is greater than a PFSS with arrays of dipole elements. A PFSS with slots, as opposed to dipoles, should produce an extension, when energised, close to the values calculated in this chapter.

When the PFSS is energised the change in the length of the slots will be comparable to the change in the length of the dipoles calculated. This will produce an insignificant change in the resonant frequency of the PFSS.

By using two PFSSs, with identical elements, a larger total change in the length of the slots can be achieved. The two PFSSs are positioned on top of each other with no gap between them. The slots in the two PFSSs are aligned and the two sheets are secured at opposite ends. This arrangement is shown in Figure 4.15.

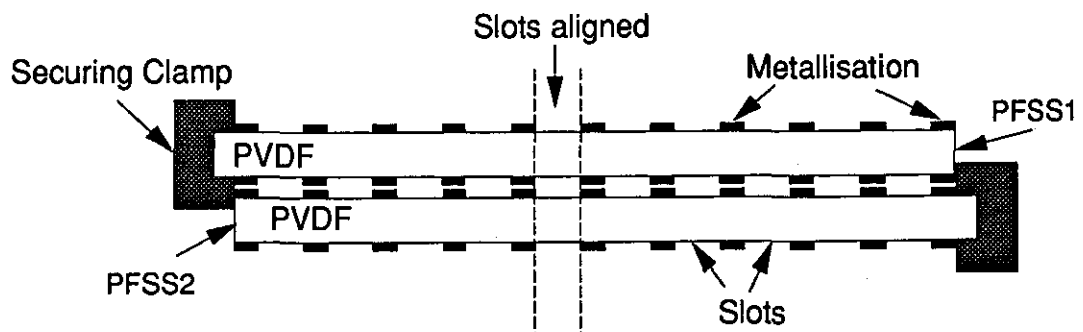


Fig.4.15: A double layer slotted PFSS

To obtain 1mm of extension from a sheet of PVDF the length of PVDF must be 1.45m. This was calculated using the *percentage length extension value* of 0.069% calculated previously.

$$1\text{mm Length Extension} = 0.069\% \times \text{Original Length}$$

$$\therefore \text{Original Length} = \frac{1\text{mm}}{0.069} \times 100\%$$

$$= 1.45\text{m}$$

If both lengths shown in Figure 4.15 are extended by 1mm the total relative contraction of each slot will be 1mm (Figure 4.16).

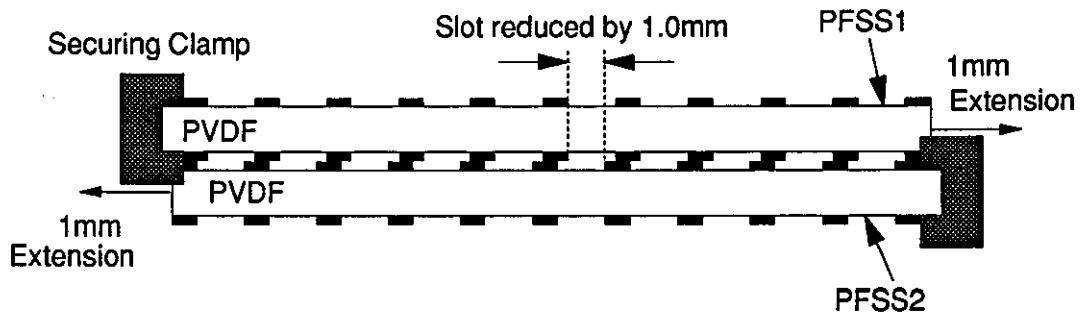


Fig.4.16: The cumulative movement at each slot of a double layer PFSS

FSSs 1.45m long cannot be manufactured using the facilities available at the University, additionally the cost and availability of PVDF sheets with these dimensions is prohibitive. PVDF is available in sheets 150mm square. Using 0.069% as the *percentage length extension value* the expected extension from these sheets was calculated as 0.103mm.

Graph 4.1 showed the resonant frequency shift obtained by altering the lengths of the dipoles on an FSS. As explained previously the graph can also be used to estimate the resonant frequency shift of a complementary slotted FSS. The Graph shows reducing the length of the slots by 0.103mm will produce an insignificant resonant frequency shift.

The slots could be etched so their width is in the direction of the extension of the PVDF. By positioning two of these piezoelectric FSSs behind each other the piezoelectric sheets could be energised to produce an effective reduction in the width of the slots on the double layer structure. If arrays of 0.1mm wide slots are aligned before energisation they should produce a shuttering effect when energised to block all of the incident microwaves. This action is shown in Figure 4.17.

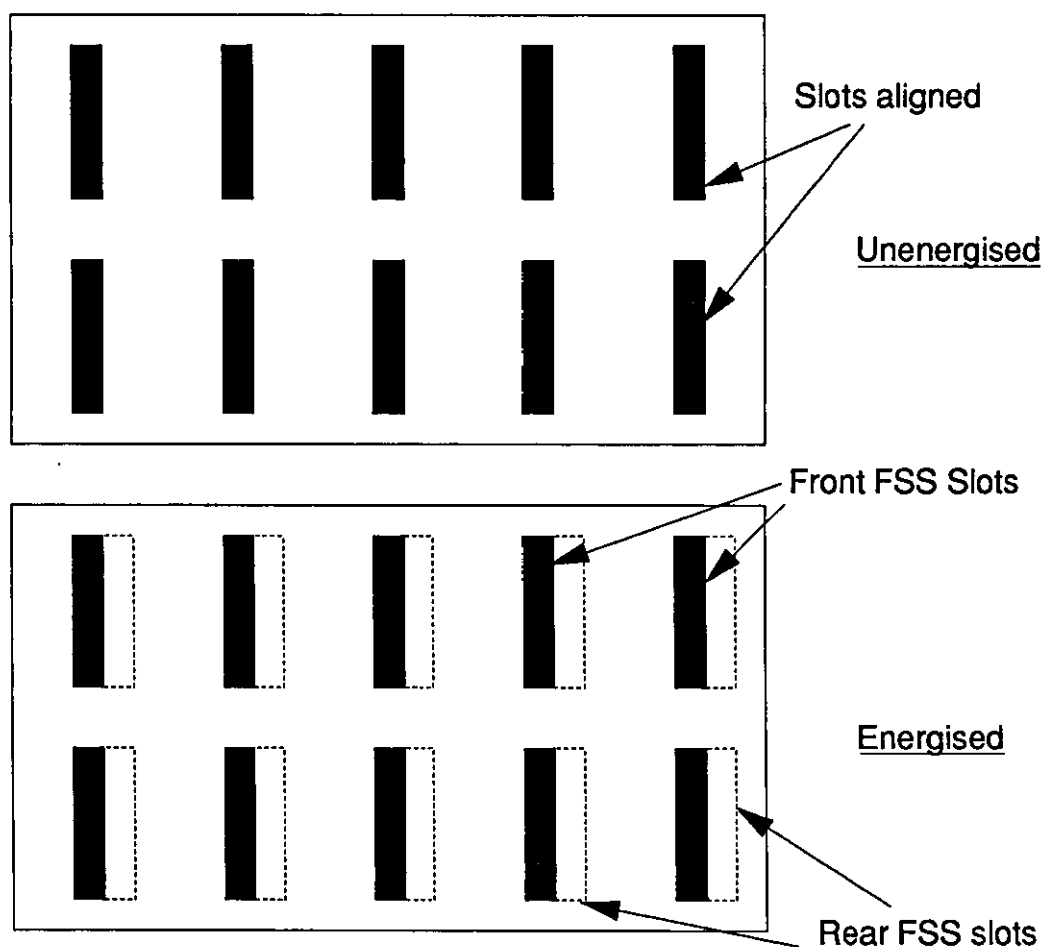


Fig.4.17: The shuttering action of PFSSs

4.4.1 Experiments with PVDF

PVDF material with a substrate thickness of $9\mu\text{m}$ and copper-nickel electrodes with thicknesses of $0.055\mu\text{m}$ was purchased. Experiments were performed to establish the extension which could be obtained in practice from this material. The copper layer of the electrode is necessary to avoid corrosion which would reduce the electrical conductivity and hence the electric field in the PVDF. The nickel layer is on the outside and was connected to the power supply via copper strips which were secured to the nickel using a silver loaded epoxy adhesive^[36]. A side view of the PVDF sheet is shown in Figure 4.18.

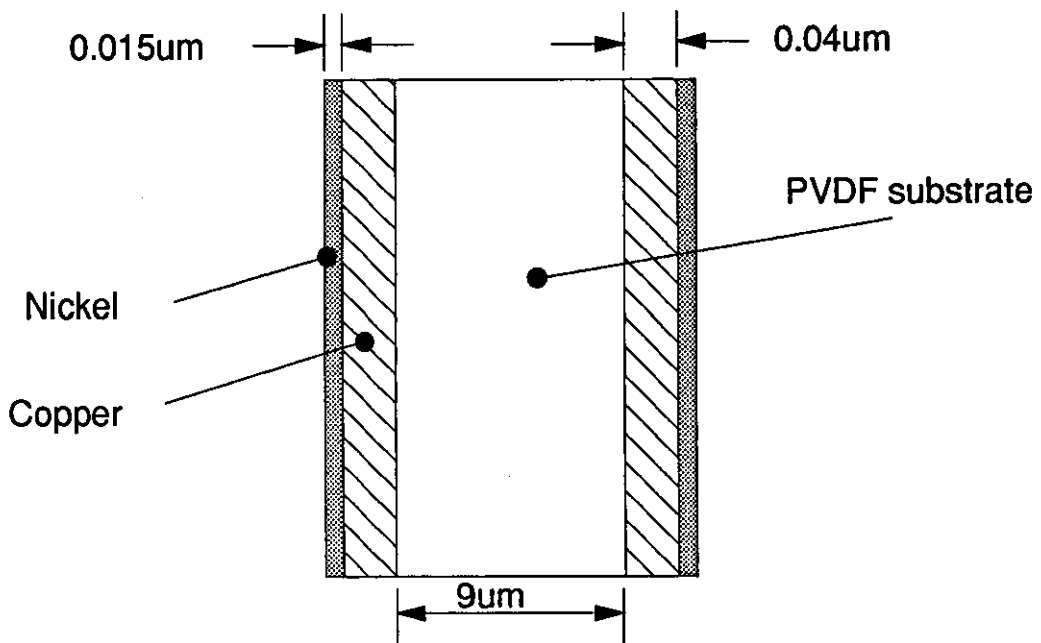


Fig.4.18: Side view of a PVDF sheet

The PVDF foils are very flimsy. Initial experiments indicated they would require an additional supporting structure if they were used in the RFSS design. Holding the PVDF in tension ensures any extension is in the required direction. If the material was allowed to expand freely it might not move in the required direction, i.e. along its length, if there was any restricting friction.

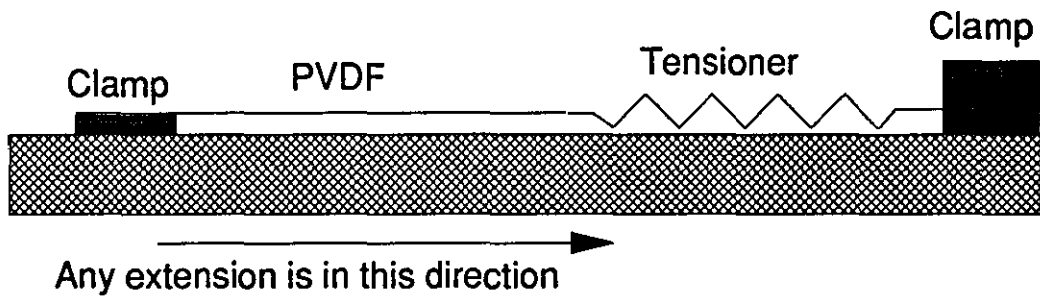


Fig.4.19: Holding The PVDF In Tension

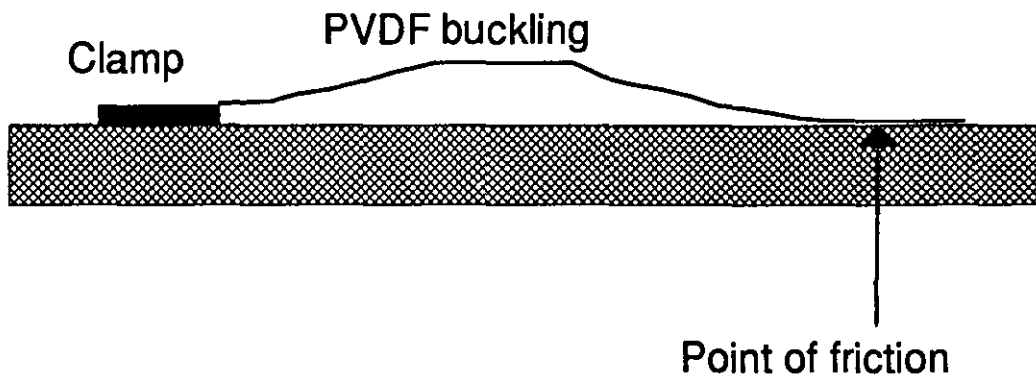


Fig.4.20: Buckling Due To Friction

A further problem with the $9\mu\text{m}$ thick PVDF foils was discovered during the initial experiments. These foils are so thin that small 'pin-holes' can appear in the PVDF during manufacture. This exposes the inside surfaces of the two electrodes - there is no longer any PVDF substrate between them, only air.

During experiments the supply voltage was increased gradually from 0V. On one foil the substrate appeared to undergo electrical breakdown and the electrodes started to arc when the supply voltage reached 20V. This voltage corresponds to an electric field of 2.22kV/mm in the PVDF. The breakdown voltage of dry air is 2.0kV/mm . The voltage at which the PVDF strip broke down suggests a pin-hole

existed in the PVDF leaving only air as an insulator between the electrodes. When the electric field exceeded the breakdown field of air (at about 20V) this pin-hole caused arcing between the electrodes.

The problems with the flimsy nature of the PVDF and the possibility of pin-holes lead to a decision *not* to use 9 μ m thick PVDF in the RFSS design.

PVDF material is also manufactured in 28 μ m thick sheets (Table 3.2). These sheets require a larger voltage to be applied in order for the maximum electric field to be created in the PVDF substrate.

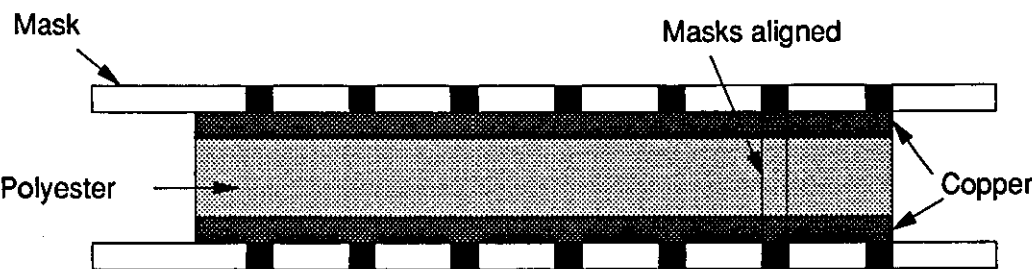
$$V = E \times t = 30V/\mu m \times 28\mu m = 840V$$

The thicker material also has the disadvantage of occupying more space between the FSSs. PVDF material with substrate thicknesses of 52 μ m and 110 μ m was also purchased. These materials, although more rigid than the 9 μ m thick foils, still require some form of supporting structure.

4.4.2 The Manufacture of FSSs

The small movements generated by the PFSS when it is energised mean close tolerances are required during the manufacture of the PFSS.

The University has experience of manufacturing single sided copper-polyester FSSs using the facilities for printed circuit board etching. Double sided FSSs have also been manufactured, these require accurate alignment of the etching masks on both sides of the copper-polyester sheet.



The dark areas on the mask are the positions where slots are etched

Fig.4.21: The masks positioned around a double sided copper-polyester sheet during the manufacture of the FSS

If the two masks are misaligned the resultant double sided FSS will have slots with reduced dimensions.

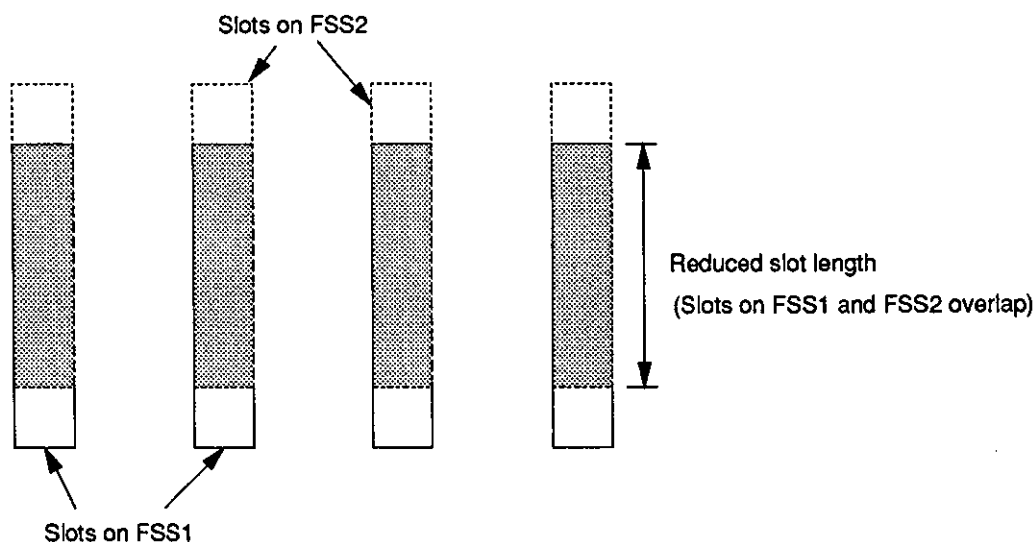


Fig.4.22: The result of misaligned masks during the manufacture of a double layer FSS

Previously manufactured FSSs had a minimum slot width of 0.2mm. The small planar displacement obtainable from piezoelectric FSSs mean the slots can only be 0.1mm wide to enable the 'shuttering' effect of the FSSs to be achieved. This means the alignment of the masks around the PVDF is very critical.

The copper-polyester sheets, or in the case of the piezoelectric FSS, the copper-nickel coated PVDF sheets, are covered with photosensitive etch resistant laminae. The masks are then accurately positioned and secured around the PVDF/copper-polyester laminated sheets and exposed to ultraviolet light. The light hardens the laminae where they are not shielded by the mask. The mask is then removed and the 'un-hardened' laminae (i.e. that which was shielded from the ultraviolet light) is chemically removed. This leaves the copper, or copper-nickel,

exposed in the areas where it is to be etched away from the polyester/PVDF sheet. Ferric chloride or ammonium sulphate is now used to etch the exposed copper from the PVDF/polyester substrate.

The high tolerances required meant the possibility of 'undercutting' during the etching procedure had to be considered. Undercutting is the term used to describe the results of the etchant seeping under the masked areas and etching some of the copper or copper-nickel electrode from these areas. This is shown in Figure 4.23. The amount of undercutting is greater for thicker copper or copper-nickel metallisation.

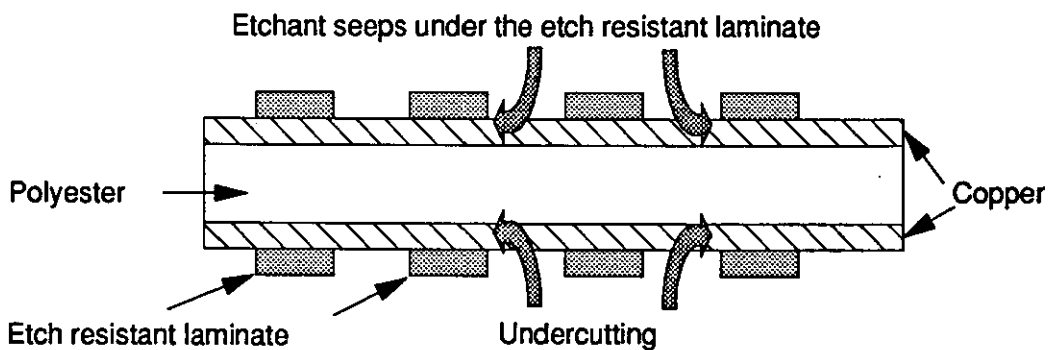


Fig.4.23: Undercutting during the manufacture of an FSS

The thin copper-nickel metallisation on the PVDF sheets helps reduce the undercutting on the PFSS. However when the slots were measured using a microscope, capable of measurements to an accuracy of $50\mu\text{m}$, they were found to be up to 0.13mm wide (i.e. undercut by up to 0.03mm).

An alternative to using a chemical etchant process is to use a laser *ablation* technique. Laser ablation involves using an excimer laser to bombard the metallised surface with atoms, typically rare gas halide atoms, which cause some of the copper-nickel atoms on the metallised surface to be repelled. The difficulty with this process stems from having to ensure the laser only removes the metal

coating and does not ablate the PVDF substrate. Lasers do have the advantage of being highly accurate and the capability to produce thin slots with sub-micron accuracy.

The laser cannot be used to *cut* through the PVDF substrate because this is needed as an insulator against the high electric fields which are applied to energise the PVDF. The electric field is greater than the breakdown of air and so arcing would occur around the edges of the slot if the PVDF was removed.

To avoid arcing between the electrodes an 'electrodeless' border has to be created around the edges of the PFSS. This can be seen around the edges of the section of the PFSS shown in Figure 4.24.

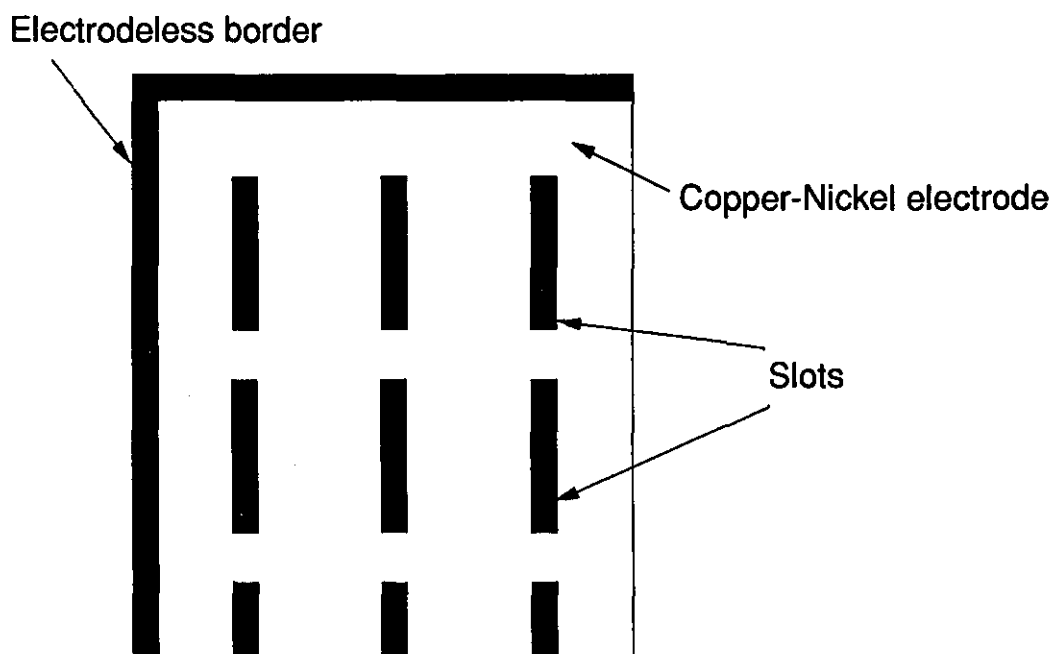


Fig.4.24: The electrodeless border around a PFSS

This chapter used computer models of an RFSS to help establish the design criteria for the Reconfigurable FSS. Methods of implementing the piezoelectric materials PZT and PVDF in the RFSS were considered along with the possibility of using existing piezoelectric actuator designs.

Experiments with PVDF were performed. These initial experiments provided important results about the mechanical properties of PVDF. The possibility of using PVDF to manufacture FSSs, as opposed to using the PVDF to move copper-polyester FSSs, was considered. Finally the method of manufacturing FSSs was described and the difficulties of manufacturing FSSs from PVDF were discussed.

5 EXPERIMENTAL AND MODELLED RESULTS

This Chapter details the results of measurements and computer models of conventional and reconfigurable FSSs. Comparisons are made between the modelled and measured frequency scans and reasons for disagreements between the two are suggested.

All measurements and models were made in the E-Plane, i.e. the electric field was perpendicular (transverse) to the FSS (TE mode). Also, unless stated otherwise, transmission response frequency scan measurements were made at normal incidence, i.e. the electric **and magnetic** fields were perpendicular to the FSS (TEM mode).

The effect the slot length and width, and the FSS substrate material and thickness have on the resonant frequency, passband bandwidth, and the transmission loss at the resonant frequency are studied. The effect of different shape FSS elements, e.g. square loops, was investigated.

Comparisons between slotted FSSs and FSSs with arrays of dipoles were made. Booker's extension to Babinet's principle is proved experimentally, justifying the use of the modal analysis software to model slotted FSSs.

5.1 The effect of dipole length on resonant frequency

5.1.1 Double Layer FSS Models

The Patent^[2] cited an example of a reconfigurable FSS (RFSS). The first stages of the research into the implementation of the reconfigurable FSS concept involved computer modelling this example. The transmission response produced from this model enabled the initial design criteria - minimising the space, S , and maximising the displacement, DS , to be established. The transmission response plots shown in Graph 4.1 in Chapter 4 are reproduced as Graph 5.1 in this chapter.

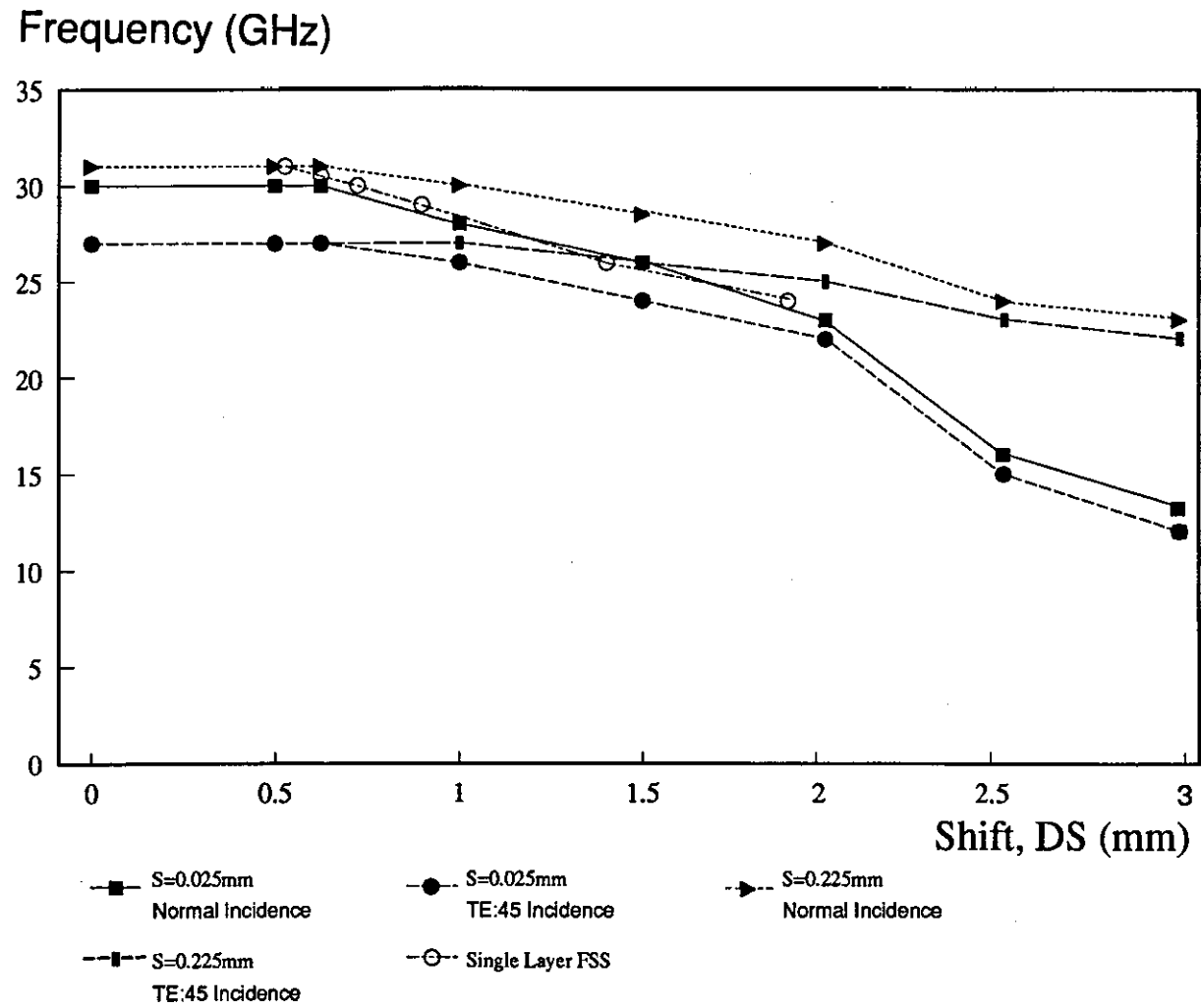
The dimensions of the dipoles on the two FSSs used in the model of Chapter 4 are listed in Table 5.1 below.

	FSS1	FSS2
Dipole Length	4.3mm	3.25mm
Dipole Width	0.4mm	0.4mm
Lattice Dimensions	6.0mm square	6.0mm square

Table 5.1: The dimensions of the dipoles

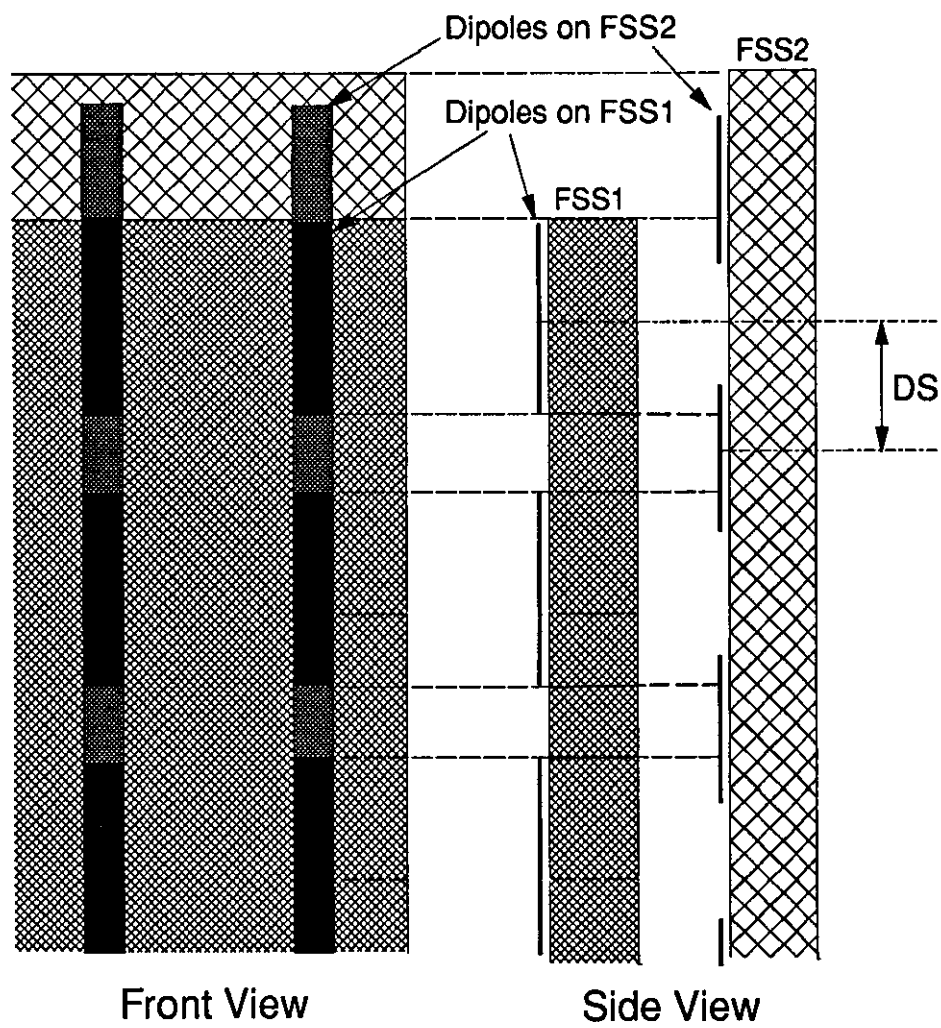
When the planar shift, DS , between the two FSSs was zero the 3.25mm long dipoles on FSS2 were positioned centrally behind the 4.3mm long dipoles on FSS1. i.e. The 3.25mm long dipoles were completely 'shadowed' from any incident microwaves by the longer dipoles on FSS1.

Graph 5.1: Computer models of a double layer FSS structure



Graph 5.1 showed no shift in resonant frequency until the shift, DS , was greater than 0.525mm. This was because the dipoles on the rear FSS remained in the 'shadow' of those on the front FSS until DS was 0.525mm. As DS was increased beyond 0.525mm the ends of the dipoles on the two FSSs started to overlap. This causes the *effective* length of the dipoles on the double layer structure to be increased.

When DS is 3.0mm the rear FSS has moved exactly half a lattice. Optically, from the front, this causes the double layer FSS structure to appear as a continuous copper strip. This is shown in Figure 5.1.




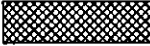


<u>Key</u>			
	Copper FSS1		Polyester FSS1
	Copper FSS2		Polyester FSS2

Fig.5.1: The double layer FSS structure with DS=3.0mm

The distance between the ends of adjacent dipoles on FSS1 is 1.7mm. (This is calculated by subtracting the dipole length, $L=4.3\text{mm}$, from the element length, $D=6.0\text{mm}$.) For this space to be completely covered by the dipoles on FSS2 the shift DS needs to be a minimum of 2.225mm. (This is calculated by adding the shift DS required to start covering the space, 0.525mm, and the distance between the ends of adjacent dipoles, 1.7mm.) For shifts DS greater than 2.225mm the 1.7mm gap between the ends of adjacent dipoles on FSS1 remain covered by the dipoles on FSS2.

Graph 5.1 shows the resonant frequency of the double layer FSS structure continues to change as the shift DS is increased beyond 2.225mm. This occurs because there is a gap, S , between the two FSSs. This gap means the two FSSs act as two closely coupled FSSs rather than a single (double layer) FSS.

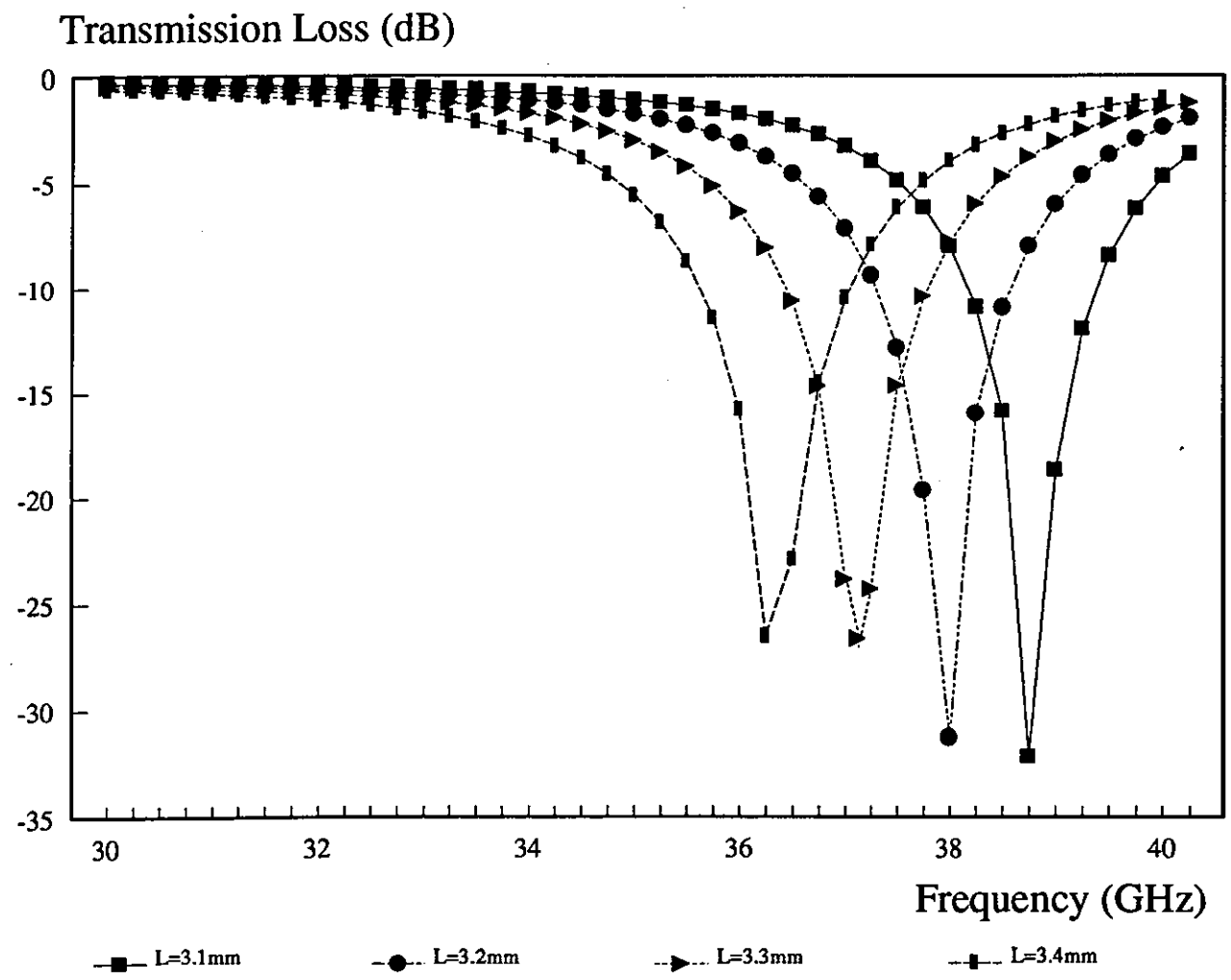
NOTE:

The first model of the single layer FSS had dipoles with a length of 4.3mm. The resonant frequency of this model was plotted at $DS=0.525\text{mm}$. The resonant frequencies of further models of the single layer FSS are also plotted. The lengths of the dipoles used in these models is equal to the value of DS plus 4.3mm (the original dipole length). This positioning of the resonant frequency plot of the single layer FSS on the Graph enables a direct comparison of the plots for single and double layer FSSs with the same *effective* dipole lengths.

5.1.2 Single Layer FSS Models

By modelling single layer FSSs with varying dipole lengths an estimate of the minimum *effective* change in dipole length necessary to produce the desired resonant frequency shift can be established.

Four FSSs were modelled. These FSSs consisted of dipoles with lengths 3.1mm, 3.2mm, 3.3mm, and 3.4mm positioned in 6mm square lattices. All the dipoles were 0.4mm wide. Graph 5.2 shows the change in resonant frequency as the lengths of the dipoles was increased. A resonant frequency shift of 2.6GHz was produced by increasing the dipole length by 0.3mm (3.4mm-3.1mm). To achieve a similar frequency shift using a double layer FSS would require a greater change in (*effective*) dipole length because of the finite gap, S , which must exist between the FSSs.



Graph 5.2: The modelled transmission response of single layer FSSs with varying dipole lengths

5.2 Modelling FSSs with arrays of slots

Chapter 4 explained the RFSS would be made from the piezoelectric film, PVDF, in order to minimise the gap S between the two FSSs. To enable the PVDF to be energised requires the electrode area to be maximised and continuous across the PVDF surface. A slotted FSS, as opposed to an FSS with arrays of dipoles, was chosen for the prototype RFSS because this maximises the electrode area and allows it to be continuous across the PVDF.

Slots cannot be modelled using the Modal Analysis Method software. For single layer FSSs an approximate model can be obtained to estimate the resonant frequency of the FSS by using Booker's extension to the Babinet's Complement principle^[37 p.498]. This involves modelling the complementary FSS, i.e. dipoles with the same dimensions as the slots positioned in the same size lattices. This only provides an approximate model. To produce a more accurate model the values of permittivity ($\epsilon_0\epsilon_r$) and permeability ($\mu_0\mu_r$) should be interchanged^[37 p.498]. This was not possible in the Modal Analysis software.

5.2.1 Experimental proof of Booker's Extension to Babinet's Principle

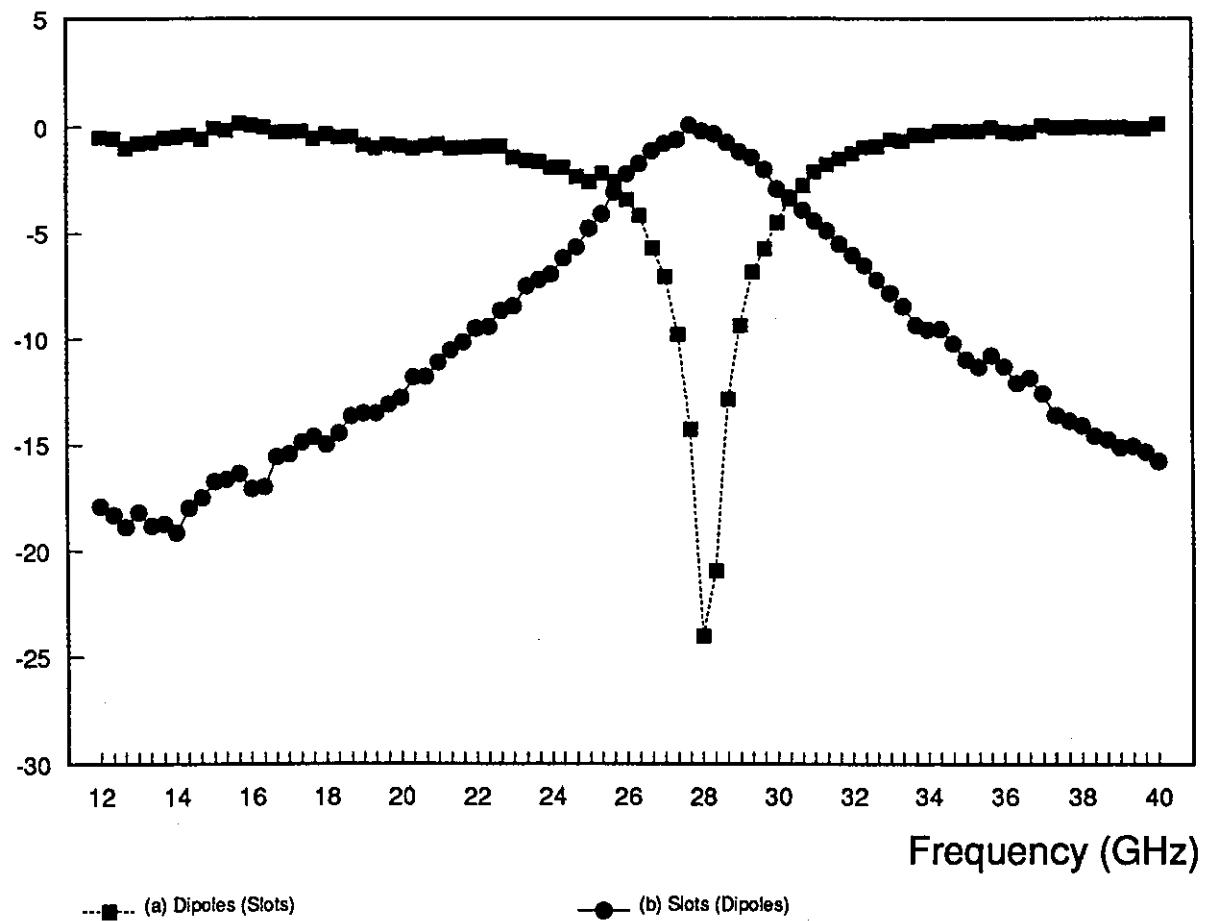
An FSS consisting of dipoles, 4.7mm long and 0.4mm wide, positioned in 6mm square lattices was manufactured from a copper-polyester sheet. The FSS had an area 150mm square.

Scans of the FSS in the J, K, and Q-bands showed a resonance at 27.8GHz where the transmission loss was -23.8dB. The -3dB bandwidth was 5.0GHz (from 25.7GHz to 30.7GHz). These frequency scans are plotted in Graph 5.3 (plot a).

A complementary slotted FSS was manufactured from copper-polyester sheets. This FSS consisted of slots, 4.7mm long and 0.4mm wide positioned in 6mm square lattices. This FSS also had an area 150mm square.

This slotted FSS was scanned over the three frequency bands, J, K and Q. These scans are also plotted in Graph 5.3 (plot b). They show a resonant frequency at 27.8GHz where the loss was 0dB. The -3dB bandwidth of 4.5GHz has lower and upper cut-off frequencies of 25.7GHz and 30.2GHz respectively.

Transmission (Reflection) (dBs)



Graph 5.3: Frequency scans of FSSs with arrays of dipoles and arrays of slots

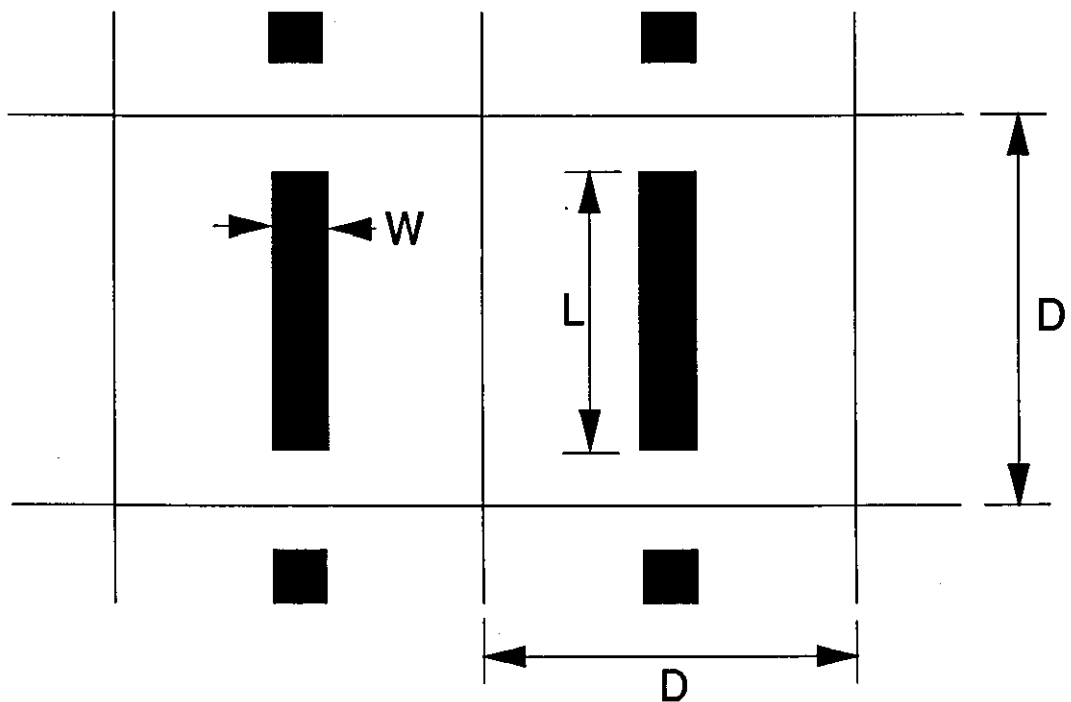
The -3dB points provide a quick indication to the accuracy of the complementary FSSs. Insignificant power is dissipated by the FSSs. This means, neglecting these insignificant losses, all of the power incident on the FSSs is either reflected or transmitted. If the two FSSs are exactly complementary, i.e. the slots are the same dimensions as the dipoles, Booker's extension to Babinet's Principle^[37 p.496] states the reflection coefficients for the FSS with arrays of dipoles will be exactly the same as the transmission coefficients for the FSS with arrays of slots.

Thus plot (a) in Graph 5.3 can be considered to show the reflection coefficients of the slotted FSS or the transmission coefficients for the FSS with arrays of dipoles. Similarly plot (b) shows either the transmission coefficients of the slotted FSS or the reflection coefficients for the FSS with arrays of dipoles. The accuracy of this statement can be seen at the -3dB points. Exactly half the power is transmitted at the -3dB frequencies the remaining power being reflected. The -3dB points should coincide for the two curves. Graph 4.3 shows the upper -3dB points differ by 0.5GHz. The lower -3dB points are the same for the two curves.

5.3 The RFSS as a Microwave Shutter

To establish an indication of the practical feasibility of the RFSS concept initial experiments using two slotted copper-polyester FSSs as a microwave 'shutter' were performed. i.e. The FSSs could be switched between a transparent mode where they allowed incident microwaves to be transmitted and an opaque mode where incident microwaves were reflected. These experiments were also used to confirm whether the design criteria established for dipole FSSs by computer modelling were applicable to the slotted FSS.

Two copper-polyester FSSs consisting of slotted elements with the dimensions shown in Figure 5.2 were manufactured.



$$L=3.2\text{mm}, W=0.4\text{mm}, D=6.0\text{mm}$$

Fig.5.2: The slot and element dimensions of the Copper-Polyester FSSs

These circular FSSs had a diameter of 300mm and were mounted in the plastic frame, shown in Photograph 5.1. The copper-polyester FSSs are flexible and, despite being pulled taught across the circular frames, could not be positioned to completely eliminate the gap, S , across their whole area. A vacuum pump was used to evacuate the space between the two FSSs. This had the effect of sucking the two FSSs together and minimised the gap S to the thickness of the polyester substrate. (FSS1 had its copper on the outside of the structure whereas FSS2 had its copper on the inside.) Silicon rubber was used to seal the FSSs to the frame and prevent air leaking into the vacuum. Figure 5.3 shows a side view of the two FSSs pulled tightly across the frames.

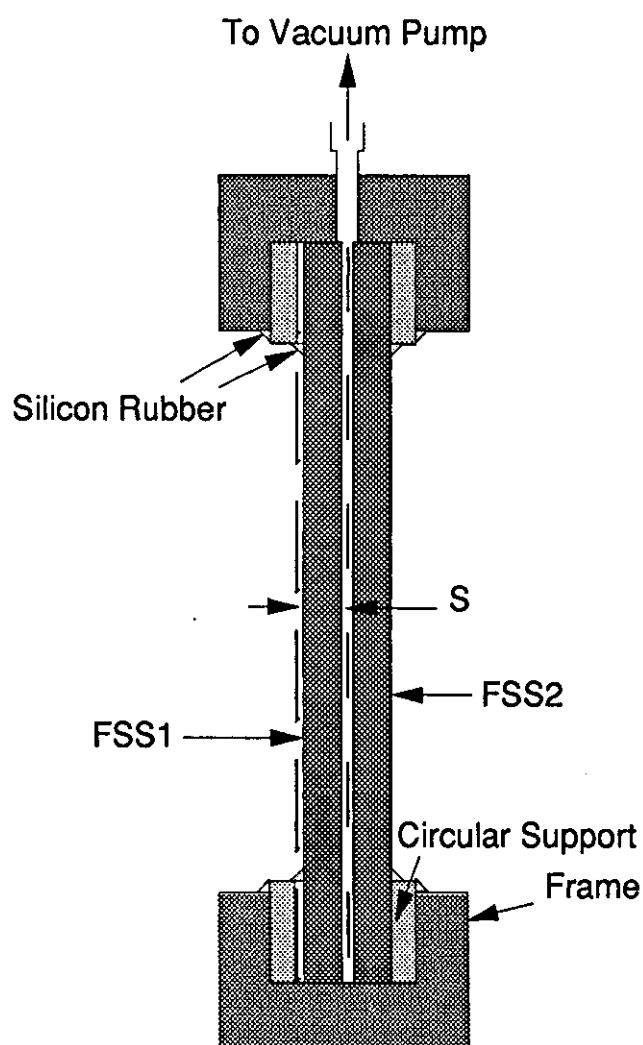
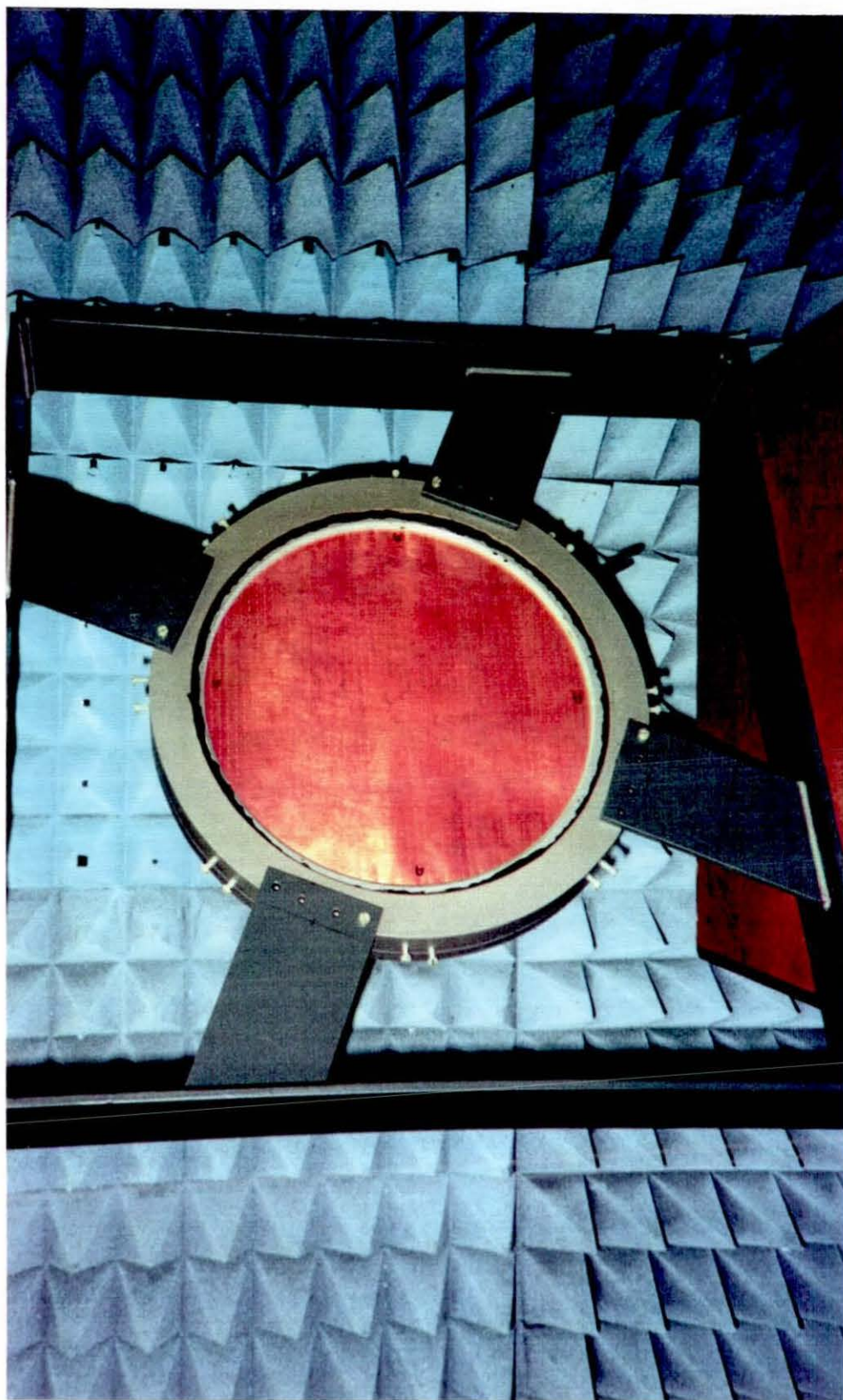


Fig.5.3: Side view of two FSSs in the 'Vacuum Frame'



Photograph 5.1: The Vacuum Frame

Figure 5.4 shows how the polyester substrates were sucked together in the slots when the vacuum was applied.

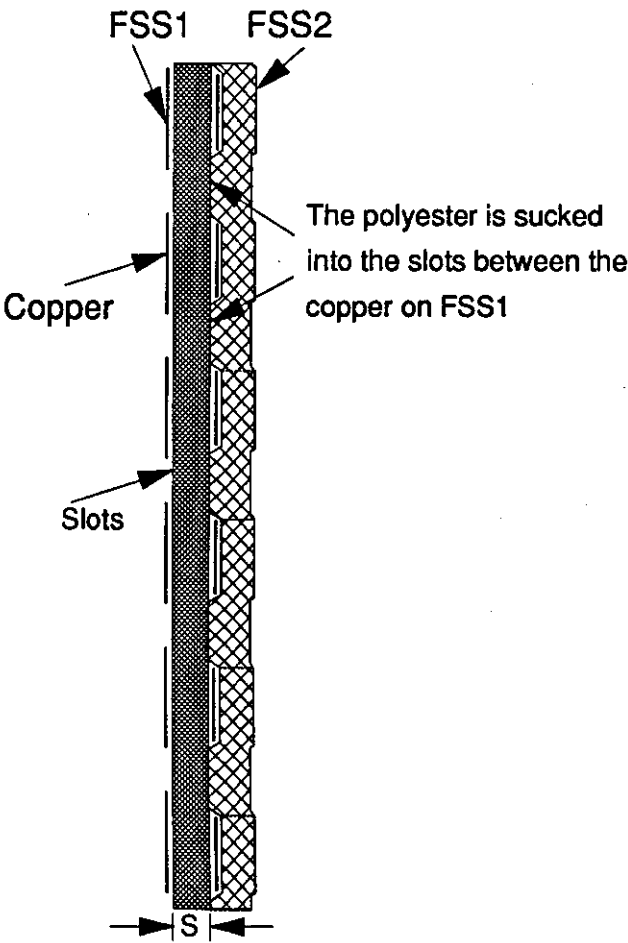


Fig.5.4: Side view Of the two FSSs with the vacuum applied

The two slotted FSSs were aligned so the 3.2mm x 0.4mm slots were positioned behind each other. The vacuum was applied sucking the two FSSs together and reducing the gap between them to 0.037mm. This structure was scanned between 25 and 40GHz. The position of the FSSs in the anechoic chamber is shown in Figure 5.6.

Graph 5.4 shows two transmission response plots, one of a modelled double layer FSS and the other of the double layer slotted FSS in the vacuum frame. The *active area* of this double layer FSS was 200mm square. Radar absorbent material (RAM) was positioned around the edges of the frame to prevent reflections and diffractions from the frame interfering with the transmission response. This RAM also obscured part of the FSSs reducing the 300mm diameter area to the 200mm square active area described above. This is shown in Figure 5.5.

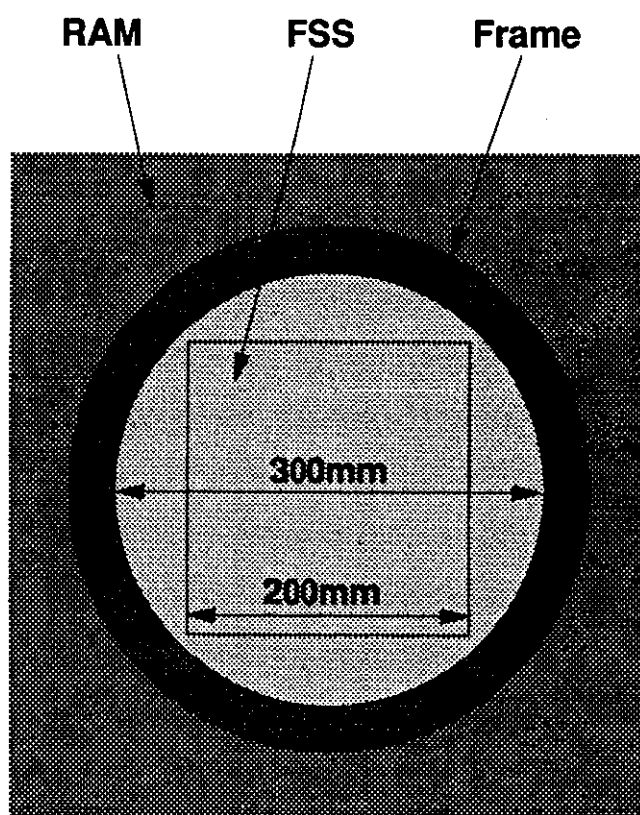
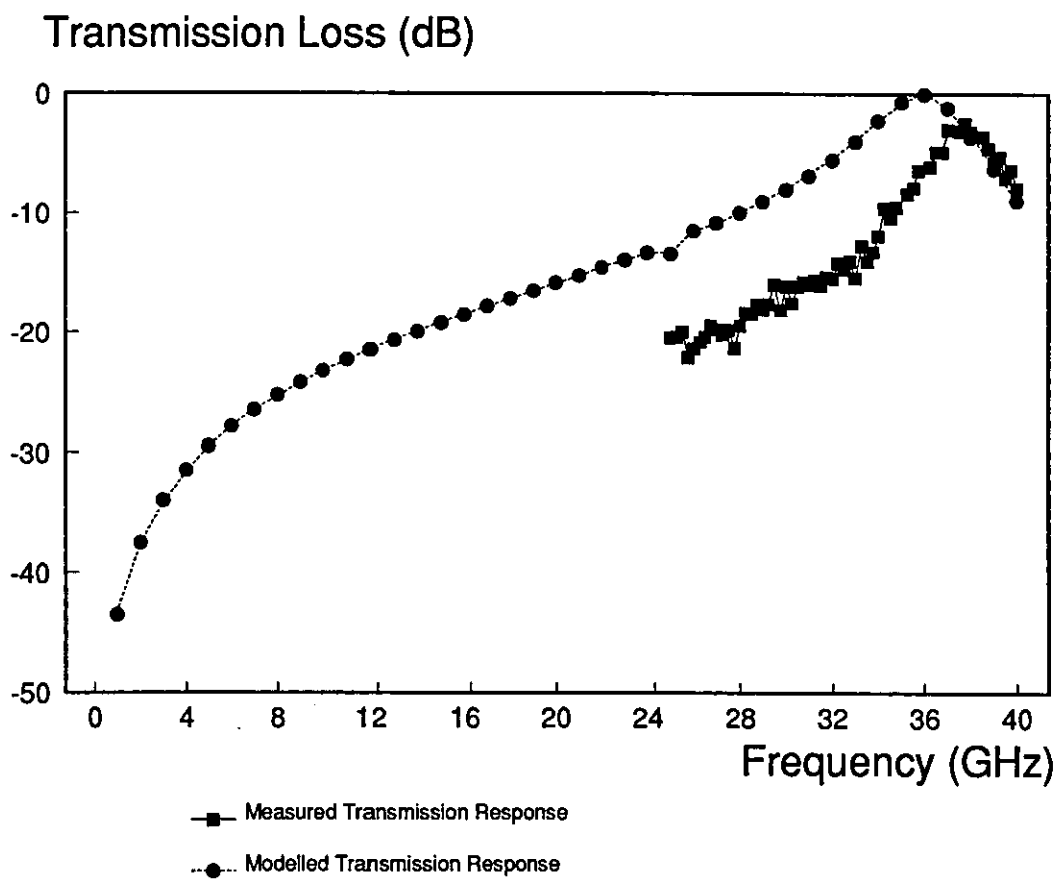


Fig. 5.5: The Active Area of the circular FSSs



Graph 5.4: The measured and modelled transmission coefficients of the double layer FSS

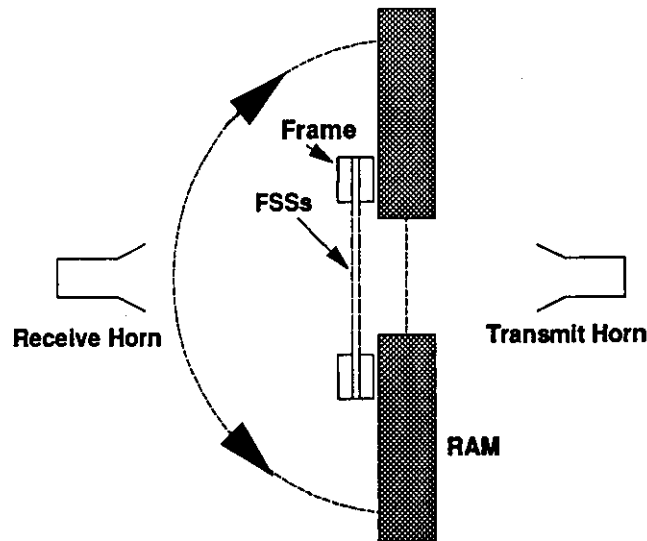


Fig.5.6: The vacuum frame in the anechoic chamber

The frequency response of the modelled FSSs plotted in Graph 5.4 was obtained using the Modal Analysis software^[21]. Section 5.2 explained this software cannot be used directly to model slotted FSSs. The frequency response plotted was produced by modelling two infinite FSSs consisting of dipoles 3.2mm long and 0.4mm wide positioned in 6.0mm square lattices, i.e. the complement of the slotted FSSs which were used in the experiments. The transmission coefficients shown in the Graph are the modelled reflection coefficients of this complementary dipole FSS.

The modelled transmission response had a resonant frequency at 36GHz, 1GHz lower than the measured transmission response. Also the measured response showed a loss of -3dB which was not seen in the model.

5.3.1 Shuttering the RFSS

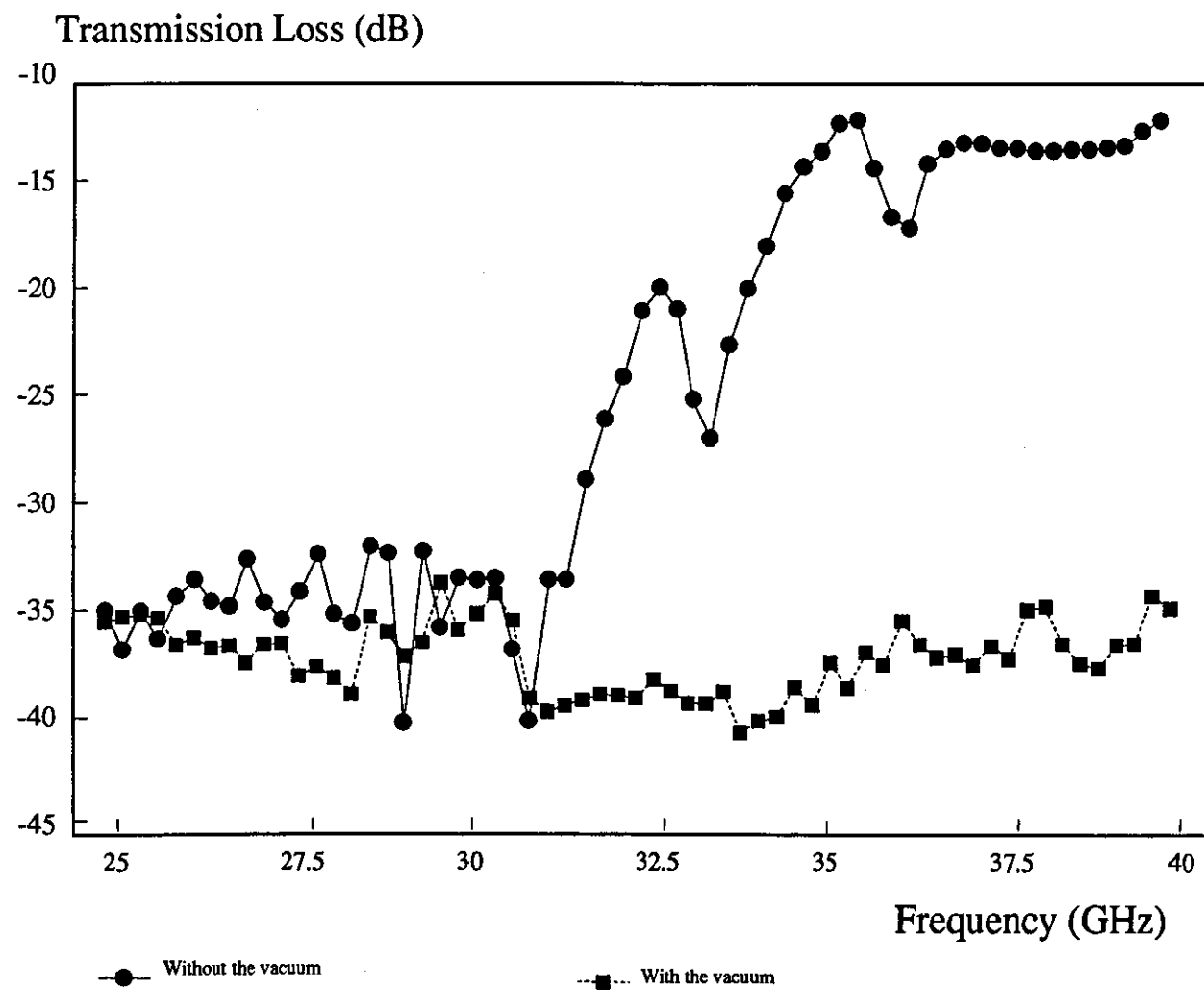
The rear FSS in the vacuum frame was now shifted by 3mm (one half of a lattice) in the direction of the width of the slots. This should prevent microwaves from passing through the FSSs at all frequencies, including the resonant frequency of 37GHz seen in Graph 5.4. i.e. Complete 'shuttering' of the FSSs should occur.

This double layer structure was now positioned in the anechoic chamber and scanned between 25 and 40GHz to establish its transmission response.

The first frequency scan, shown in Graph 5.5, was made without the vacuum applied. A second scan, also shown in this graph, was made after the space between the FSSs was evacuated. This minimised the gap, S , to just the thickness of the polyester substrate, 0.037mm.

This graph shows the importance of keeping the gap between the FSSs to a minimum in order that the RFSS can be reconfigured. When the vacuum was not applied the space between the FSSs was estimated to vary between 1mm and 3mm. Even with this small gap the Graph shows the structure allowed microwaves to leak through.

Graph 5.5: The effect of a gap S between the FSSs



5.4 The suitability of PVDF in the manufacture of FSSs

The piezoelectric material, PVDF, is obtainable in sheets 150mm square, 150mm by 300mm, or in continuous 300mm wide rolls. The thicknesses available are 9, 28, 52, and 110 μ m. Earlier experiments (Section 4.4.1) showed the 9 μ m thick material to be impractical in this application because of its flimsy nature and the possibility of pin size holes in the PVDF substrate causing an electrical breakdown between the high voltage electrodes.

A 150mm square sheet of 28 μ m thick PVDF was surrounded by RAM and positioned between the transmit and receive horns in the anechoic chamber. The 150mm square sheets were used because they were considered large enough to approximate an infinite FSS when operated at 30GHz.

This piezoelectric sheet (with un-etched copper-nickel electrodes) was scanned at frequencies from 12 to 40GHz. The received signal did not exceed -30dB at any frequency. This indicates the electrodes are good reflectors of microwaves and PVDF is a suitable material for the manufacture of an FSS. At power levels below -30dB the accuracy of the spectrum analyser was not considered reliable.

This experiment was repeated with PVDF sheets 52 μ m and 110 μ m thick, and with the sheets rotated by 90° to establish whether their polarization, which determines their direction of expansion - the 'stretch' direction, has any effect on the reflectivity. All experiments showed an insignificant amount of power, less than -30dB, was transmitted.

5.4.1 Comparisons between PVDF and Copper-Polyester FSSs

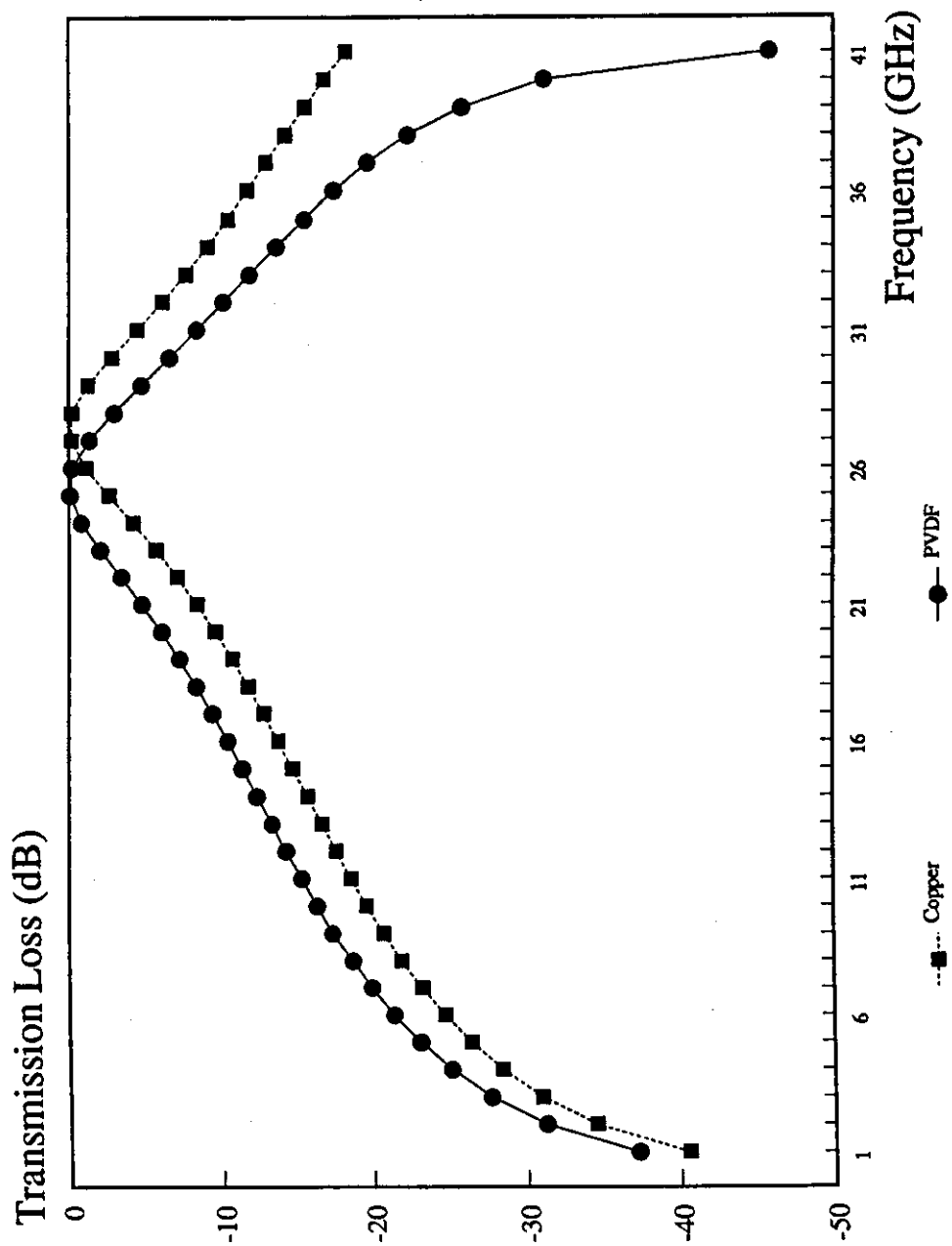
5.4.1.1 Modelled PVDF and Copper-Polyester FSSs

A double sided piezoelectric FSS consisting of arrays of dipoles, 4.8mm long and 0.4mm wide, separated by the 28 μ m thick PVDF substrate was modelled using the Modal Analysis software. The values of relative permittivity (ϵ_r) and loss tangent ($\tan\delta$) used in the model were 12.5 and 0.02 respectively. The dipoles were positioned in 6.4mm square lattices.

Babinet's Complement of this FSS is a double layer FSS with arrays of slots. The reflection coefficients produced from the model act as an approximation to the transmission coefficients of this Babinet's complementary slotted FSS. Graph 5.6 shows the frequency response of this model along with the frequency response of a modelled copper-polyester FSS with the same size dipoles and element dimensions.

The electrical parameters used to model the copper-polyester FSS were 3.25 (ϵ_r) and 0.005 ($\tan\delta$)^[34], the polyester substrate was 24 μ m thick. This FSS was modelled as a single layer FSS because the copper laminate is only on one side of the substrate. The reflection coefficients of this model, which are shown in Graph 5.6, are an approximation to the transmission coefficients of a complementary slotted FSS.

A comparison of the two FSSs (copper-polyester and PVDF) shows the PVDF FSS to have a slightly lower resonant frequency than the copper-polyester FSS; 25GHz as opposed to 27GHz.



Graph 5.6: The transmission response of modelled copper-polyester and PVDF FSSs.

5.4.1.2 Measurements of PVDF and Copper-Polyester FSSs

Two FSSs were manufactured with slots 4.8mm long and 0.4mm wide in a 6.4mm square lattice. One FSS was double sided and constructed from PVDF; the other was a single sided FSS constructed from a copper-polyester sheet. The measured transmission responses of the two FSSs are shown in Graph 5.7.

Comparing the transmission responses of the copper-polyester and the PVDF FSS shown in Graph 5.7 shows the PVDF FSS to have a much larger bandwidth and a greater loss at resonance.

At the resonant frequency of 21.3GHz the PVDF FSS (PFSS) exhibited a loss of -9.87dB. The -3dB bandwidth extended from 13.6 to 27.8GHz, i.e. a bandwidth of 14.2GHz. The copper-polyester FSS had a resonant frequency at 26GHz where the transmission loss was -0.2dB, and a bandwidth of only 5.1GHz, between 23.5GHz and 28.6GHz. The larger bandwidth, or 'flattening', of the transmission response of the PFSS could be due to it being a double layer structure^[1 p.603].

Ideally the conductive areas of an FSS have infinite conductivity. This was assumed for the copper-polyester FSSs and enabled Booker's extension to Babinet's Principle to be proved in Section 5.2.1. In this proof the lower -3dB frequencies of two complementary copper-polyester FSSs coincided and the upper -3dB frequencies differed by only 0.5GHz. Booker's extension of Babinet's Principle states the -3dB frequencies of complementary structures will coincide if no power is dissipated in the structures^[37 p.496]. The copper metallisation did not have any significant electrical resistance, hence no power was dissipated in the FSS.

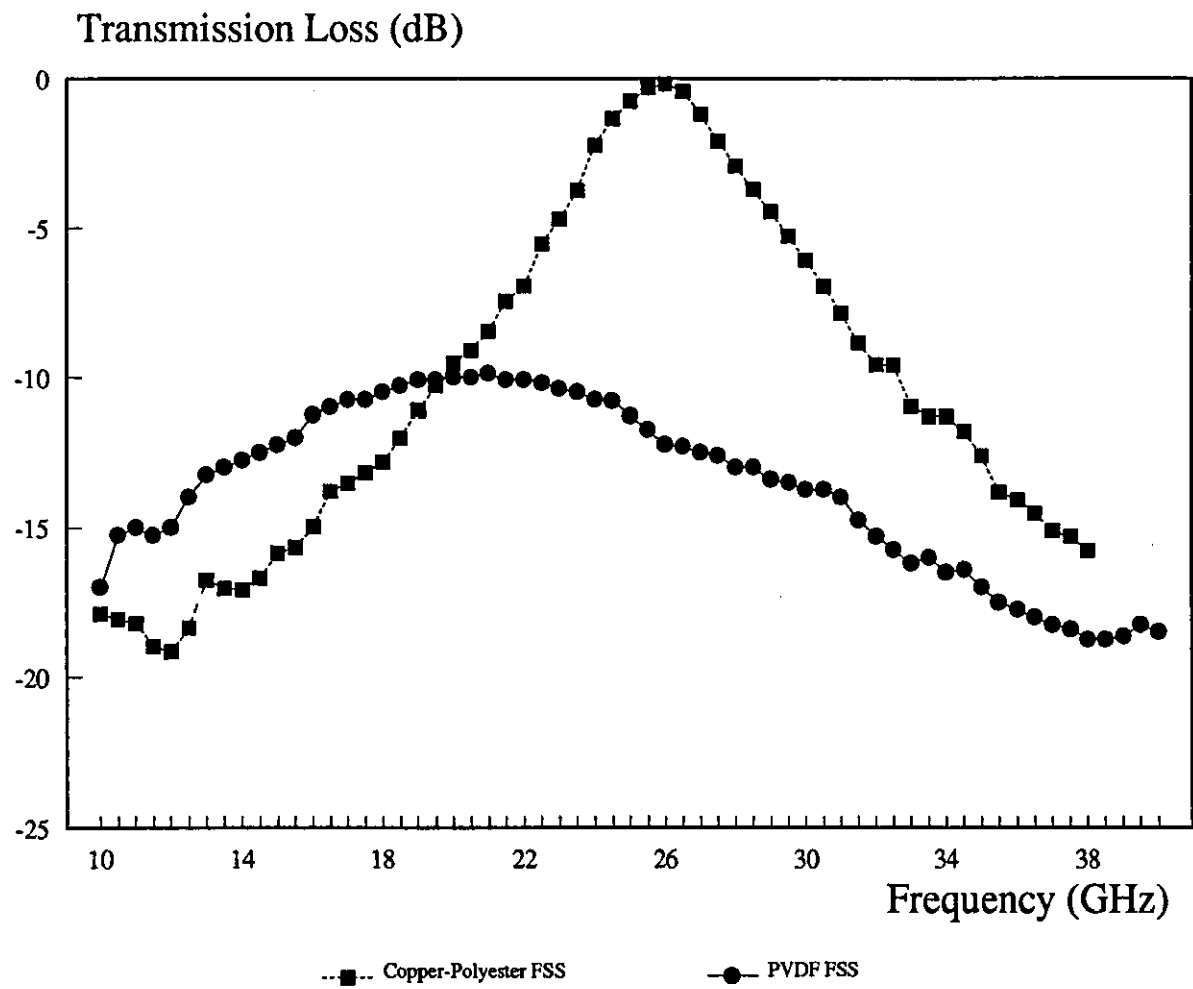
The electrodes on the PFSSs were a lot thinner than the metallisation on the copper-polyester FSSs (0.055µm as opposed to 24µm). The thinner metallisation has a larger resistance because of its smaller cross sectional area.

(The resistance is given by the equation:

$$\text{Resistance (R)} = \frac{\text{Resistivity } (\rho) \times \text{Length (l)}}{\text{Cross Sectional Area (CSA)}}$$

and the cross sectional area is the product of the thickness and width of the metallisation)

This metallisation resistance could dissipate some power and account for the 10dB loss at resonance of the PFSS which was scanned to produce Graph 5.7.



Graph 5.7: The measured transmission responses of Copper-Polyester and PVDF FSSs.

5.4.1.3 Comparisons between modelled and measured results

The transmission responses plotted in Graph 5.6 were produced from models of FSSs with the same element dimensions as those scanned to produce the curves of Graph 5.7.

The modelled and measured transmission response plots of the copper-polyester FSSs compare well. A modelled resonance at 27GHz compares with a measured resonance at 26GHz; the bandwidths of the modelled and measured transmission responses were 5GHz and 5.1GHz respectively. Both the copper-polyester FSS transmission response plots (modelled and measured) have an insignificant loss at resonance.

The modelled PVDF FSS had a resonant frequency of 25GHz and a loss at resonance of -0.1dB, this compares with the measured resonance and loss of 21.3GHz and -9.87dB respectively. The inaccuracies between modelled and measured frequency responses could be caused by the values of ϵ_r and $\tan\delta$ used in the model not being realistic of the actual properties of the PVDF substrate. The values used were quoted for a frequency of 10kHz (see Table 3.3), the FSS was operated at between 10 and 40GHz.

5.5 Methods of mounting the PFSSs

The experiments with two closely coupled FSSs in the vacuum frame (Section 5.3.1) confirmed the conclusion drawn from the initial modelling of the FSSs that the space, S , between the FSSs should be minimised. The experiments also demonstrated the importance of keeping the FSSs flat. It was estimated the slack between the two FSSs, when the vacuum was not applied, could cause the gap S to vary by up to 3mm. The graph of S and DS against resonant frequency (Graph 5.1) indicates this would have a significant effect on the resonant frequency.

5.5.1 The Sliding Frame

The copper-polyester FSSs were pulled taut across the circular frames in Section 5.3 and secured using double sided tape around their circumferences. This is not possible with the PVDF FSSs because they do not remain a constant size. When the PVDF is energised it would expand and become slack.

By keeping the PVDF tight, in the direction of piezoelectric expansion, the buckling, which occurs when the material becomes slack as described above and shown in Figure 5.7, can be avoided.

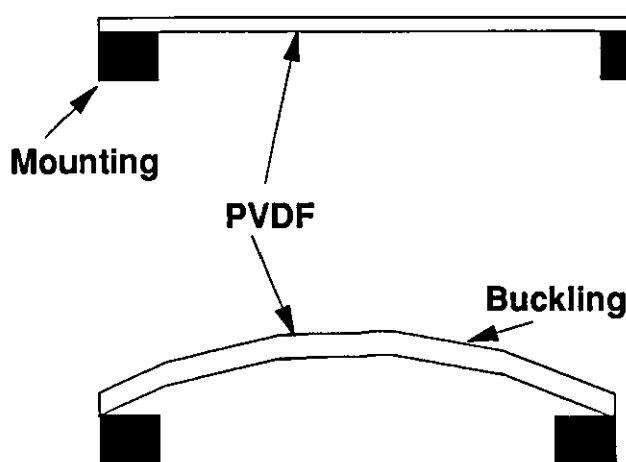


Fig.5.7: A cross sectional view showing the effect of securing the PVDF FSS in the circular frame

The small piezoelectric extension produced in the PFSS must be concentrated along its length, not in the direction shown in Figure 5.7. A frame was developed to hold the PVDF flat and taut so any piezoelectric extension would be in the length direction. Figure 5.8 shows this *Sliding Frame*.

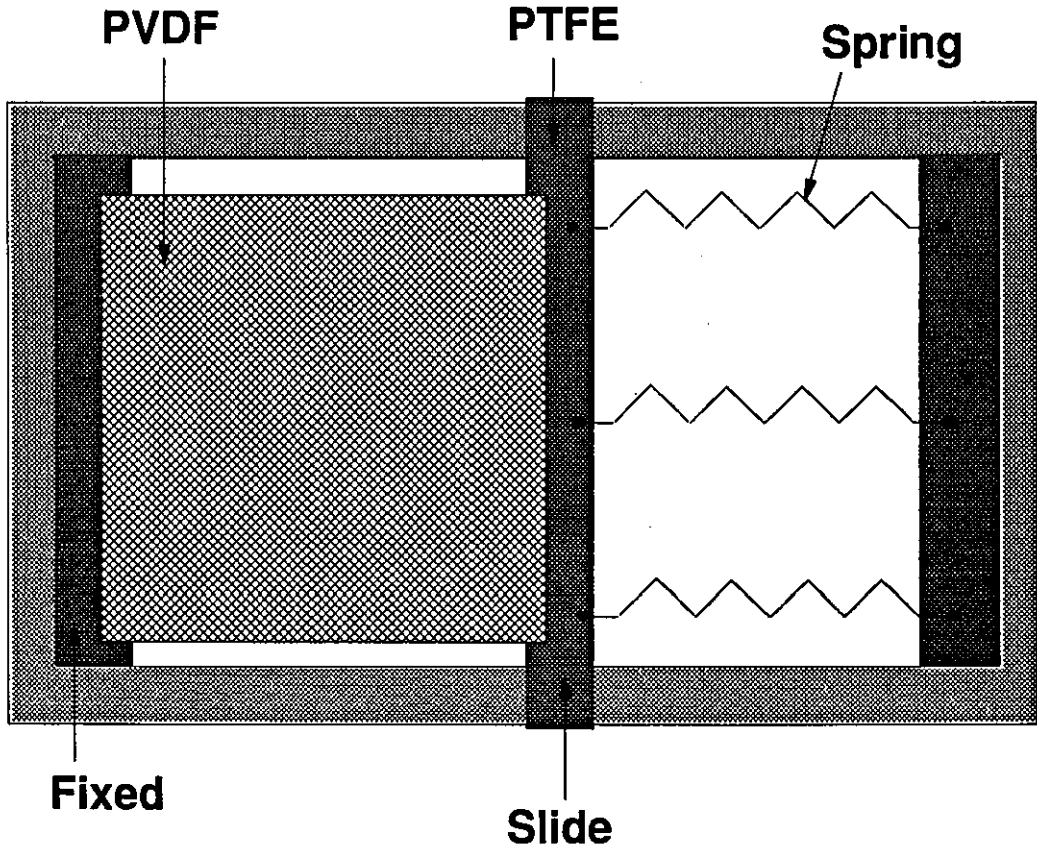


Fig. 5.8: A PVDF FSS pulled tight in the Sliding Frame

Elastic springs in the frame pull the PTFE slide towards the right. The PVDF FSS is attached to this slide and held taut and flat in the frame. The slide was made from PTFE because this material has a low coefficient of friction allowing the PFSS to expand and contract freely whilst remaining taut in the frame.

Implementing the Sliding Frame in practice was difficult. The small extension produced when the PVDF was energised was not uniform across its width. This could be due to the poling axis of the PVDF not being the same as the axial length of the sheet of PVDF.

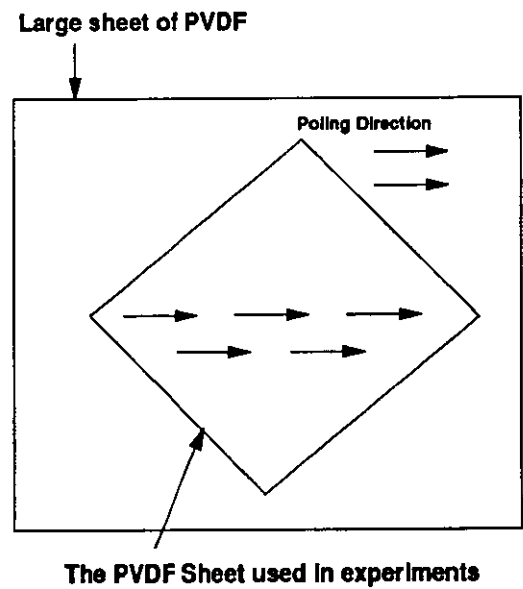


Fig. 5.9: Poling and axial directions of PVDF

Alternatively the irregular expansion of the PVDF could be due to an unequal charge distribution across its surface. This is unlikely however because of the low resistivity of the copper-nickel electrodes on the PVDF sheet. (The resistivities of copper and nickel are $5.76 \times 10^{-7} \text{ S/m}$ and $1.45 \times 10^{-7} \text{ S/m}$ respectively^[34].)

If the PVDF does not expand linearly across its width the slide in the frame will not hold the PFSS taut across its entire surface. Areas of the PFSS will become slack and buckle. This buckling means the distance between the two PFSSs, S , when they are both installed in the frame will not be constant. The buckling is shown in Figure 5.10.

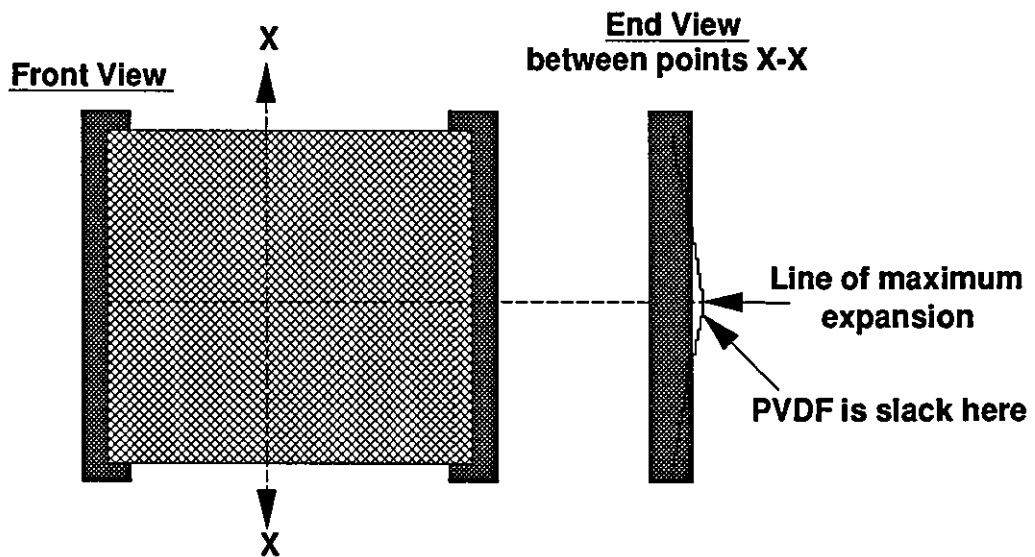


Fig. 5.10: Buckling of an irregularly extended PVDF FSS

A further cause of the PVDF buckling was inaccurate alignment on the slide and clamp. The PTFE slide and clamp have to be secured parallel to each other on the PVDF sheet. Additional problems included adjusting the elastic tensioners so they pulled equally and securing the PVDF to the slide and frame using the conductive epoxy adhesive. A conductive epoxy was necessary to enable the electrical connections to be made to the PVDF. These complications instigated research into alternative methods of securing the two PFSSs flat and at a minimum separation S .

5.5.2 A PTFE Frame

The low frictional resistance of PTFE can be utilised to 'sandwich' the PVDF FSSs flat. Two PFSSs could be positioned between two sheets of 1.6mm thick PTFE. These PTFE sheets would clamp the PFSSs flat but still allow them to extend. The electrical properties of PTFE are^[39]:

ϵ_r	2.0
$\tan\delta$	0.0001-0.0002

5.5.2.1 The transmission response of PTFE

The transmission response of two 1.6mm thick PTFE sheets, with no gap, S , separating them and no FSSs sandwiched between them were computer modelled. The model produced the plot shown in Graph 5.8.

This graph shows there was no loss at 33GHz, this corresponds to the frequency at which the total thickness of the material is one half of the wavelength of the microwaves in the material (λ_m).

$$\text{viz. } c = f \lambda$$

(eqn.5.1)

where c is the speed of light ($3 \times 10^8 \text{m/s}$),

f is the frequency,

λ is the wavelength in *free space*;

thus:

$$\begin{aligned} \lambda &= \frac{c}{f} \\ &= \frac{3 \times 10^8}{33 \times 10^9} \\ &= 9.09 \text{mm} \end{aligned}$$

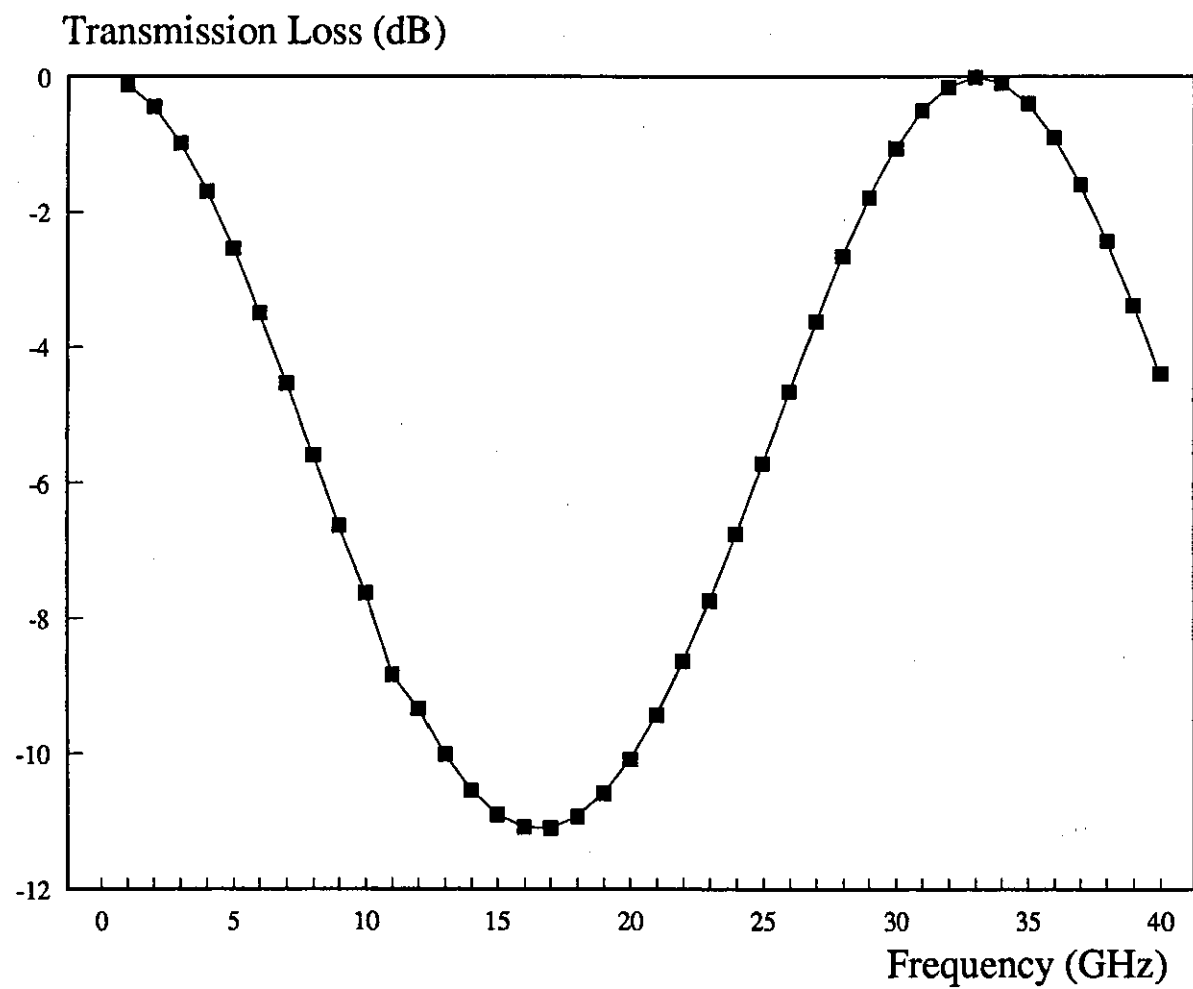
$$\text{Since } \lambda_m = \frac{\lambda}{\sqrt{\epsilon_r}}$$

(eqn. 5.2)

where λ_m is the wavelength in the PTFE material,
 λ is the wavelength in free space,
 ϵ_r is the relative permittivity of the PTFE;

$$\begin{aligned} \lambda_m &= \frac{9.09 \times 10^3}{\sqrt{2}} \\ &= 6.42 \text{ mm} \end{aligned}$$

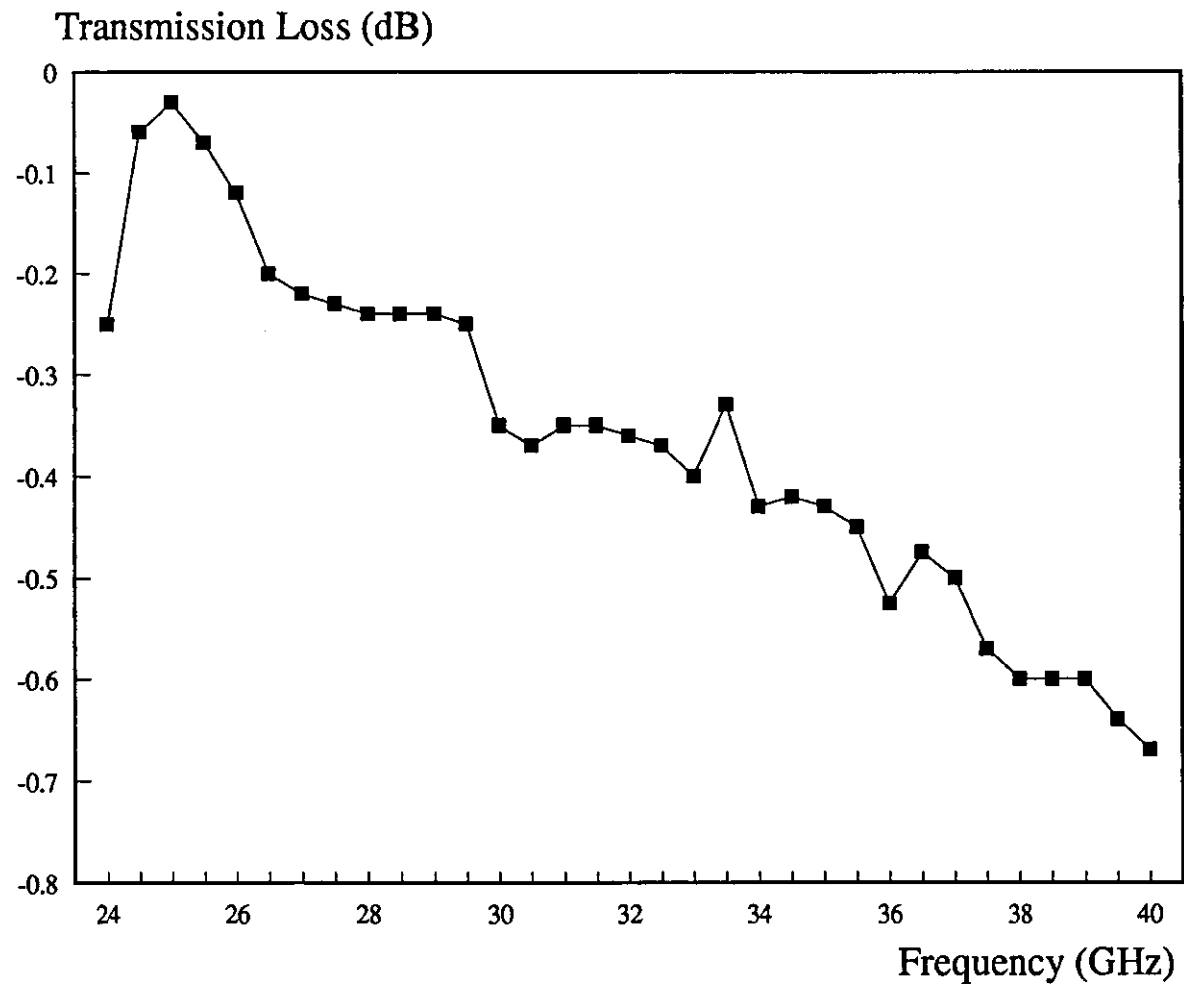
The wavelength of the microwaves in the PTFE material (6.42mm) is (approximately) twice the total thickness of the two 1.6mm thick PTFE sheets being modelled.



Graph 5.8: The modelled transmission response of two 1.6mm thick PTFE sheets

Two sheets of PTFE were scanned in the anechoic chamber at frequencies between 24GHz and 40GHz. The scan, plotted in Graph 5.9, shows a loss of 0.4dB at 33GHz, the frequency at which the computer model predicted no loss. The minimum transmission loss occurred at 25GHz. Using equations 5.1 and 5.2 the thickness of the material required to produce no loss at 25GHz was calculated as 4.24mm, i.e two PTFE sheets 2.12mm thick. A micrometer was used to measure the PTFE and it was found to be 1.6mm (± 0.01 mm) thick.

The difference between the modelled and measured transmission response could be due to the two PTFE sheets not being clamped completely together. This would allow a small gap to exist between them. Another possible explanation for the discrepancy between the measured and modelled transmission responses could be the value of ϵ_r used in the calculations being incorrect.



Graph 5.9: The measured transmission response of two 1.6mm thick PTFE sheets

5.6 The effect of the FSS geometry on the resonant frequency

An alternative to maximising the resonant frequency shift of an FSS by maximising the displacement, DS , is to design an FSS with a resonant frequency which is highly dependent on the positions of the two component FSSs. i.e. A small displacement, DS , causes a large resonant frequency shift.

Other shaped FSS elements were considered for manufacturing the RFSS. These included FSSs with tripoles^[18], square loops^[16,17], and square patches^[11]. The RFSS requires elements with a shape which only has to be altered by a small amount to produce a significant change in the resonant frequency.

5.6.1 Square Loops

Square loops resonate at a frequency which can be calculated using the equation:

$$f = \frac{l \times c}{4}$$

where: f is the resonant frequency,

l is the length of the perimeter of the loop,

and c is the speed of light (3×10^8 m/s).

Slots, and dipoles, resonate at a frequency calculated from the equation:

$$f = \frac{l \times c}{2}$$

Slotted FSSs only allow transmission of microwaves which are polarised with their magnetic field (the H-Field) along the length of the slot, and their electric field (the E-Field) across the width of the slot. This is shown in Figure 5.11.

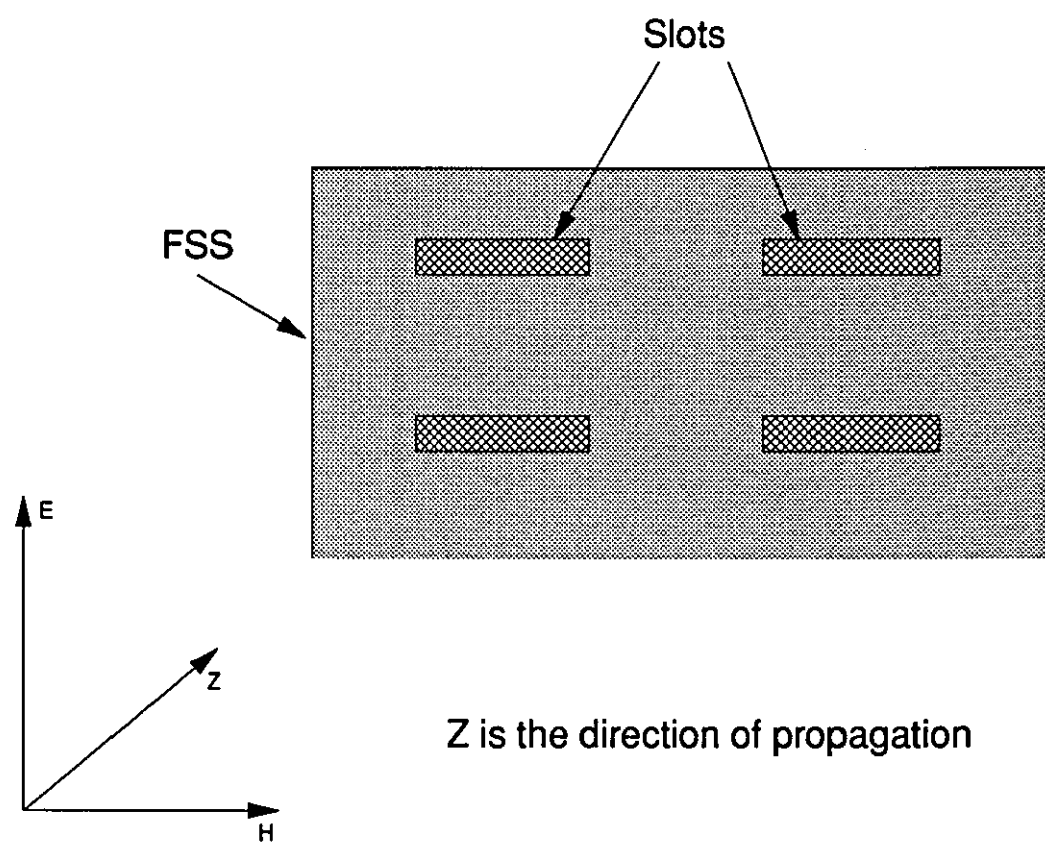


Fig.5.11: Polarisation of the microwaves relative to an FSS slot

Conversely FSSs consisting of arrays of dipoles only allow transmission of microwaves with a polarisation such that the E-Field is directed along the length of the dipoles and the H-Field is directed across the width of the dipoles. This is shown in Figure 5.12.

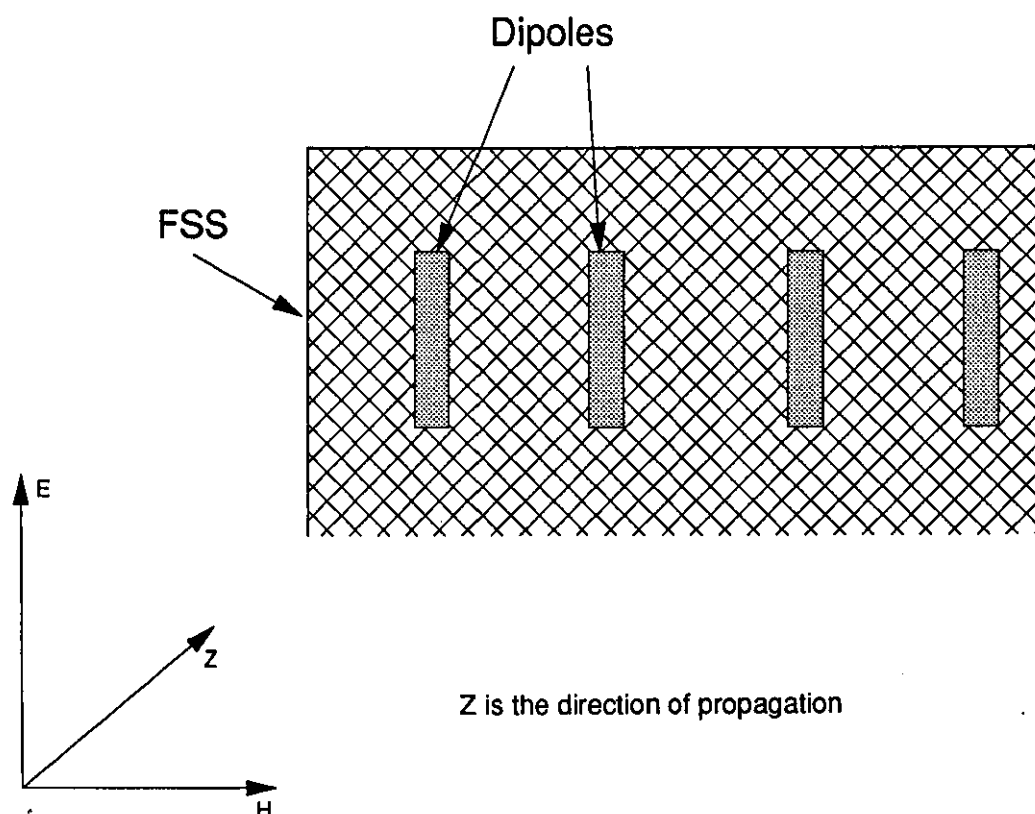


Fig.5.12: Polarisation of the microwaves relative to an FSS dipole

If the E-Field is in the direction of the length of the slots on an FSS it will not allow transmission and will, theoretically, reflect all of the microwave power.

An FSS with arrays of slotted square loops is transparent to microwaves which have an H-Field parallel with any of its sides. Thus if the FSS is transparent in one orientation it will also be transparent if the polarisation of the incident microwaves are rotated by 90° . This is shown in Figure 5.13.

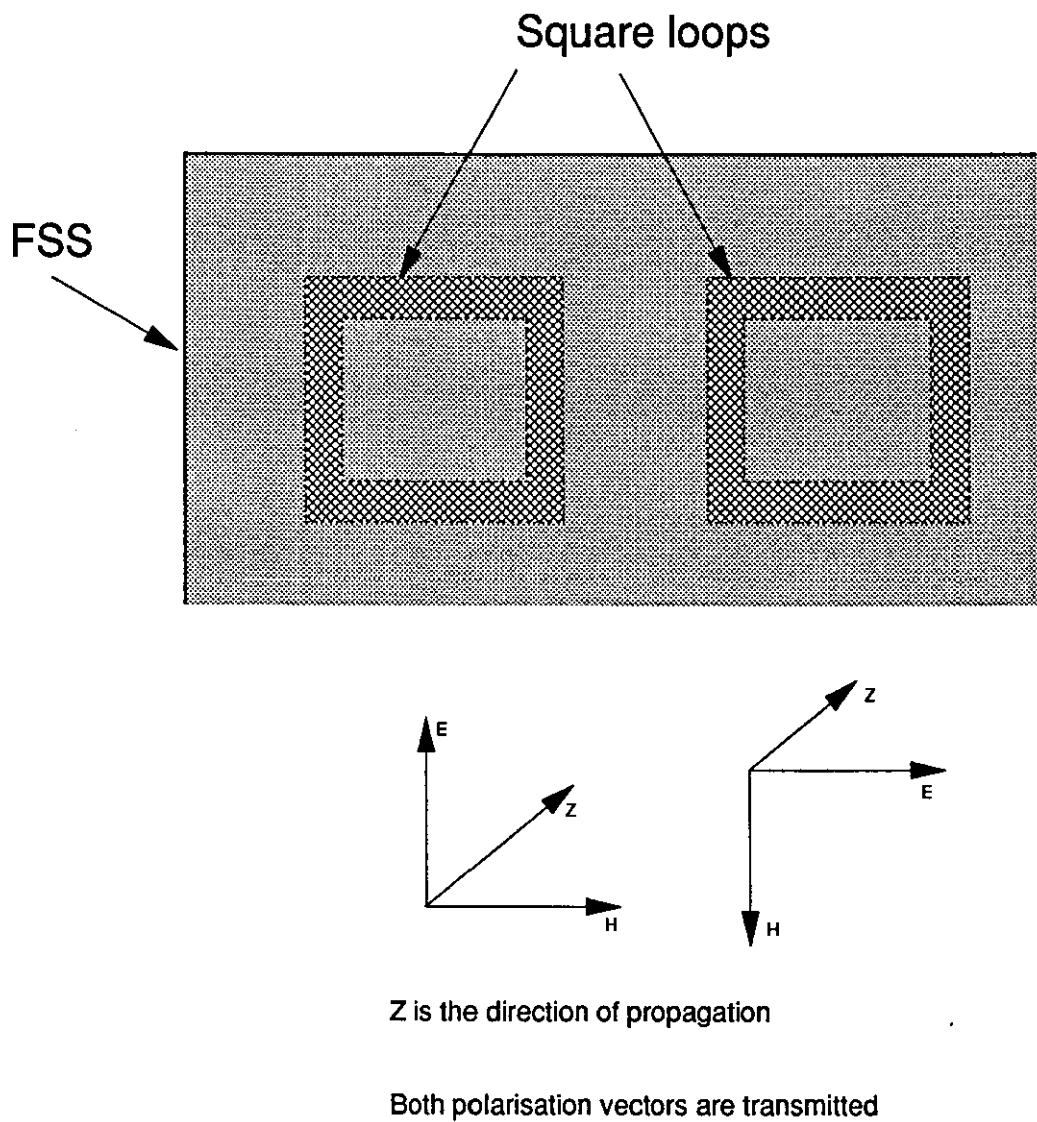
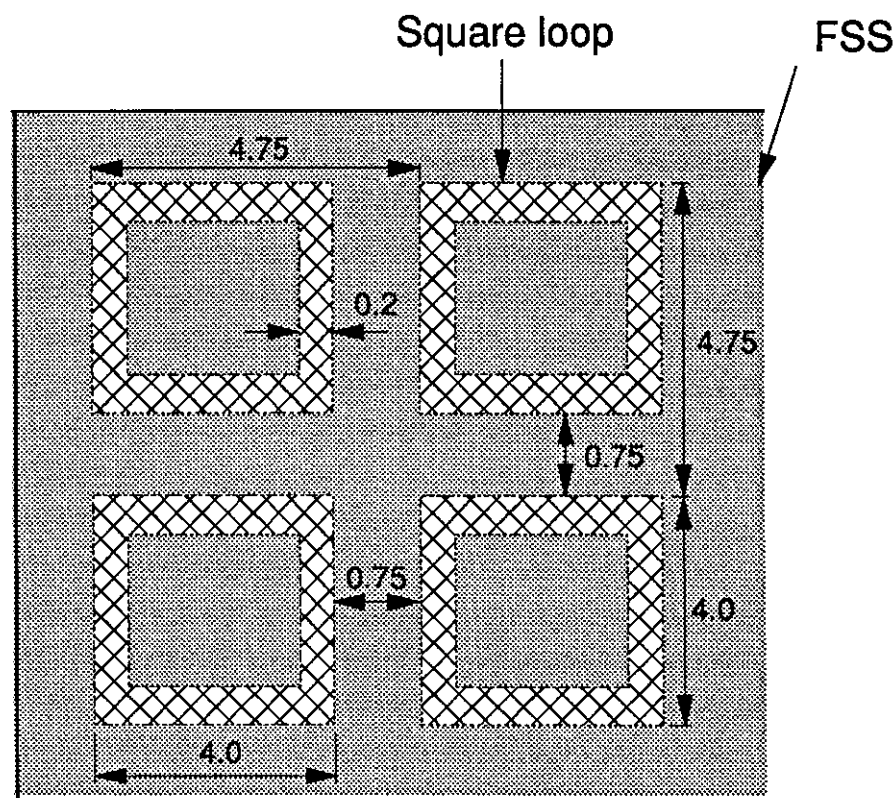


Fig.5.13: Polarisation vectors rotated by 90° are still transmitted by an FSS with square loops

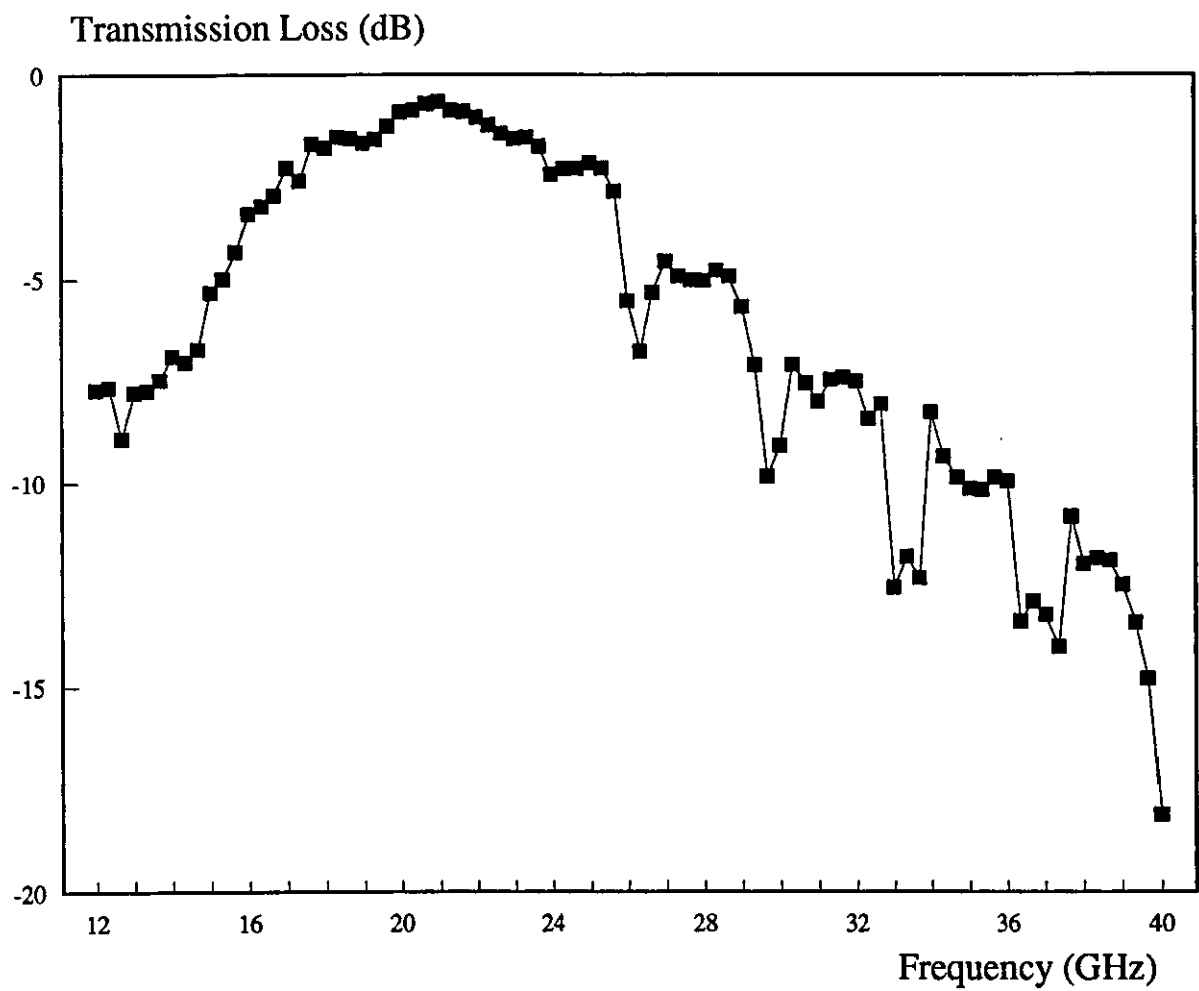
5.6.1.1 The Frequency Response of Square Loops

An FSS consisting of slotted square loop elements with the dimensions shown in Figure 5.14 was manufactured from a copper-polyester sheet. A frequency scan of this FSS in the anechoic chamber showed a resonance at 20.7GHz where there was a loss of -0.75dB. This frequency scan is shown in Graph 5.10. The FSS was modelled using the modal methods software, the transmission response produced by the model is plotted in Graph 5.11. The resonant frequency in the model was 22GHz.

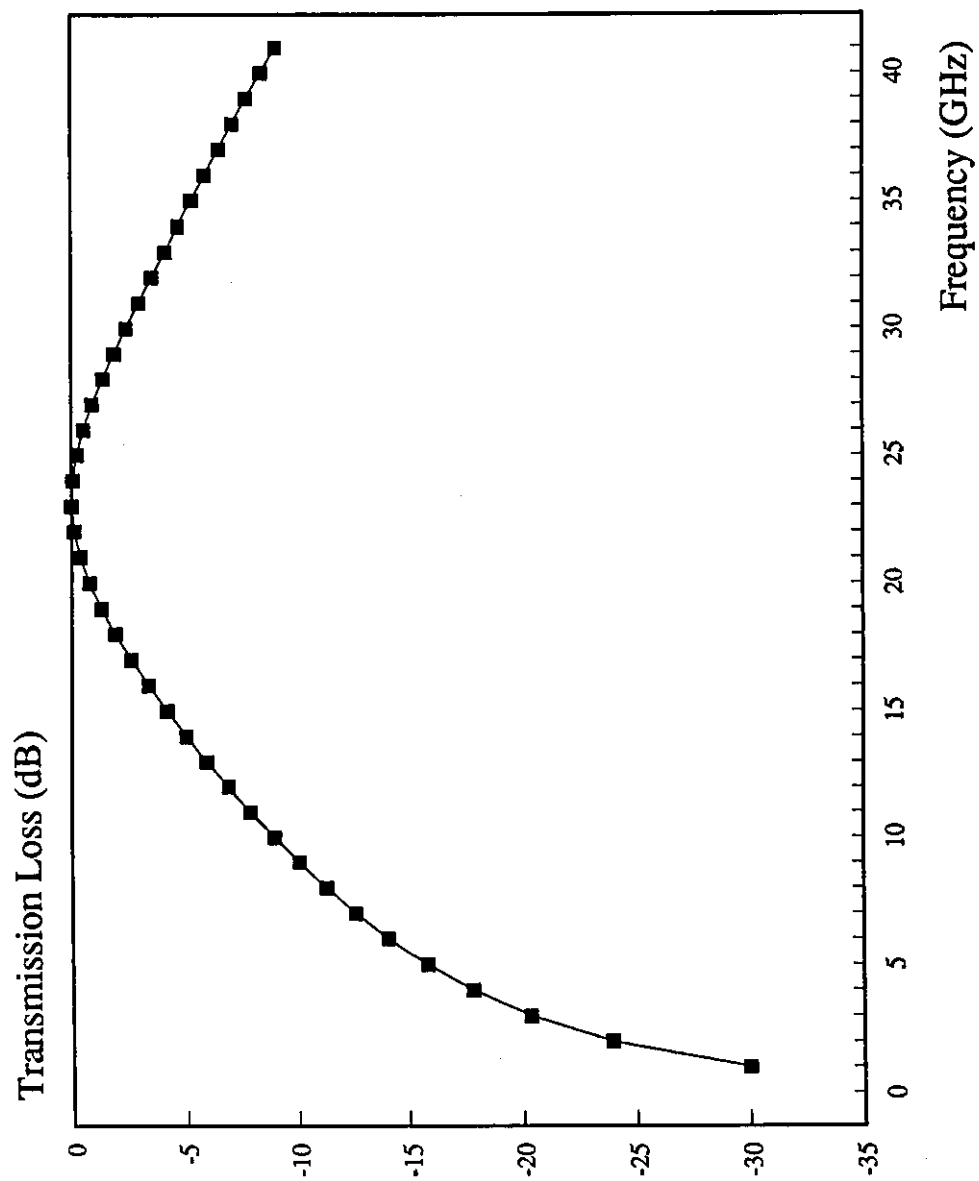


All dimensions are in millimetres

Fig.5.14: A section of the slotted square loop FSS



Graph 5.10: The measured transmission response of the slotted square loop FSS

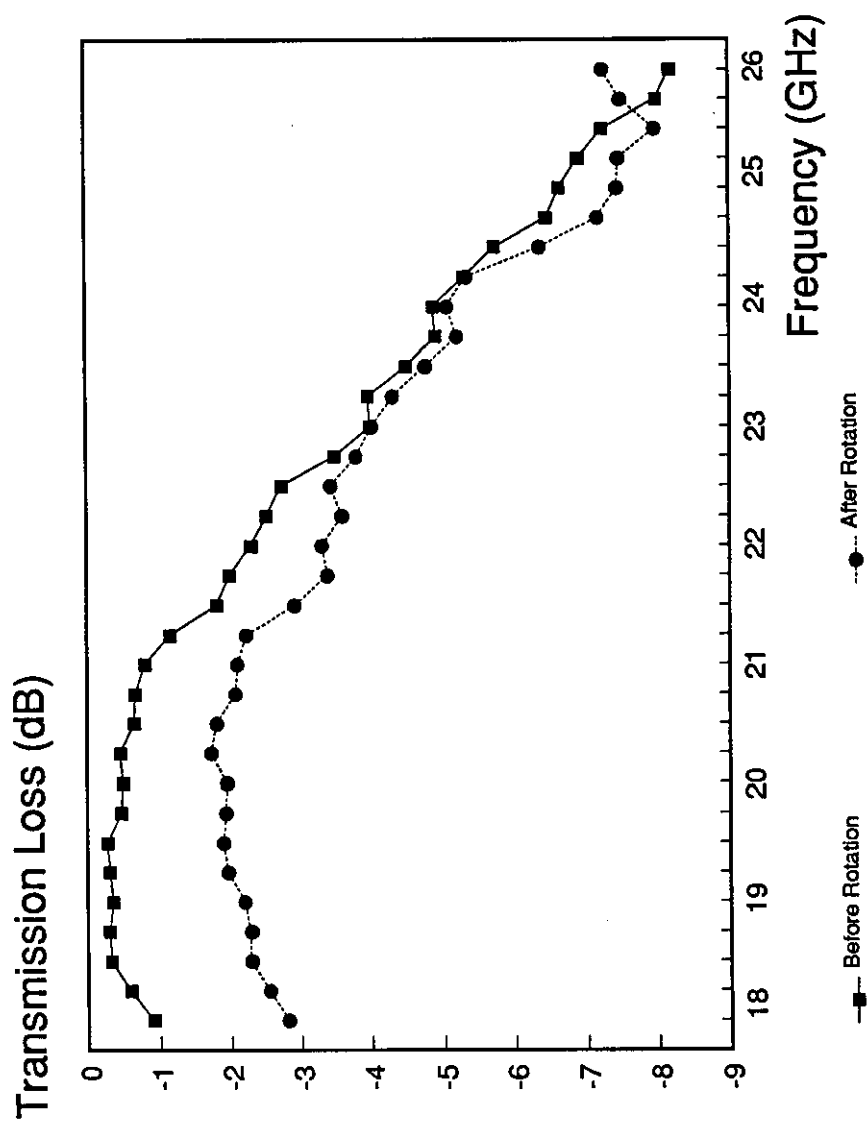


Graph 5.11: The modelled transmission response of the slotted square loop FSS

A second FSS with identical dimensions was now positioned behind the first in the vacuum frame. The two FSSs were aligned and the vacuum pump was used to evacuate the space between them and minimise the gap, S . It was difficult to achieve ideal alignment because the square loops had to be positioned accurately in both the horizontal and the vertical directions. Misalignment of 0.2mm in either direction meant two sides of the loop would not be visible. The straight slotted FSSs (Section 5.3) only had to be aligned accurately in the vertical direction, misalignment in the horizontal direction only resulted in a slightly shorter RFSS slot length. (A reduction in slot length of 0.2mm produces an insignificant change in resonant frequency at the frequencies being considered, this can be seen from Graph 5.1.)

The FSSs were aligned as accurately as possible and scanned in the K and Q frequency bands. The vacuum frame was then rotated by 90° and a further two frequency scans in the K and Q bands were made. The resonant frequency should be the same before and after the FSSs are rotated if the square loops on the two FSSs are correctly aligned.

Careful realignment of the FSSs was made until frequency scans made before and after the RFSS structure was rotated by 90° produced resonances at about the same frequency. Graph 5.12 shows the K-band transmission responses. There is less than 0.2GHz difference in the resonant frequency of these two plots.



Graph 5.12: Frequency scans of the double layer slotted square loop RFSS before and after a 90° rotation with the loops on the two FSSs aligned

The front FSS was now shifted by 0.2mm in the vertical direction. This leaves the RFSS with the 3.8mm long horizontal slots shown in Figure 5.15. A frequency scan of this structure in the anechoic chamber showed the 23.3GHz resonant frequency had a transmission loss of -3dB. This is plotted in Graph 5.13.

The RFSS was rotated by 90° and scanned again. The FSSs now blocked the transmission of microwaves producing a loss of at least -17.5dB at all frequencies in the K-band. This frequency scan is also plotted in Graph 5.13. The 'blocking' effect of the RFSS is due to the H-Field being across the width of the slots.

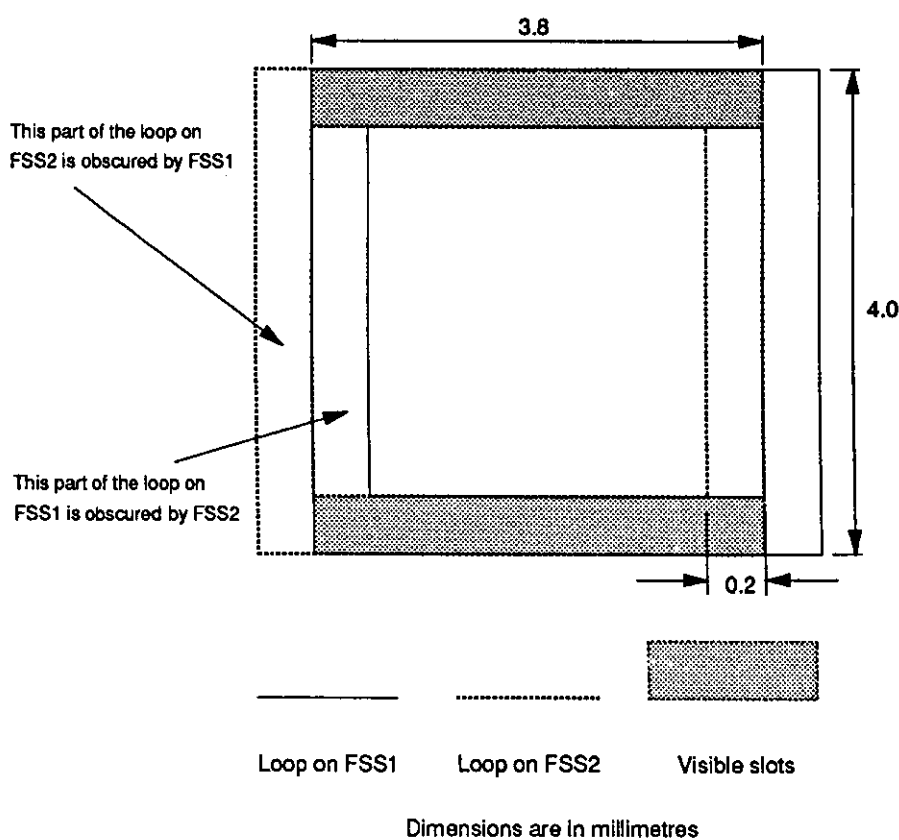
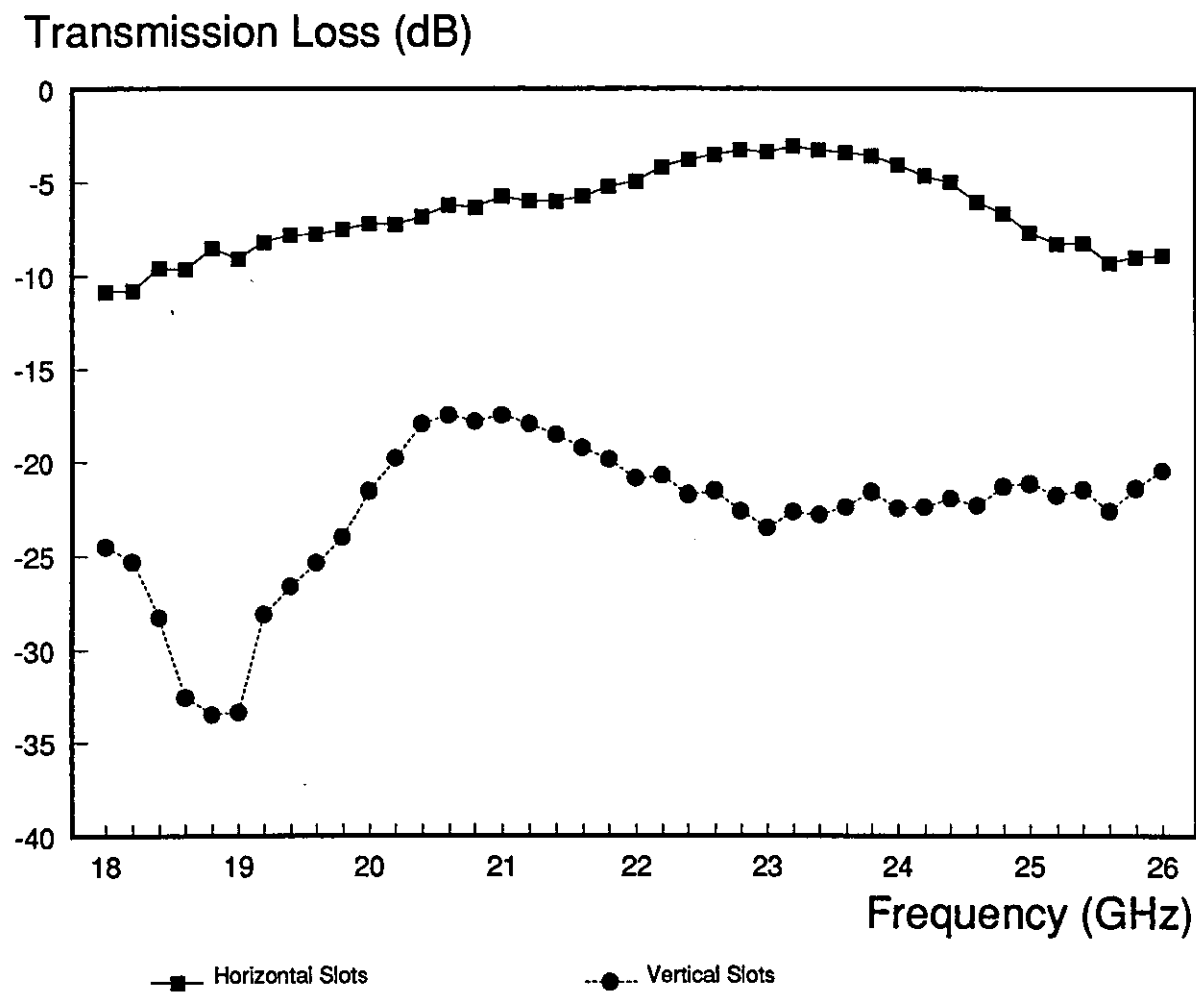


Fig.5.15: The 'visible' slots after a shift of 0.2mm

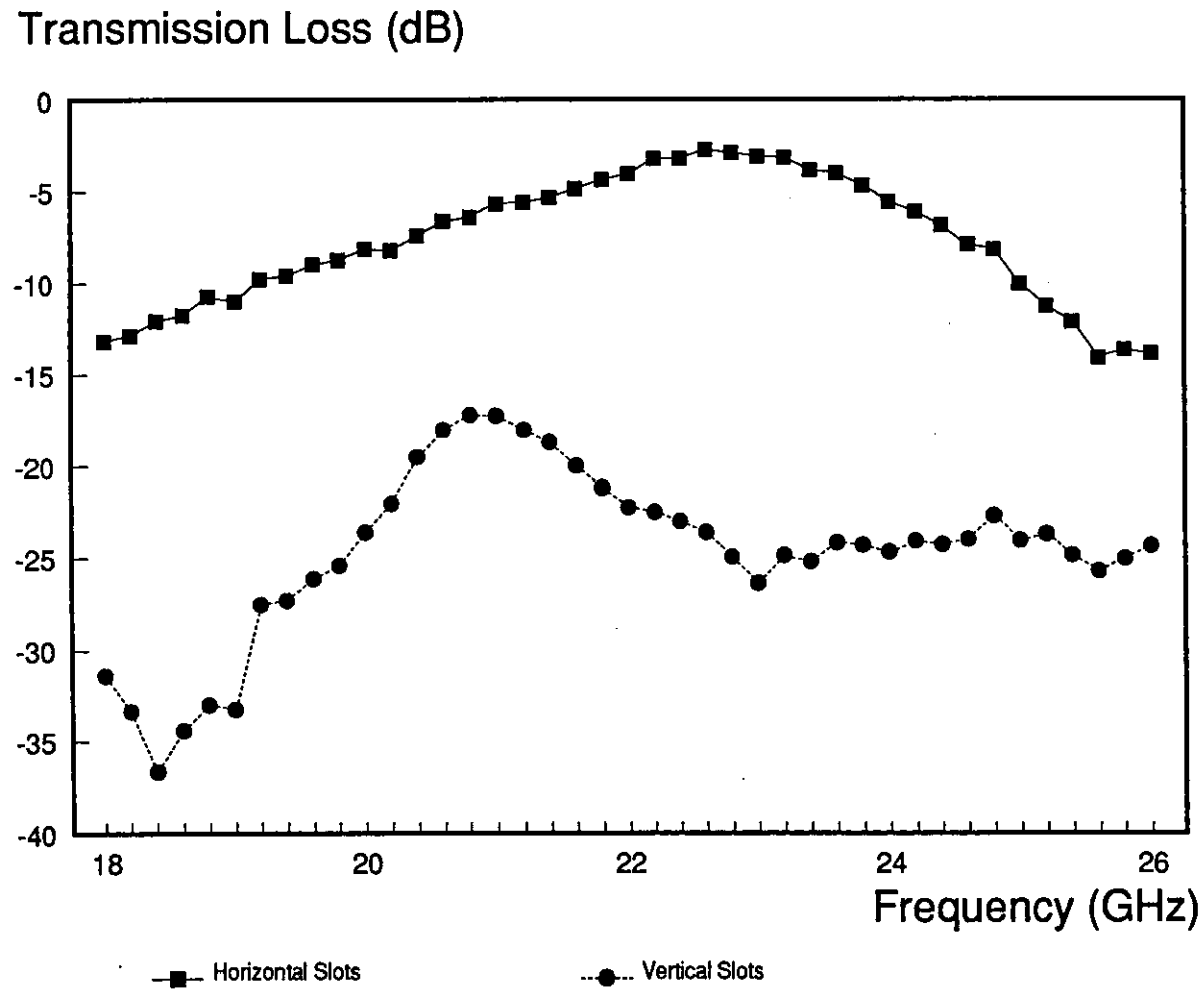


Graph 5.13: Transmission and blocking effect of the RFSS after shifting the front FSS by 0.2mm

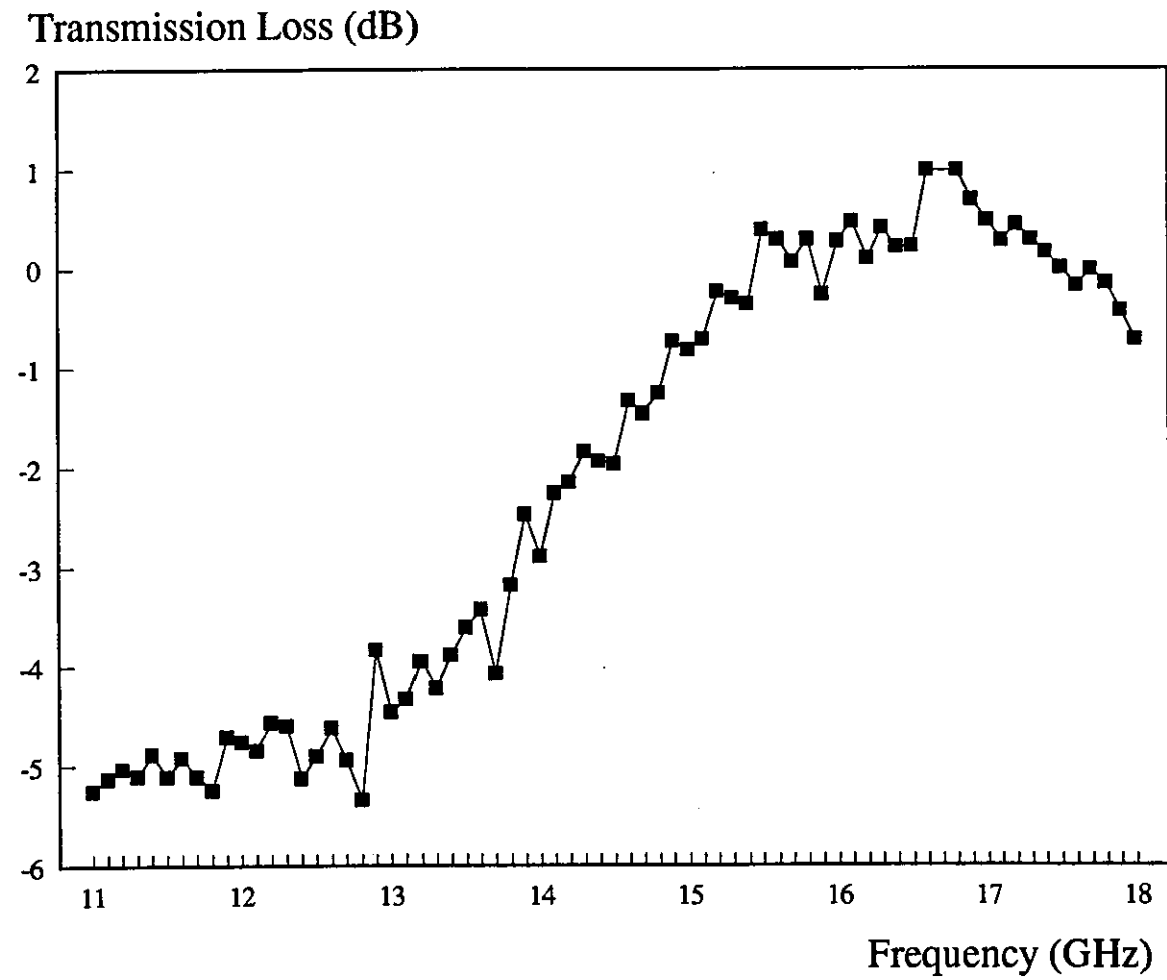
The front FSS was now shifted by a further 0.5mm leaving 3.3mm of slot length visible. The RFSS was rotated back 90° so the H-Field was along the length of these slots. A frequency scan of this structure showed the resonant frequency had reduced to 22.8GHz where the loss was -2.6dB. This is plotted in Graph 5.14. Rotating the structure by 90° and scanning again showed the shuttering effect as seen before in Graph 5.13. The minimum loss had now reduced to -17.0dB. This transmission response is also plotted in Graph 5.14.

5.6.1.2 The effect of the Perspex Frame on the Square Loops

The effect of sandwiching the FSSs between perspex sheets was now investigated. A single square loop FSS was sandwiched between two 6mm thick sheets of perspex. A frequency scan in the J -band showed the FSS-perspex structure had a resonance at 16.8GHz where there was a gain in transmitted power of +0.91dB. This frequency scan is plotted in Graph 5.15. The gain is probably caused by a combination of the resonant frequency of the FSS and standing waves in the perspex sheets. Positioning the FSS between the perspex has shifted the resonant frequency by 3.9GHz from 20.7GHz (Graph 5.10).



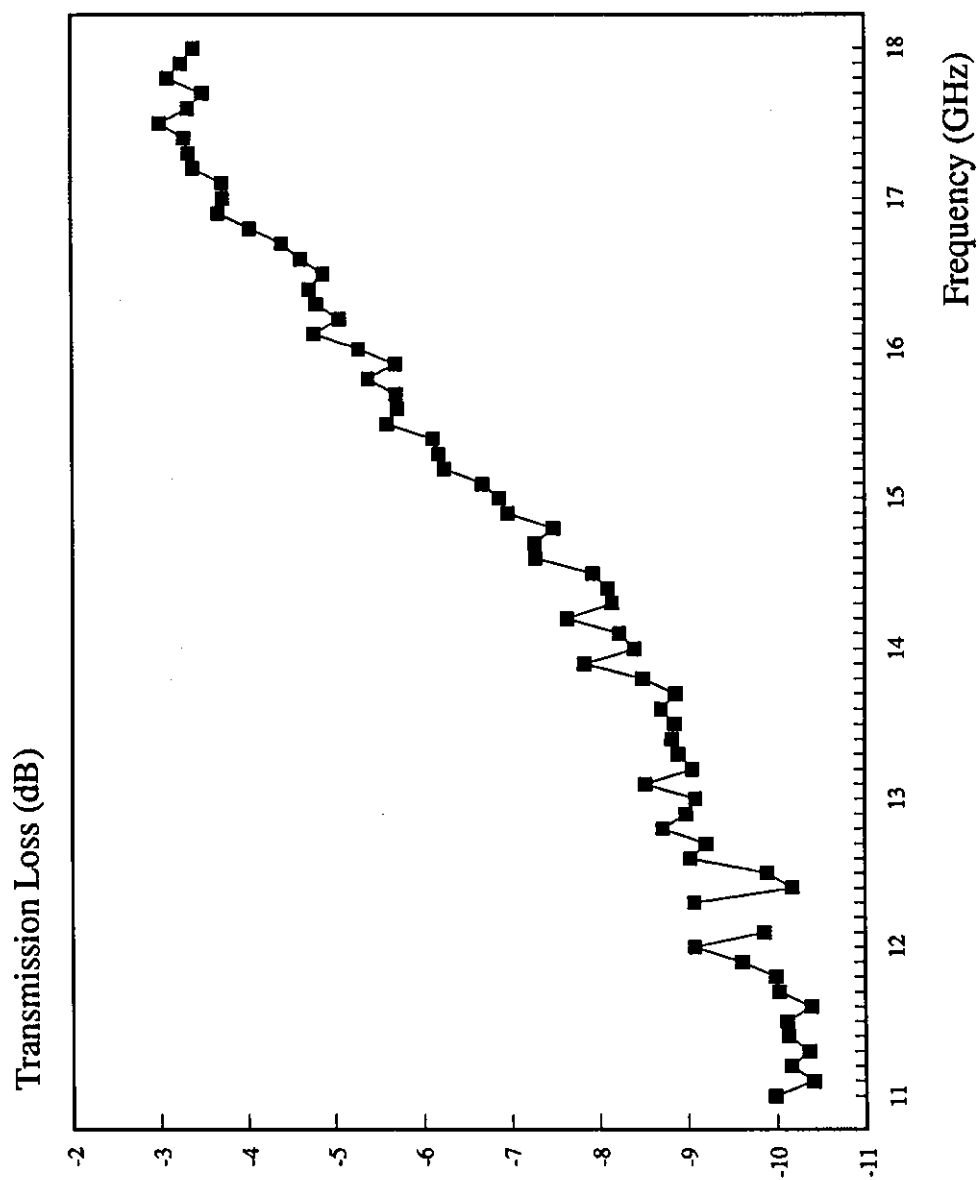
Graph 5.14: Transmission and blocking effect of the RFSS with 3.3mm long slots



Graph 5.15: Transmission response of the FSS between perspex sheets

A second, identical, FSS was now positioned behind the first. Both FSSs were sandwiched between the perspex sheets. The loops on the two FSSs were aligned and the structure was scanned in the anechoic chamber (Graph 5.16). The resonant frequency did not alter significantly but the transmitted power at the resonant frequency (17.5GHz) was reduced to -3dB.

The vacuum frame incorporated fine adjustment screws which allowed the FSSs to be moved once they were aligned. The perspex frame did not incorporate this facility and so the effect of accurately moving the FSSs to align only parts of the square loops was not possible.



Graph 5.16: Transmission response of two FSSs between the perspex sheets

5.6.2 Different Length Slots

The 'shuttering' effect produced by the slotted FSSs in the vacuum frame can be adapted to produce a frequency shift as opposed to a total frequency block.

Two copper-polyester FSSs were manufactured. Both FSSs had alternate columns of lattices containing long and short slots. The long slots had a length of 4.9mm and the short slots a length of 3.3mm. On the first FSS the shorter slots were positioned centrally between the longer slots. On the second FSS the shorter slots were positioned 0.2mm (the width of a slot) offset from the centre. This can be seen clearly in Figure 5.16.

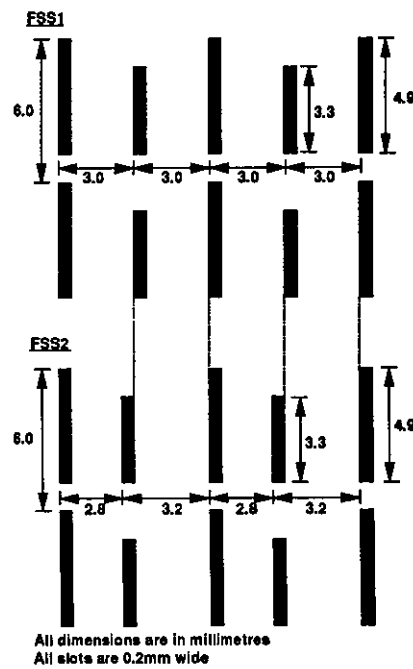


Fig. 5.16: The slot positions on two double slotted FSSs

When the FSSs were laid on top of each other the long slots could be aligned whilst the shorter slots were blocked. A movement of 0.2mm in the direction of the width of the slots allowed the shorter slots to be aligned whilst the longer slots were blocked. This is shown in Figure 5.17.

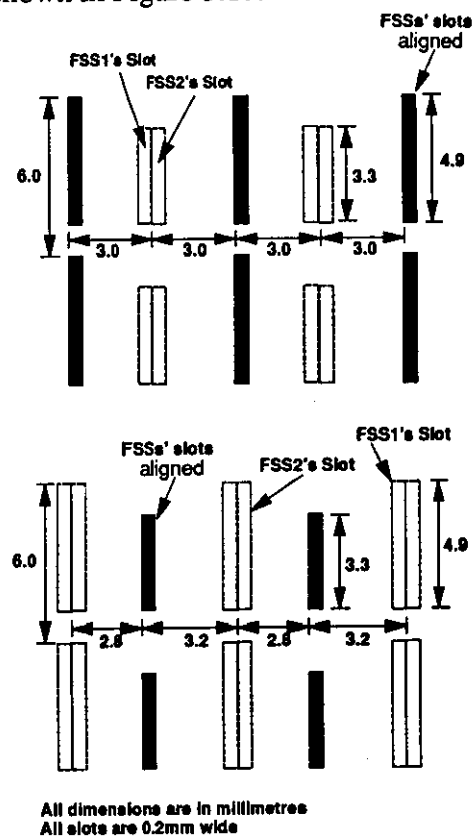


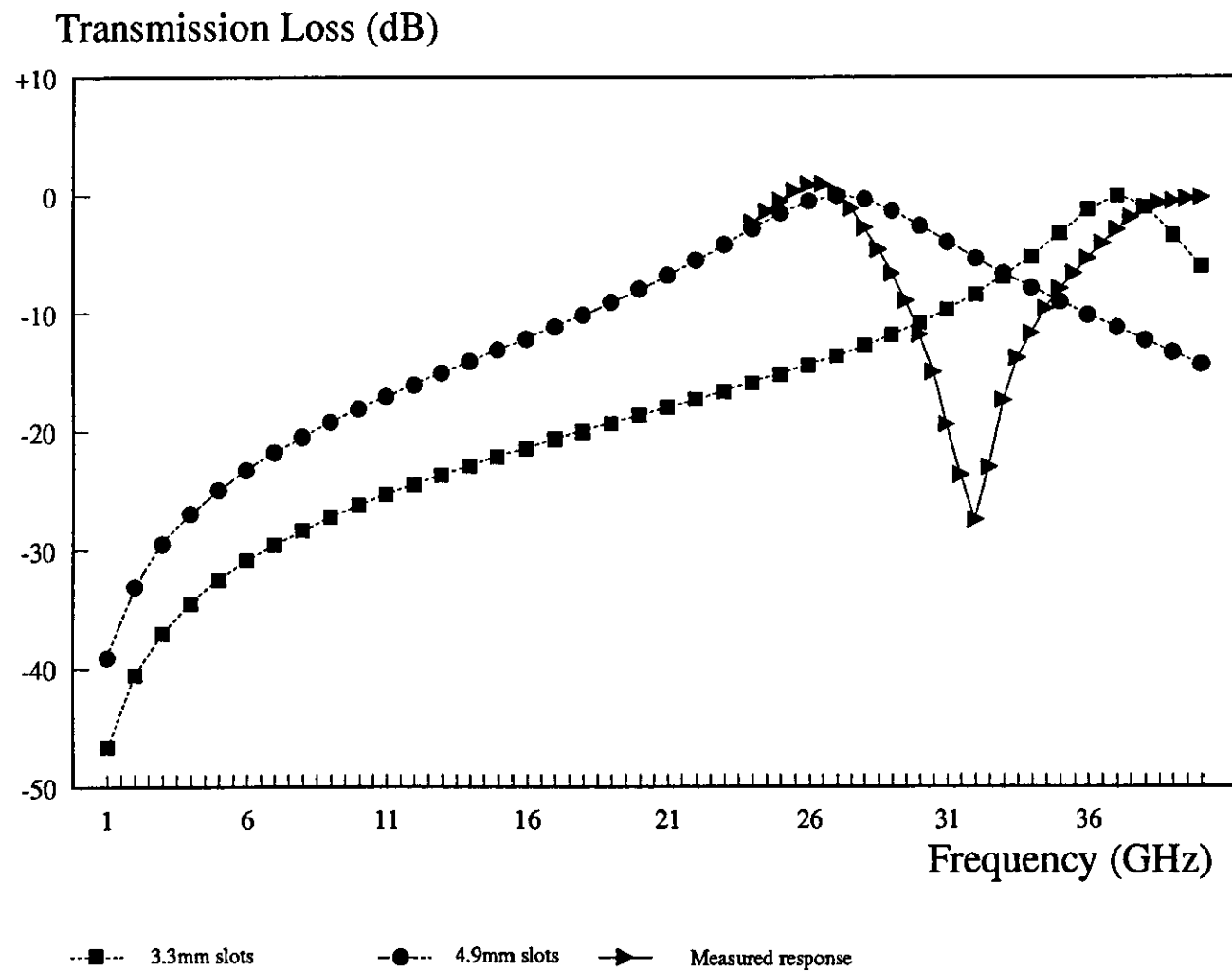
Fig. 5.17: The alignment of the two double slotted FSSs

The frequency responses of the two FSSs were measured in the anechoic chamber. The incident angle of the FSS in this experiment was adjusted to 5° to avoid standing waves between the transmit and receive horns and the FSSs distorting the shape of the transmission response.

Both FSSs had the same transmission response, this is plotted in Graph 5.17. This indicates the position of the shorter slots, relative to the longer slots, has no significant effect on the frequency response. Both FSSs had nulls at 31.8GHz and two peaks at 26.3GHz and approximately 40GHz. The upper frequency peak could not be measured accurately because it was beyond the upper cut-off frequency of the Q-band waveguide and the spectrum analyser.

FSSs consisting of slots of more than one length cannot be modelled. However models of two FSSs, one with 4.9mm long slots and one with 3.3mm long slots were modelled. The transmission responses produced from these models had resonant peaks at 27GHz (4.9mm long slots) and 37GHz (3.3mm long slots). These transmission responses are plotted along with the measured transmission response of the double slotted FSS in Graph 5.17.

The higher frequency peak in the measured transmission response is attributed to the 3.3mm slot. This peak appears 3GHz higher than in the modelled frequency response. This discrepancy could be caused by the longer slot on the FSS interacting with the shorter slot. The computer model did not take into account any interaction between the long and short slots because they were modelled separately.



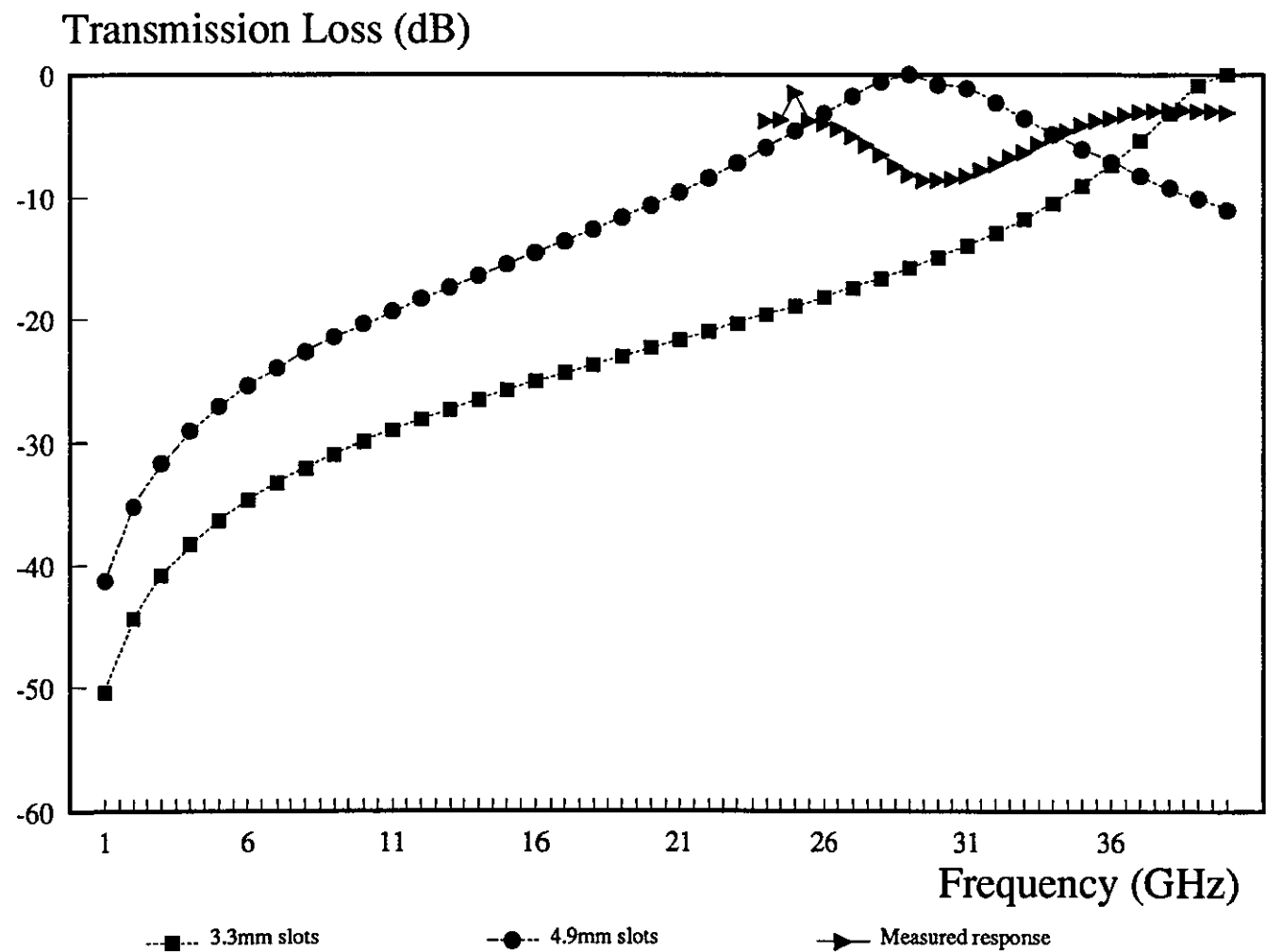
Graph 5.17: The transmission response of the double slotted FSSs

5.7 PVDF FSSs

FSSs with the same dimensions as the copper-polyester FSSs shown in Figure 5.16 were manufactured from PVDF. These FSSs were scanned between 24 and 40GHz. Graph 5.18 shows this frequency response which includes a null at 30GHz and two peaks at 25GHz and approximately 40GHz. This frequency response is similar to the frequency response of the copper-polyester FSS (Graph 5.17) although the null is not as deep (-8.9dB in the PVDF FSS transmission response compared with -30.0dB in the copper-polyester FSS). Also the bandwidth of the two peaks is broader - a characteristic of PVDF FSSs noted in previous experiments (Section 5.4.1.2). The Graph also shows the modelled transmission responses of PFSSs with slots 4.9mm and 3.3mm long.

A D.C. voltage of 840V was applied to the copper-nickel electrodes on the PFSS to produce an electric field in the 28 μ m thick substrate of 30V/ μ m. This had no effect on the transmission response of the PFSS.

Graph 5.18: The transmission response of the PVDF double slotted FSSs



5.7.1 PFSSs in the PTFE frame

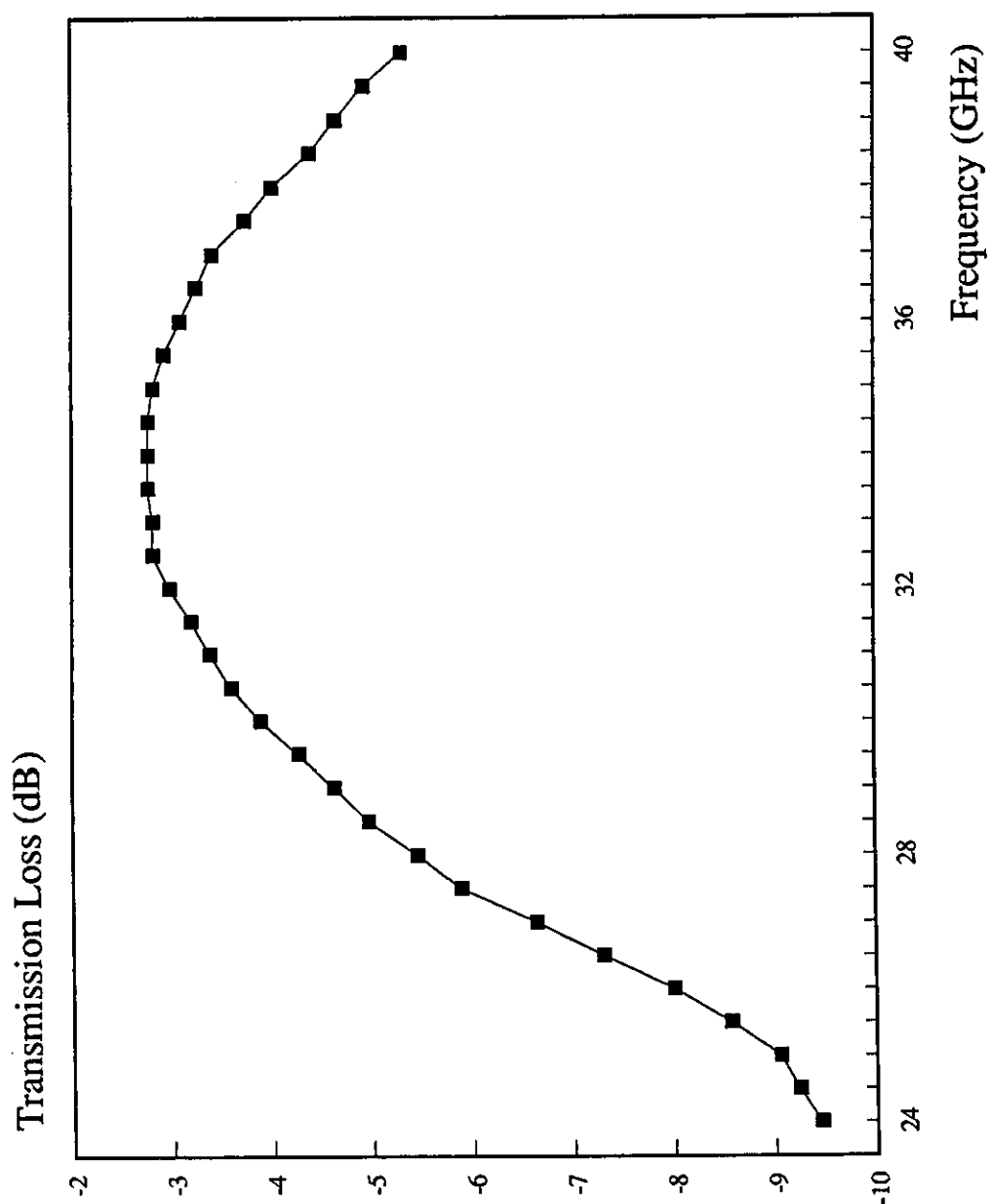
The piezoelectric FSS was now positioned between two sheets of 1.6mm thick PTFE and its transmission response was measured in the anechoic chamber (Graph 5.19). This frequency response has only one resonant peak in the Q-band at 33.6GHz; without the PTFE the FSS had two resonant peaks (Section 5.7). The peak in Graph 5.19 was attributed to the shorter slots (3.3mm) and is shifted from its resonant frequency of greater than 40GHz in Graph 5.18 by the PTFE.

With the PFSS between the PTFE sheets the structure cannot be modelled using the computer software. The software can only be used to model double layer FSSs with a single separating substrate or a single layer FSS sandwiched between up to five dielectric materials. The structure in this instance is a combination of these two cases.

All frequency scans of FSSs between PTFE were made at incident angles of 5°. This was to avoid standing waves produced in the PTFE from distorting the results.

Two piezoelectric FSSs with the same dimensions as the copper-polyester FSSs shown in Figure 5.16 were positioned between the PTFE with their longer slots aligned and their shorter slots blocked. A frequency scan of this structure showed it to be lossy with no clearly defined resonance. Alignment of the two FSSs between the PTFE is difficult. The PTFE is opaque preventing correct alignment from being confirmed visually. Also the alignment tolerance required is high - an accuracy of better than $\pm 0.2\text{mm}$, the width of the slots on the FSSs, is necessary to obtain any transmission through the structure.

Repeated attempts at alignment to obtain a frequency response with a satisfactory resonance were unsuccessful.



Graph 5.19: The transmission response of a PVDF double slotted FSS positioned between two PTFE sheets

5.7.2 PFSSs in the perspex frame

Sheets of *clear* perspex, 6mm thick, could be positioned either side of the PFSSs. This would clamp the PFSSs flat and allow their alignment to be made accurately. The electrical properties of perspex are:

ϵ_r	2.8
$\tan\delta$	0.014

These properties could influence the frequency response of the double layer FSS structure.

5.7.2.1 Shuttering the PFSSs

Piezoelectric sheets 150mm square can only be shifted by 0.1mm when they are energised. To achieve the complete microwave blocking effect of the FSSs demonstrated in the vacuum frame (Section 5.3.1) with 0.2mm wide slots requires the slots to be initially offset by half a slot width as shown in Figure 5.18.

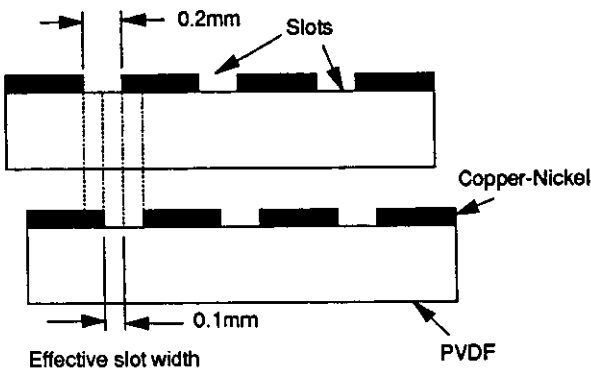


Fig. 5.18: Side view of the double layer FSS with slots offset by one half of the slot width

When these PFSSs are energised the cumulative movement of the slots will be 0.1mm (theoretically) and the slots will be completely blocked, as shown in Figure 5.19.

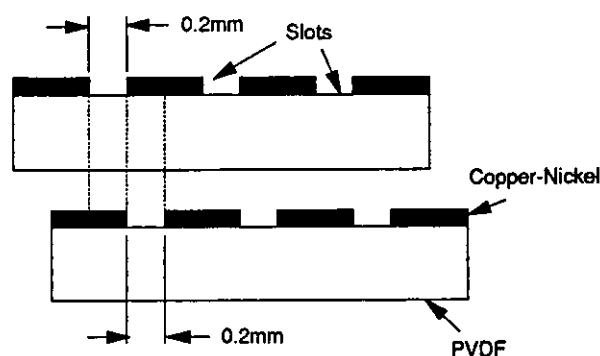


Fig. 5.19: Side view of the double layer FSS with the PVDF energised and the slots completely blocking the microwaves

The manufacturing facilities at the University do not enable slots 0.1mm wide to be etched. This is a restriction imposed by the minimum pen width used to draw the artworks used in the manufacture of the FSS (Section 4.4.2). The research has indicated the necessity of having narrow slots to enable the complete blocking action to be achieved. This justified having the PFSSs manufactured from artworks produced by an external photoplotting bureau at an increased expense. The slots drawn on these artworks were 0.1mm wide.

A piezoelectric FSS with 3.55mm x 0.1mm slots positioned in 6.0mm square lattices was modelled. Values of 12.50 and 0.02 were used for the electrical properties ϵ_r and $\tan\delta$ respectively as in the previous piezoelectric FSS models. The modelled transmission response is plotted in Graph 5.20. This shows a resonance at 38.0GHz where there was no loss in transmission. This piezoelectric FSS was now manufactured and its frequency response was measured in the anechoic chamber. An active PFSS area of 100mm square was used during the measurements, i.e. this was the area of PFSS visible to the microwaves. The remainder of the PFSS was covered with RAM.

This was necessary to prevent microwaves leaking around the edges of the FSSs.

Early experiments with FSSs showed the importance of ensuring no diffracted microwaves leaked around the edges to the receiver horn. The 100mm square active area of the PFSS in the current experiment was achieved by cutting a 100mm square aperture in a 300mm square sheet of RAM. The thickness of the RAM sheet had to be minimised to prevent experiments at 5° and 10° incident angles, which were necessary to avoid standing waves, from causing a significant 'microwave shadow' to be cast over the PFSS by the edge of the RAM. This 'microwave shadow' is shown in Figure 5.20.

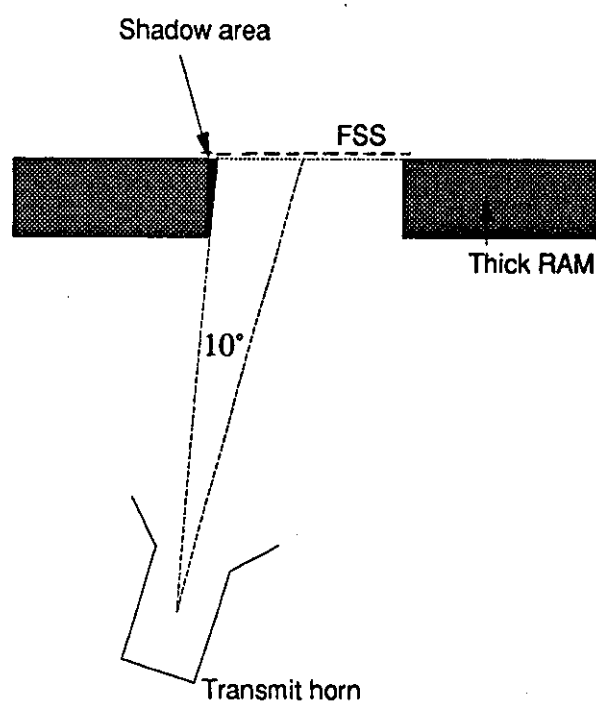
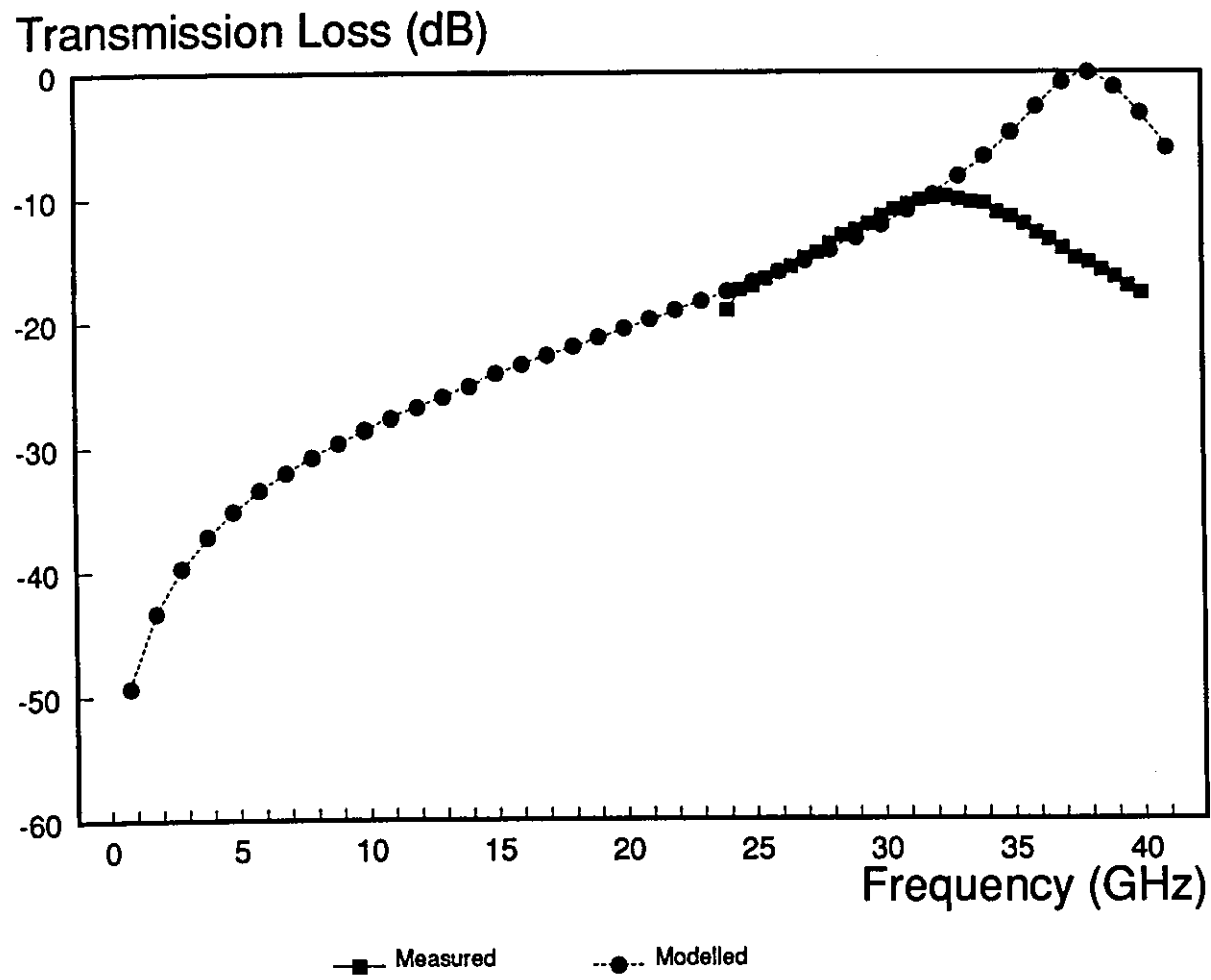


Figure 5.20: A 'microwave shadow' cast over the PFSS by the RAM

The absorbent properties of the thin RAM were measured in the J, K, and Q-bands. The RAM did not completely absorb the incident microwaves; at 24GHz the transmitted power, through the RAM was measured as -18dB. To overcome this problem a sheet of aluminium foil was secured to the rear of the RAM causing any microwaves which did pass through to be reflected, by the aluminium sheet, back through the RAM. This second pass through the RAM absorbs the transmitted power further preventing any significant power from reaching the transmit horn.

The transmission response of the narrow slotted PFSS is shown in Graph 5.20 along with the modelled response. The measured transmission response had a loss of -10dB at the resonant frequency of 32.5GHz. This resonance is 5.5GHz lower than the modelled response. The modelled PFSS variables were checked and the dimensions of the PFSS used in the experiment were checked. The correct variables and dimensions had been used. A second frequency scan of the PFSS produced the same transmission response. This inconsistency between measured and modelled results was not as large between previous models and measurements. The large bandwidth of the PFSS, which was evident in the transmission response of other PFSSs, was also present in this PFSS. The -3dB bandwidth was 8.2GHz (between 28.3GHz and 36.5GHz).



Graph 5.20: Modelled and measured transmission response of 3.55mm x 0.1mm slotted PFSS

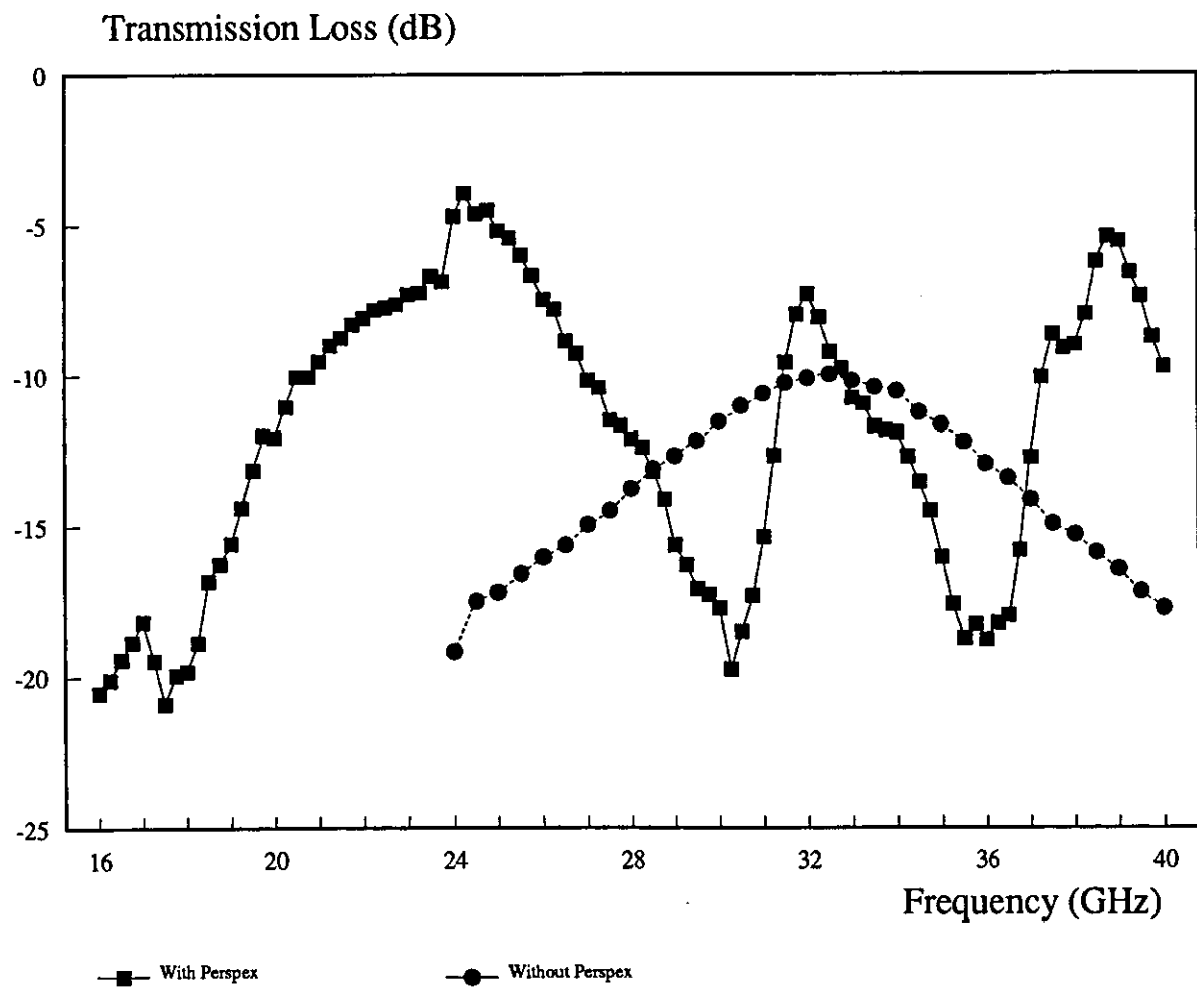
5.7.2.2 Shuttering the PFSSs in the perspex frame

The piezoelectric FSS was now positioned between two 6mm thick perspex sheets. The perspex caused a shift in resonance from 32.5GHz in the Q-band down to 24.2GHz in the K-band. The loss at resonance was reduced to -4dB from -10dB. The plot of this transmission response is shown in Graph 5.21 along with the plot of the transmission response before the PFSS was sandwiched between the two perspex sheets.

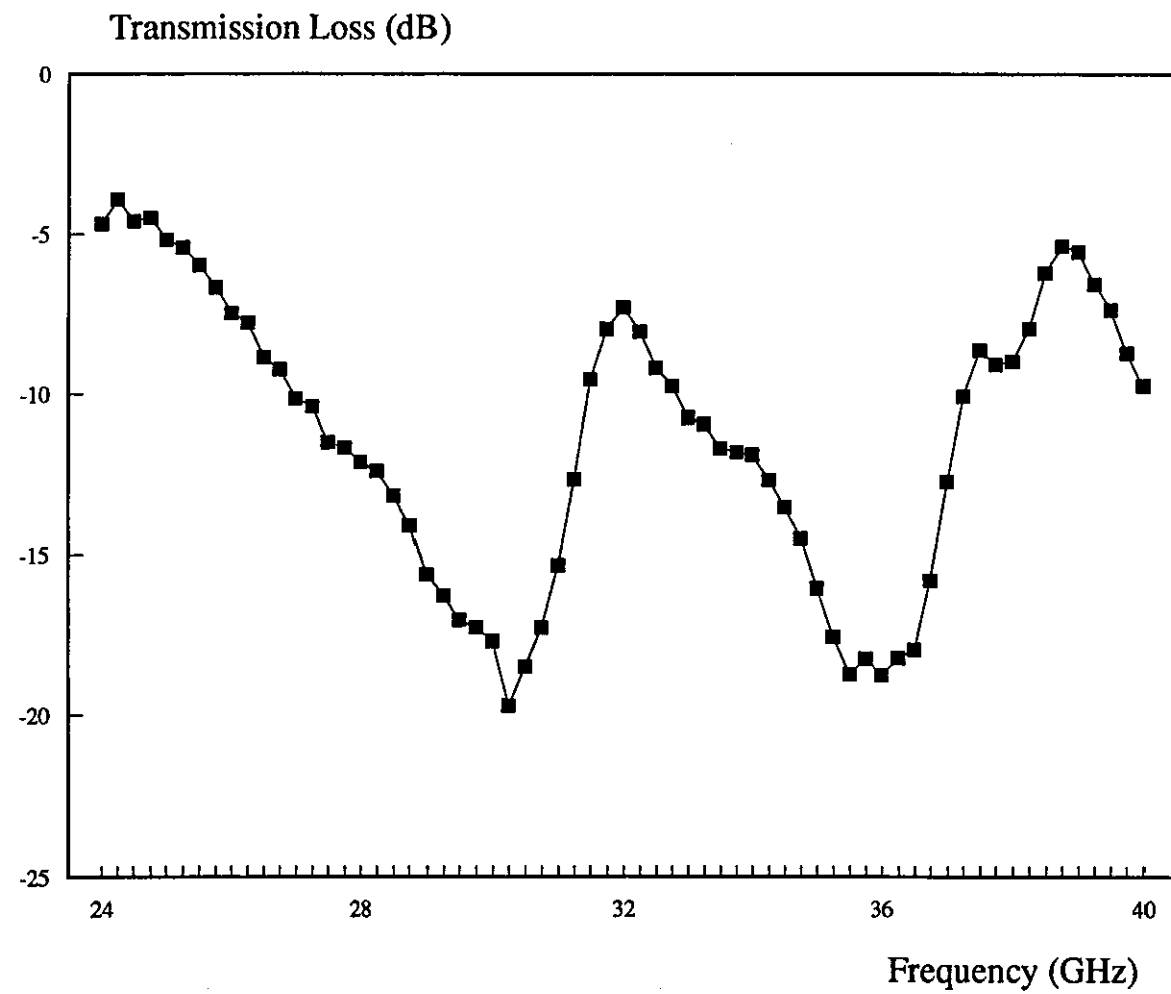
The perspex also caused peaks in the transmission response at 32GHz and 38.9GHz. These were attributed to standing waves in the perspex; they occurred at 6.9GHz intervals ($38.9\text{GHz} - 32\text{GHz} = 6.9\text{GHz}$). Another standing wave peak was expected at 25.1GHz ($32\text{GHz} - 6.9\text{GHz}$), this is close to the resonant frequency of the PFSS-perspex structure. This standing wave could have been the cause of the lower loss at the resonance frequency when the perspex sheets were used. The resonance peak is not a symmetrical shape, it has a slight 'squint'. This squint also indicates the peak is a combination of the PFSS resonance and the standing wave in the perspex.

When the piezoelectric sheet was energised there was no change in the transmission response.

Two PFSSs were now positioned between the perspex, secured at opposite ends, with their slots aligned. This structure produced standing waves in the Q-band as before. These standing waves could not be eliminated by altering the incident angle. Graph 5.22 shows the transmission response of this structure.



Graph 5.21: The measured transmission response of the PFSS with and without the perspex sheets



Graph 5.22: The transmission response of two PFSSs between perspex sheets

Energising the two PFSSs by applying a voltage (813V) across their electrodes caused a small length extension and a corresponding reduction in transmitted power. The maximum reduction in transmitted power was 0.2dB at 33.2GHz. The voltage, 813V, was the maximum which could be applied. At voltages above this the electrodes started to arc through the PVDF substrate. The PFSS-perspex structure used in this experiment (Figure 5.21) did not allow free movement of the PFSSs. After the energisation voltage was removed the piezoelectric sheets were found to have produced a static charge preventing them from contracting.

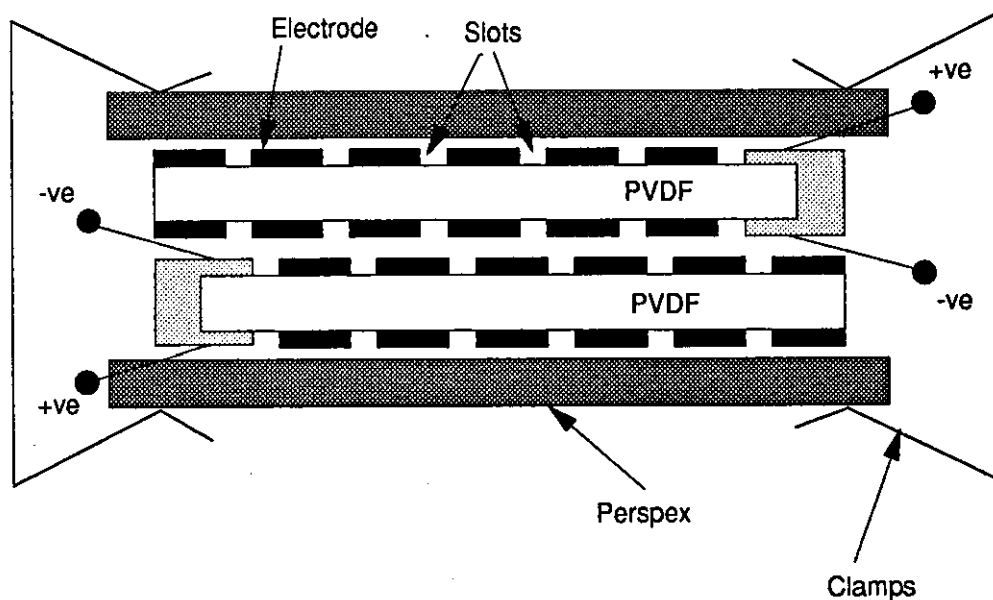


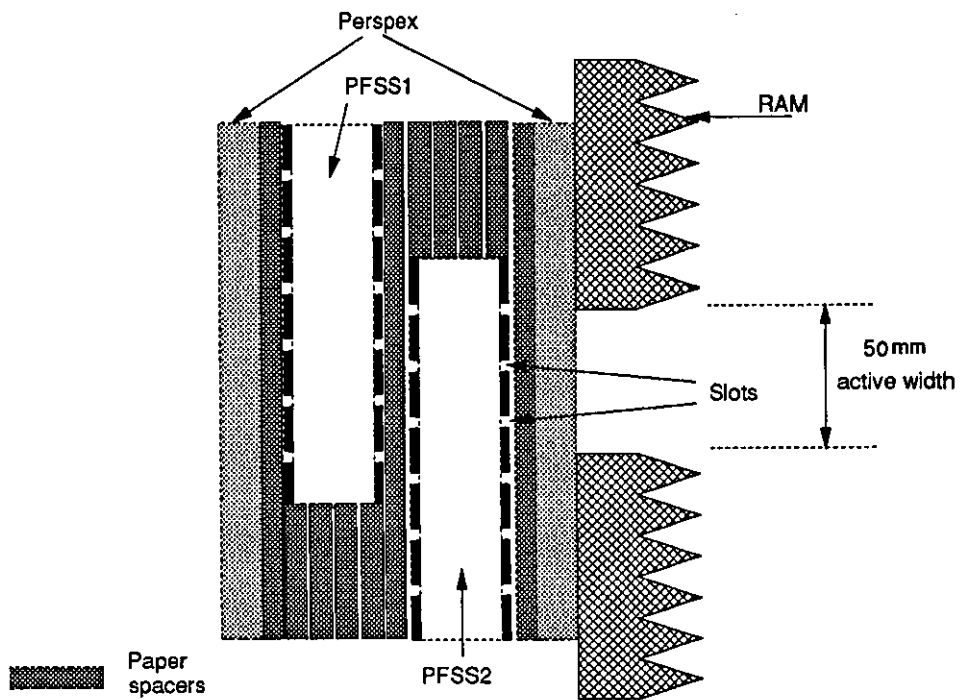
Fig. 5.21: The PFSS-Perspex structure

Thin sheets of paper were positioned between the perspex and PFSS to prevent this static charge from building up.

A frequency scan of this structure in the K-band (with the paper between the perspex and PFSSs) showed some multiple reflections and a loss of -18.0dB at 24.6GHz. With a single PFSS (Graph 5.21) the loss was -4 dB at 24.2GHz. Energising the PFSSs caused a further loss of 2.46dB as the PVDF sheets moved and produced the shuttering effect.

This shuttering effect was not ideal - slight gaps were visible on some slots indicating inaccuracies in the manufacture of the PFSSs and alignment of the PFSSs between the perspex sheets.

A greater movement could be obtained by offsetting the PFSSs so only their ends, which produced the maximum movement, overlapped. This is shown in Figure 5.22; the active RFSS area has been reduced to 50mm x 150mm. Thin sheets of paper were used as spacers positioned between the perspex where the PFSSs did not overlap to ensure they laid flat. RAM was used to cover this area of the PFSSs and prevent microwaves leaking through to the transmit horn.



NOTE: The slots on the two PFSSs are not aligned so the structure is acting as a microwave shutter

Fig. 5.22: A side view of the RFSS structure with offset PFSSs

The PFSSs used in this experiment had 3.55mm x 0.1mm slots (PFSS1) and 4.8mm x 0.2mm slots (PFSS2). These PFSSs were aligned so only 0.1mm movement was necessary to cause total shuttering of the RFSS structure. This can be seen in Figure 5.23.

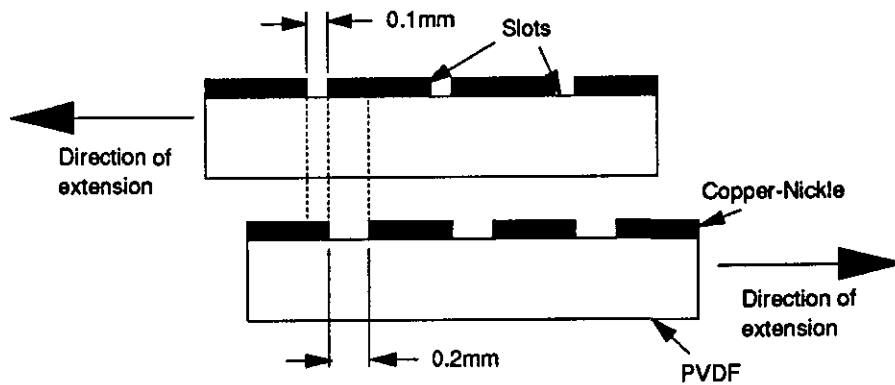
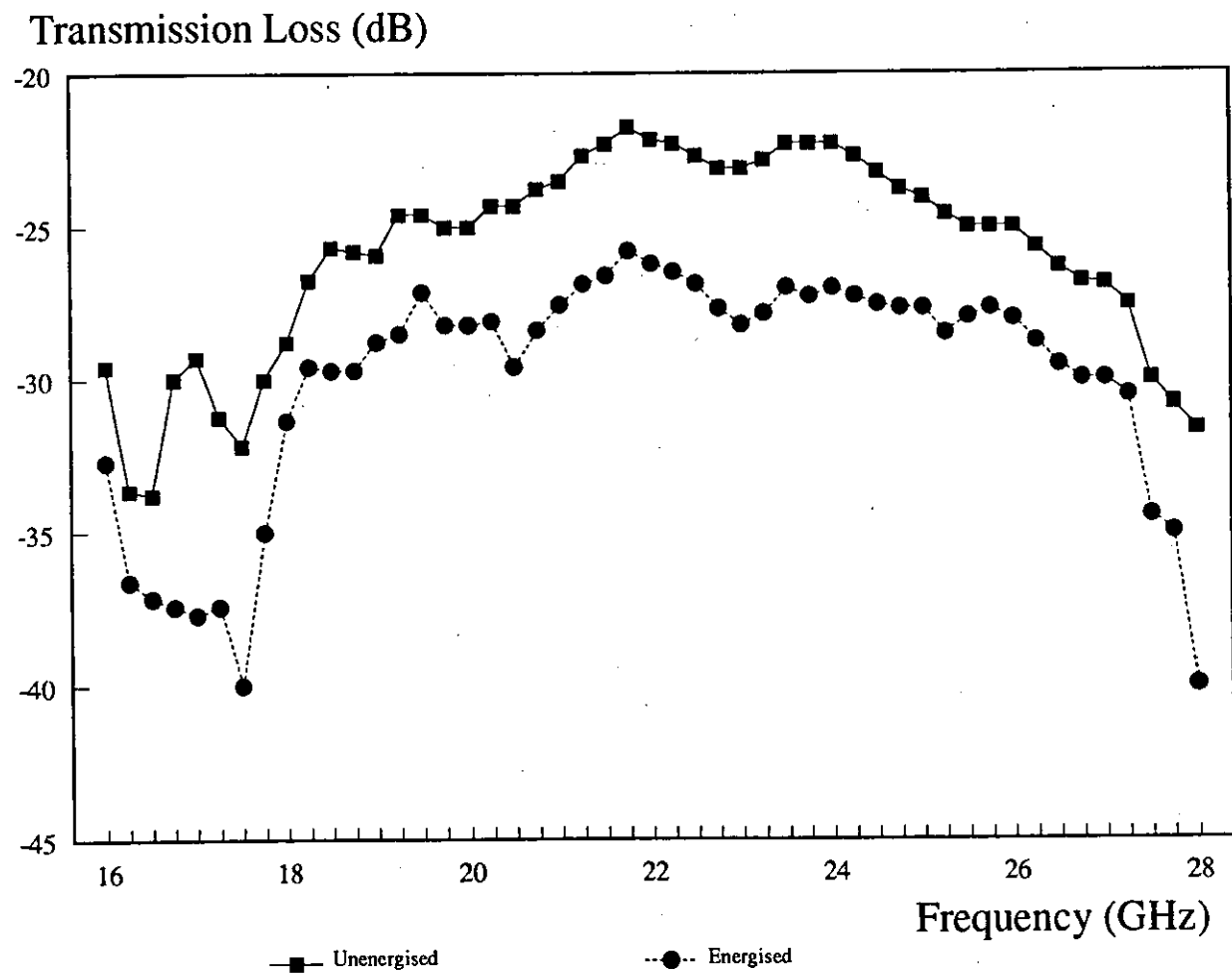


Fig. 5.23: The two PFSSs providing total shuttering after only 0.1mm PVDF extension

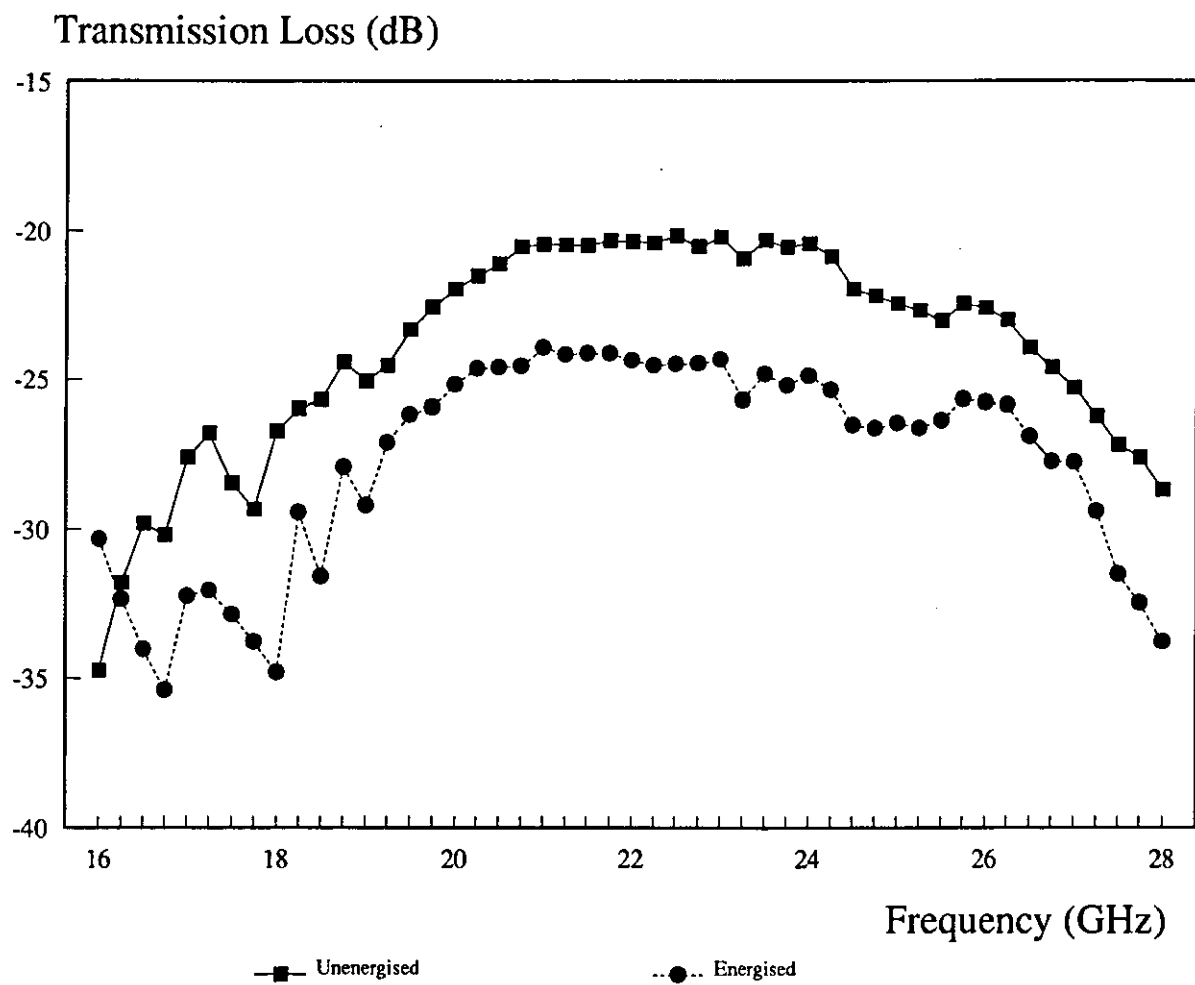
Graph 5.23 shows the frequency response of this structure with no energisation voltage applied and when energised to 840V. The graph shows the structure to have a very broad bandwidth and to be very lossey (-21.6dB before energisation). Energisation of the PFSSs did not cause complete shuttering. The transmitted power was only reduced, at the resonant frequency (21.75GHz) by 4.3dB.



Graph 5.23: The transmission response of the double layer PFSS-Perspex structure

A solid PVDF sheet was scanned in an earlier experiment, (Section 5.4), this allowed approximately -30dB of power to be transmitted. This indicates the -25.6dB of transmitted power when the PFSSs are energised is approaching the level which can be expected from total shuttering. The RFSS needs to provide more transmitted power in the un-energised state.

The PFSSs were repositioned between the perspex to try and improve the alignment of the slots. A second scan of the transmission response before and during energisation produced the plots shown in Graph 5.24. These show a change in transmitted power at the resonant frequency (21.75GHz) of -3.82dB when the RFSS was energised.



Graph 5.24: The effect of energising the RFSS (after realignment of the slots)

5.8 The effect of the gap, S , between the FSSs

The sheets of paper which were positioned between the perspex and PFSSs in the previous experiment were removed and the two PFSSs were realigned between the perspex sheets with their slots offset by half a lattice. This is shown in Figure 5.24. This positioning of the PFSSs was the same as that used in earlier experiments with the vacuum frame to demonstrate the full shuttering of the RFSS.

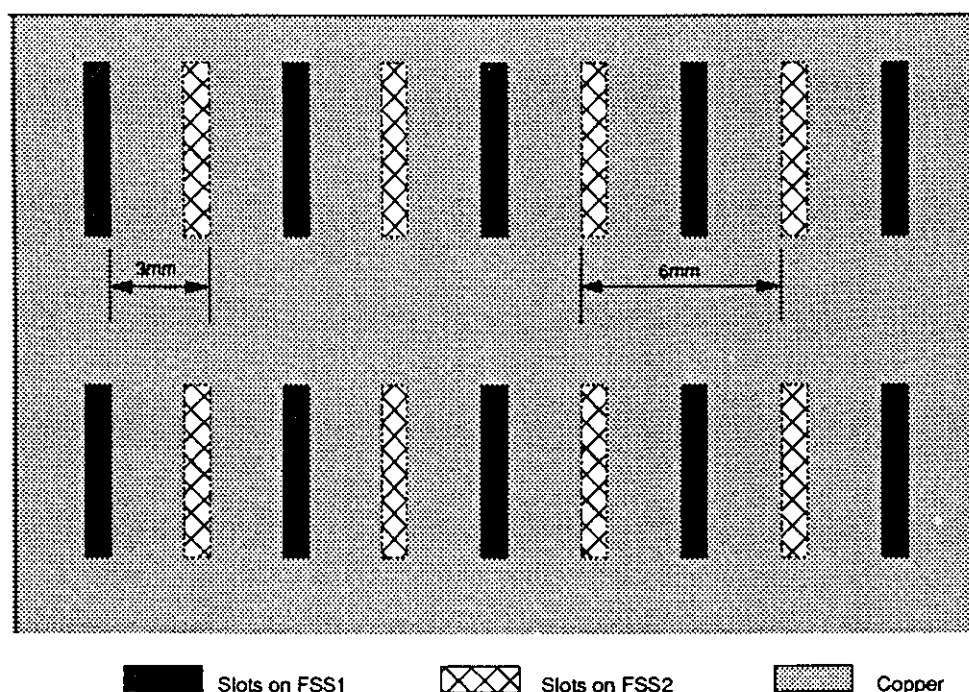


Fig. 5.24: The PFSS positioning to demonstrate the shuttering effect

This arrangement was scanned and found to allow a significant amount of leakage to the receive horn. At 24.4GHz -14.7dB of power leaked through the double layer structure. The sheets of paper were now repositioned between the perspex and the PFSSs, the purpose of this was to push the two PFSSs together and minimise any gap, S , between them.

The paper reduced the transmitted power to less than -30dB at 24.4GHz and a maximum of -27.5dB at 27.2GHz.

5.9 The effect of varying the slot length

The Patent^[2] initially suggested producing a reconfigurable FSS which could be controlled to resonate at different frequencies. Difficulties in achieving this continual range of reconfigurability occurred because the piezoelectric materials can only produce a small physical movement. This prevents shifting of the FSS by an amount which produces a significant frequency shift. The initial modelling of the a single FSS showed a change in dipole length of 0.3mm was necessary to obtain a resonant frequency shift of 2.6GHz (Graph 5.2,Section 5.1.2).

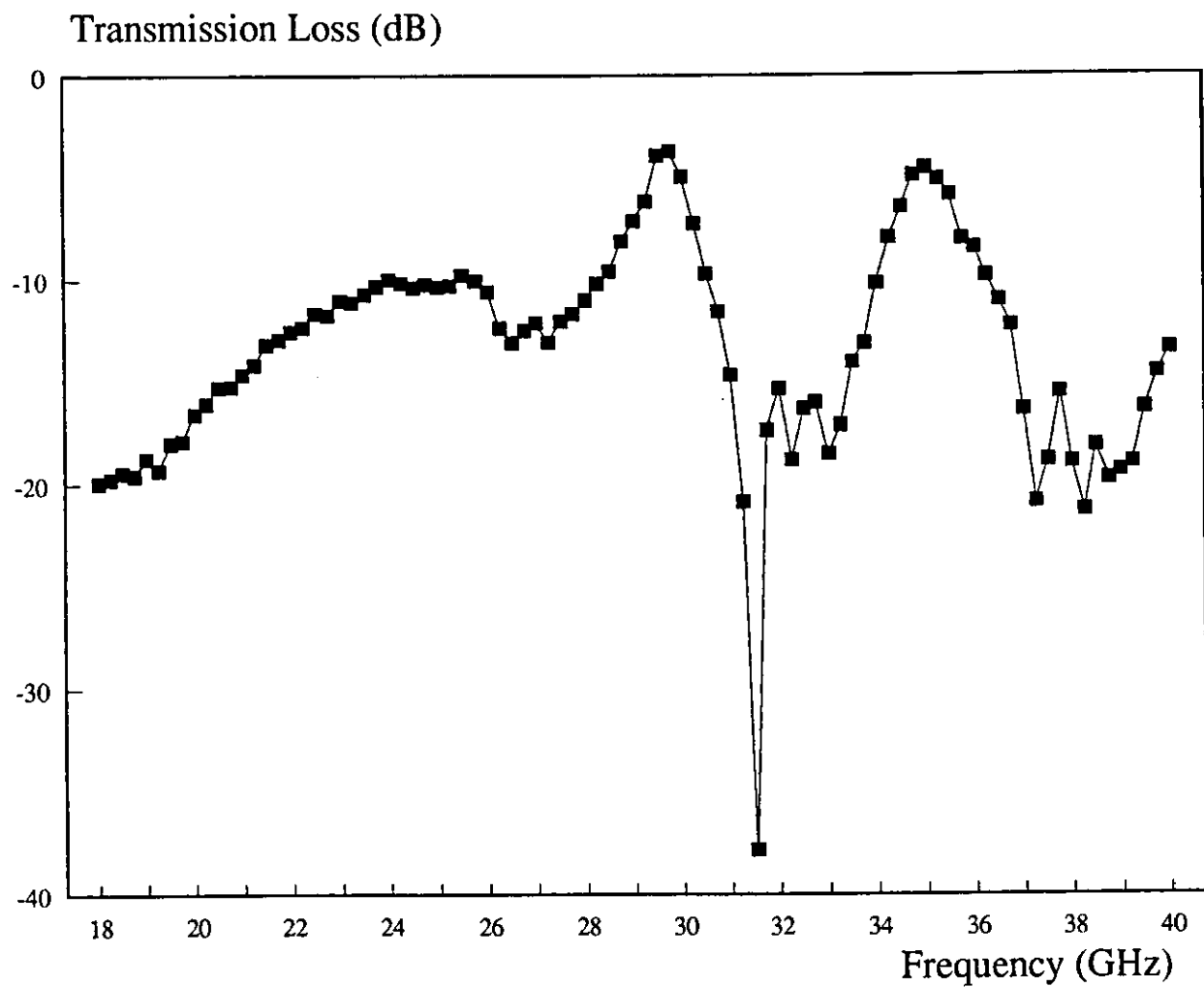
5.9.1 Variation in slot length of FSSs in the perspex frame

Two copper-polyester FSSs were manufactured with slots 3.2mm long and 0.2mm wide in 6mm square lattices.

The effect of positioning one of these FSSs between two 6mm thick perspex sheets was studied. The perspex-FSS-perspex structure was scanned in the Q-band. The perspex introduced standing waves into the transmission response making it difficult to establish the resonant frequency. Graph 5.25 shows a plot of the transmission response of the FSS between the perspex sheets. Graph 5.26 shows frequency scans of just the perspex sheets.

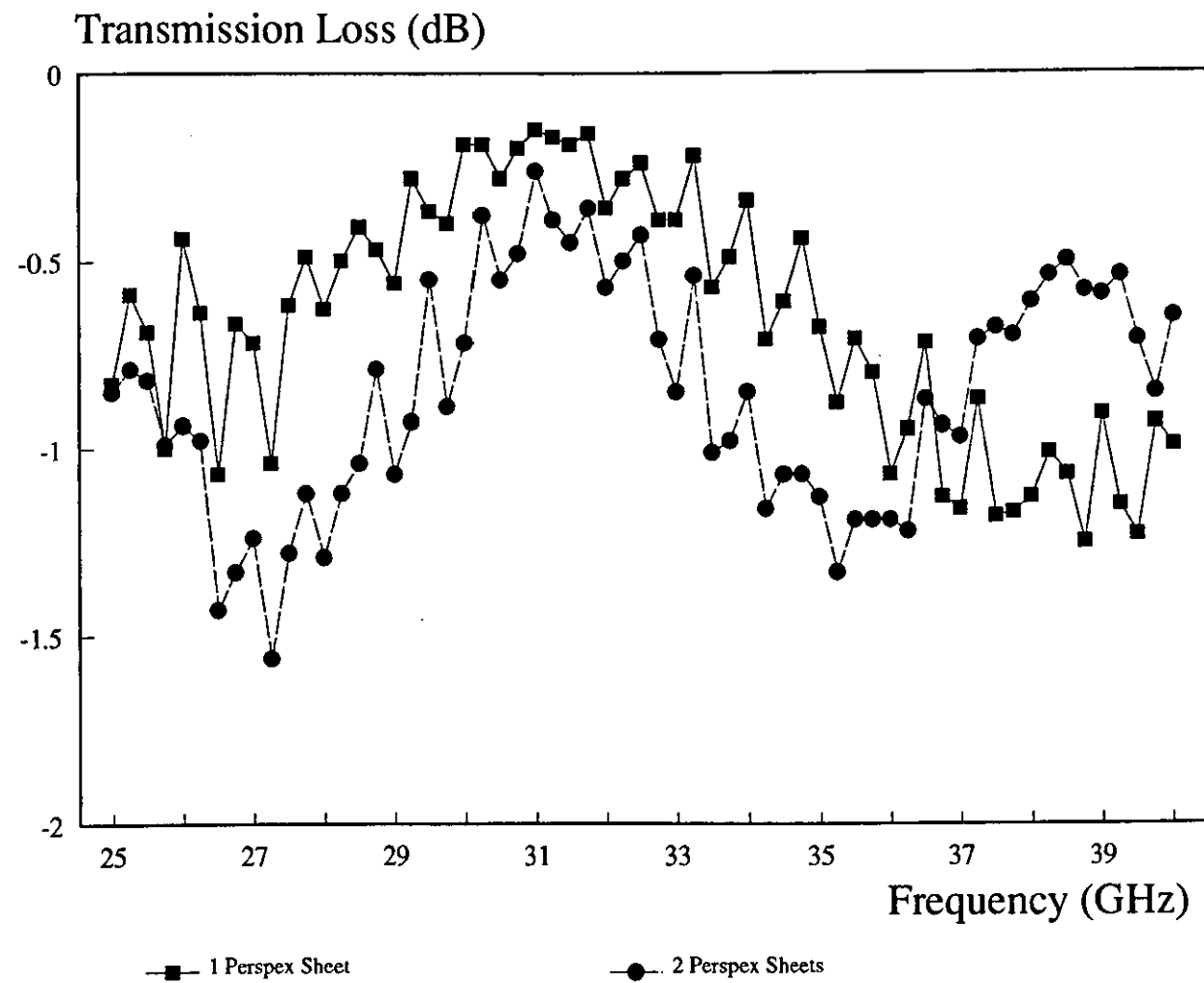
Graph 5.27 shows the plot of a frequency scan of a single 6mm thick perspex sheet positioned in front of the FSS. The slots on this copper-polyester FSS were 3.2mm long and 0.4mm wide.

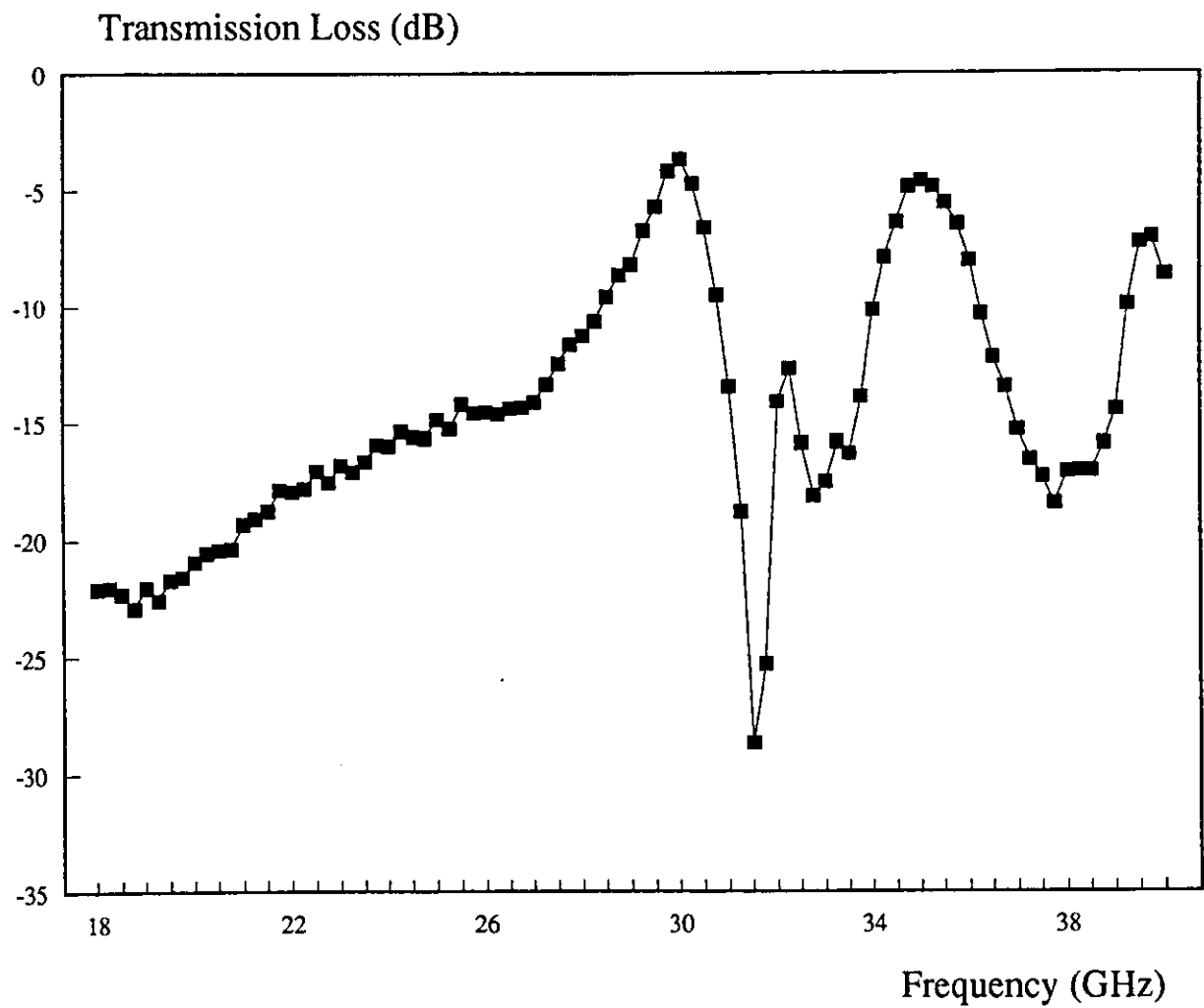
The standing waves which occur when the FSS is positioned behind or between the perspex sheets were also seen in the computer models. The modelled transmission responses are shown in Graph 5.28.



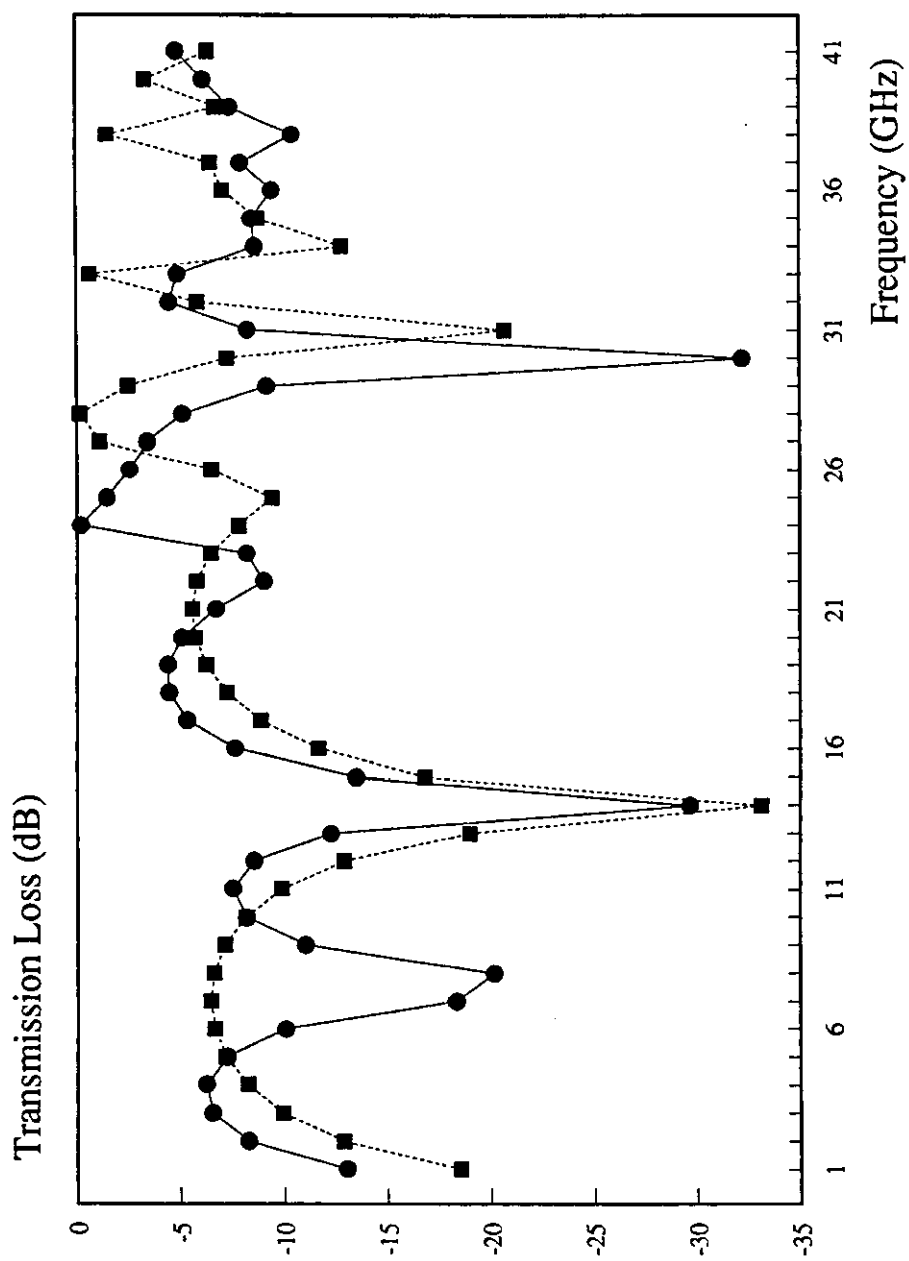
Graph 5.25: The transmission response of the FSS sandwiched between two 6mm thick perspex sheets

Graph 5.26: The transmission response of 6mm thick perspex sheets





Graph 5.27: The transmission response of a single sheet of 6mm thick perspex in front of an FSS



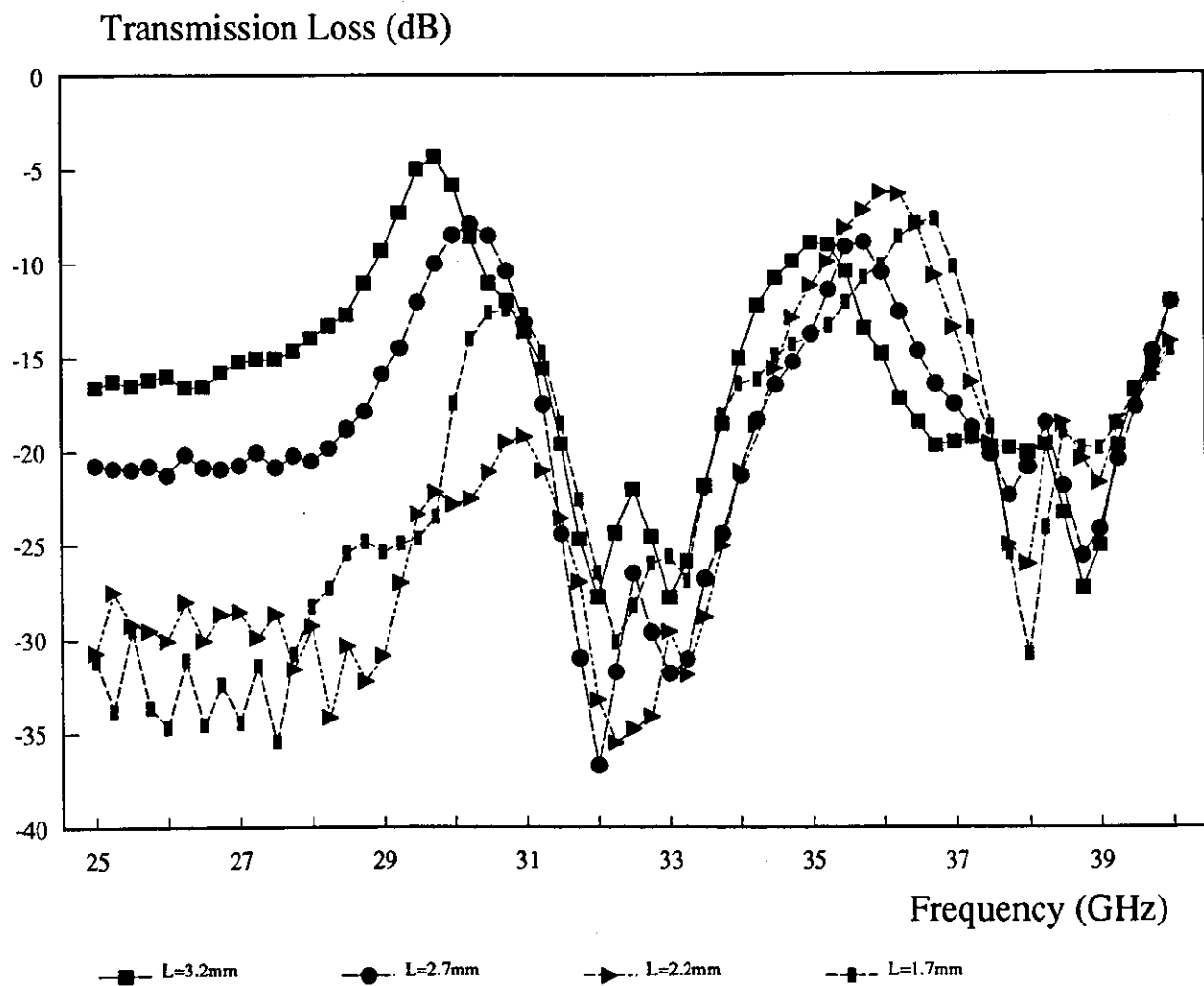
Graph 5.28: The modelled transmission frequency response of an FSS positioned between two 6mm thick perspex sheets and an FSS behind one 6mm thick perspex sheet

Two FSSs were now positioned between the perspex sheets and scanned in the Q-band. Both FSSs had slots 3.2mm long and 0.2mm wide. One FSS was then shifted in steps of 0.5mm in the length direction of the slots. This has the effect of reducing the *effective* slot length. Graph 5.29 shows four transmission response curves of the perspex-FSS structure with slot lengths of 3.2mm, 2.7mm, 2.2mm, and 1.7mm. There are two obvious 'peaks' in these plots. The frequency at which the peaks occurred increased as the slot length was reduced.

Table 5.1 summarises the transmission frequency curves shown in Graph 5.29.

Slot Length(s) (L) (mm)	Shift (DS) (mm)	Resonant Frequency Loss At Resonance			
		Peak 1		Peak 2	
		Freq. (GHz)	Loss (dB)	Freq. (GHz)	Loss (dB)
3.2	0	29.8	-4.5	35.1	-8.5
2.7	0.5	30.2	-8.0	35.7	-8.5
2.2	1.0	31.0	-18.5	36.2	-6.5
1.7	1.5	30.8	-12.0	36.5	-7.5

Table 5.1: Variation in resonant frequency and loss at resonance for the Perspex-FSS-Perspex structure



Graph 5.29: The transmission response of the RFSS with four different effective slot lengths

The frequency of the second peak in the transmission response increases at between 0.6 and 0.3GHz per 0.5mm *effective* slot length reduction. The loss at this second peak remained fairly constant varying by only 2.0dB. The frequency of the first peak did not alter by a consistent amount for the shifts DS of 0.5mm.

The second peak in the frequency scan appeared at the same frequency when measurements were made with both one sheet of perspex in front of the FSS and when two sheets of perspex were sandwiched around the FSS. This suggests the peak is 'FSS dependent', as opposed to being dependent on the perspex sheet(s), and confirms the movement of the second peak seen in Graph 5.29 was due to the reduction in RFSS slot length.

5.10 The effect of varying the PVDF substrate thickness

PVDF is available in thicknesses of 9, 28, 52, and 110 μ m. The 9 μ m thick sheets were considered unsuitable for use in the RFSS application because the material is susceptible to small pin holes. These can cause the electric field applied across the material to breakdown as described in Section 4.4.1.

The previous experiments have highlighted the flimsy nature of the 28 μ m thick PVDF which makes it difficult to concentrate the piezoelectric expansion in the desired direction.

PVDF sheets 110 μ m thick are a lot more rigid than 28 μ m thick material and would enable the extension to be concentrated in the desired direction. The disadvantages of using 110 μ m thick PVDF include the large energisation voltage required to establish a 30V/ μ m electric field (3.3kV) and the possibility of greater loss in the passband of any manufactured PFSSs.

Two PFSSs with 110 μ m thick substrates were manufactured. Both FSSs had 3.55mm long slots positioned in 6.0mm square lattices. One PFSS had an area 150mm square and the other an area 300mm x 150mm. The slots in both PFSSs were 0.4mm wide. The longer PFSS was manufactured to investigate the possibility of obtaining a larger extension when the PVDF was energised. Section 4.2.2 explained how when the PVDF is operated in its length extension mode the extension is proportional to the original length. This can be seen from equations 4.1 and 4.5, rewritten and combined here to produce equation 5.3:

$$d = \frac{\text{Strain}}{\text{Applied Field}} = \frac{\epsilon}{E} \left(\frac{m}{V} \right)$$

(eqn.4.1)

$$\text{Strain } (\epsilon) = \frac{\text{Length Extension } (\delta l)}{\text{Original Length } (l)}$$

(eqn.4.5)

$$d_{31} = \frac{\epsilon}{E} = \frac{\delta l/l}{E} = \frac{\delta l}{El}$$

(eqn.5.3)

$$\therefore \delta l = El \times d_{31}$$

(eqn.5.4)

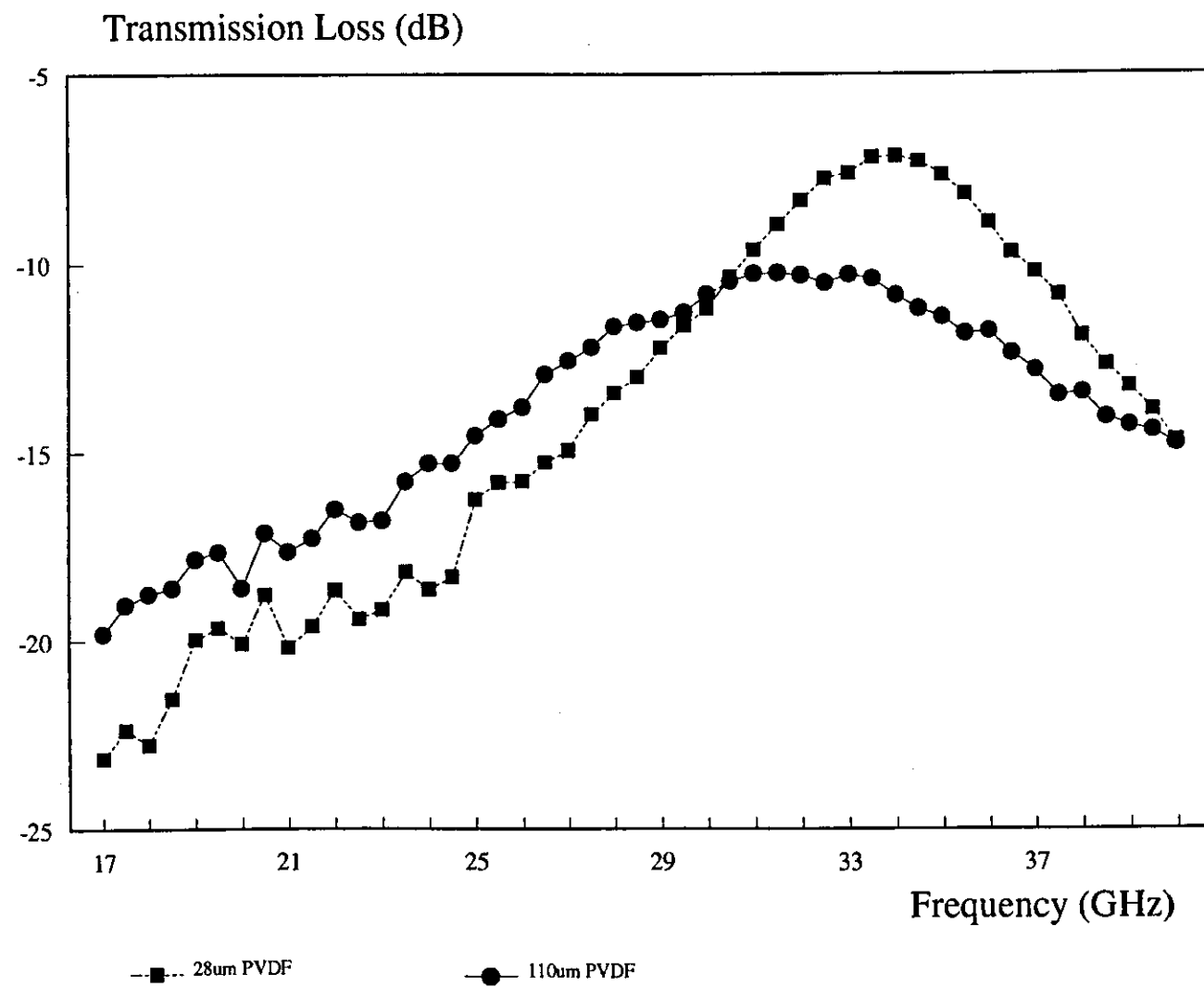
i.e. the extension δl will double if the length, l , is doubled

Frequency scans of the PFSSs were made in the K- and Q-bands. Plots of these scans are shown in Graph 5.30. Very broad bandwidths are seen with resonances at 33.8GHz (28 μ m thick PVDF) and 31.8GHz (110 μ m thick PVDF). The loss at the resonant frequencies was -7dB and -10.3dB for the 28 μ m and 110 μ m thick PVDF substrates respectively. Table 5.2 summarises the effect of increasing the PVDF thickness.

PVDF Thickness (μ m)	Resonant Frequency (GHz)	Loss At Resonance (dB)	-3dB Bandwidth (GHz)
28	33.8	-7.0	6.0
110	31.8	-10.3	10.5

Table 5.2: The effect of increasing the thickness of the PVDF substrate

Graph 5.30: Frequency scans of PFSSs with 28 μ m and 110 μ m Thick substrates

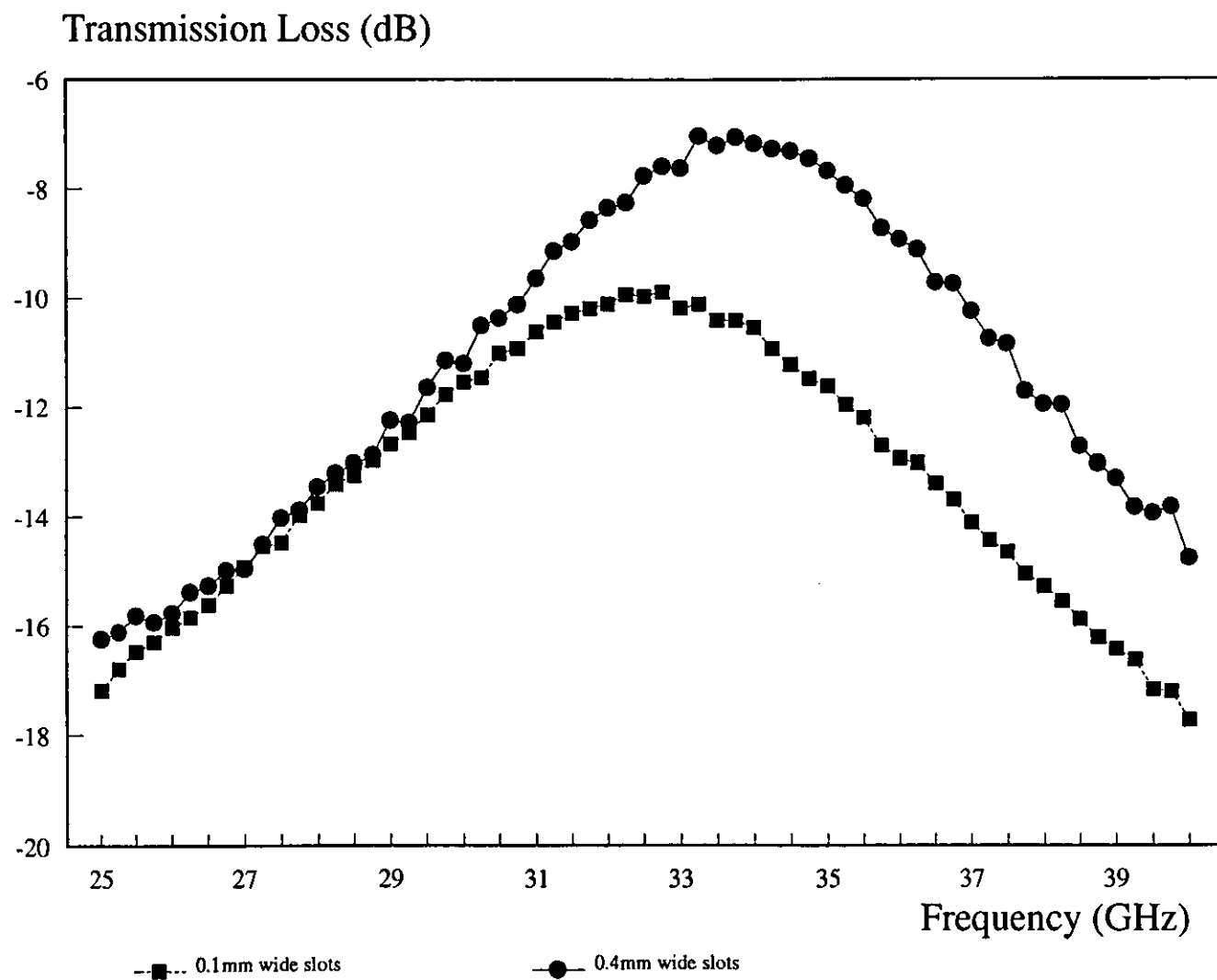


5.11 The effect of varying the width of the slots

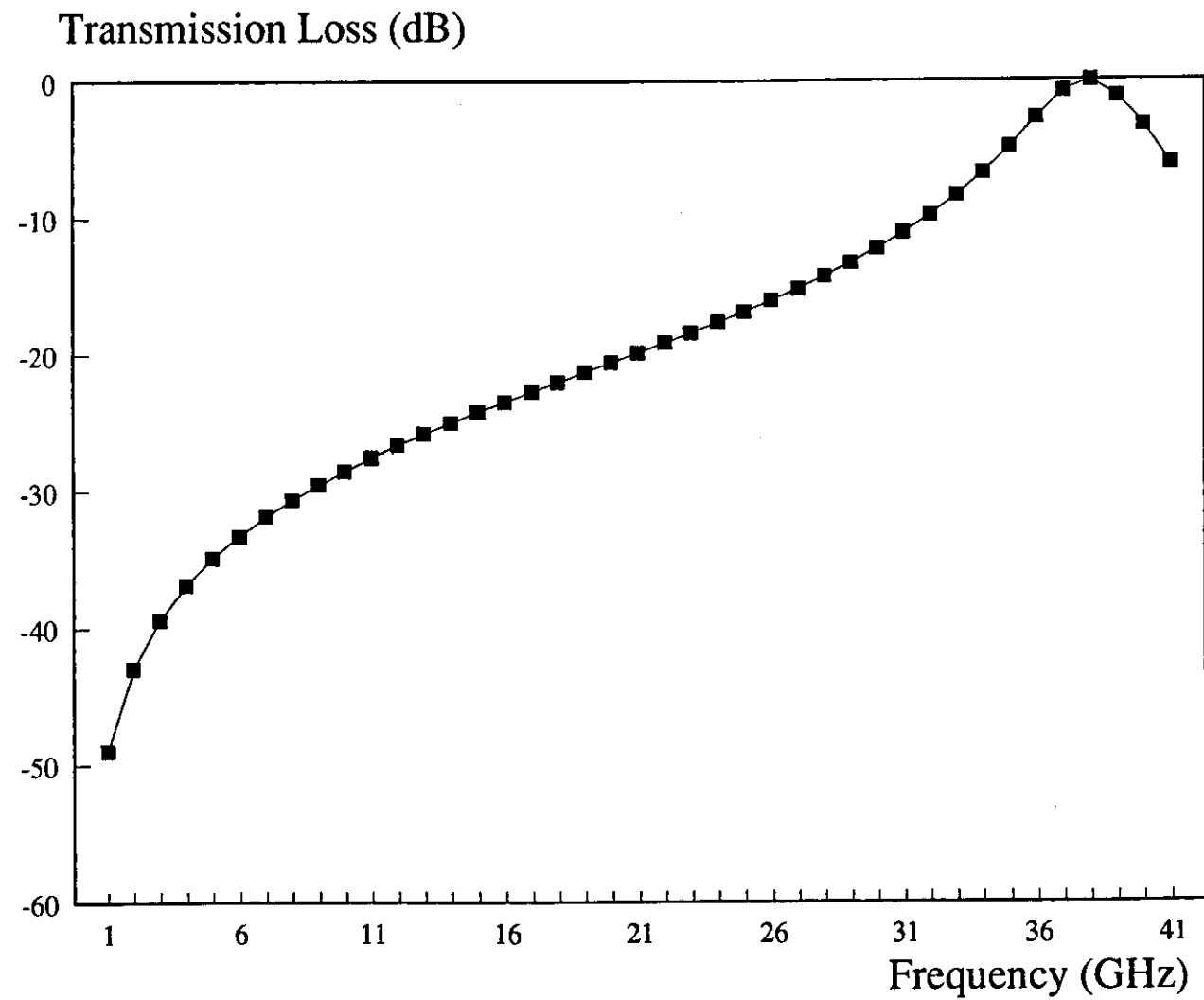
Another 28 μ m thick PFSS with 3.55mm long slots was scanned in the Q-band. The slots on this PFSS were 0.1mm wide and had a resonant frequency at 32.5GHz. This compares with the resonance of 33.8GHz for the PFSS with 0.4mm wide slots (Graph 5.30). The PFSS with narrower, 0.1mm wide, slots also had a greater loss, -10.0dB, than the PFSS with the wider slots. Frequency scans for both FSSs in the Q-band are shown in Graph 5.31.

These measurements indicate a high loss at the resonant frequency of the PFSS can be caused by narrower slots and a thicker PVDF substrate.

The computer software used for modelling the FSSs does not take account of the width of the slots on the FSS and so could not be used to model the effect of narrower slots. The software was used to model a PFSS with 3.55mm long slots. This is shown in Graph 5.32 with a resonance at 38.0GHz. This is higher than the measured resonances but follows the trend of earlier PFSS models where the measured resonant frequency occurred at a lower frequency than the modelled resonance. This experiment suggests the slot width has a greater affect on the resonant frequency than was initially thought and could be the cause of the discrepancy between measured and modelled transmission responses.



Graph 5.31: The effect of varying the width of the slots on the PFSS



Graph 5.32: The modelled transmission response of the 28μm thick PFSS with 3.5mm long slots

5.12 Energisation of the PFSSs

A second PFSS with slots 3.55mm long and 0.2mm wide was manufactured from a sheet of PVDF 300mm long, 150mm wide, and 110 μm thick. The two 300mm long PFSSs were positioned so they overlapped by an area 150mm square at their unsecured ends, i.e. the ends which moved due to the extension of the material. The slots on the two FSSs were aligned in the overlapped area.

The purpose of this experiment was to maximise the movement of the slots on the PFSS and obtain complete shuttering.

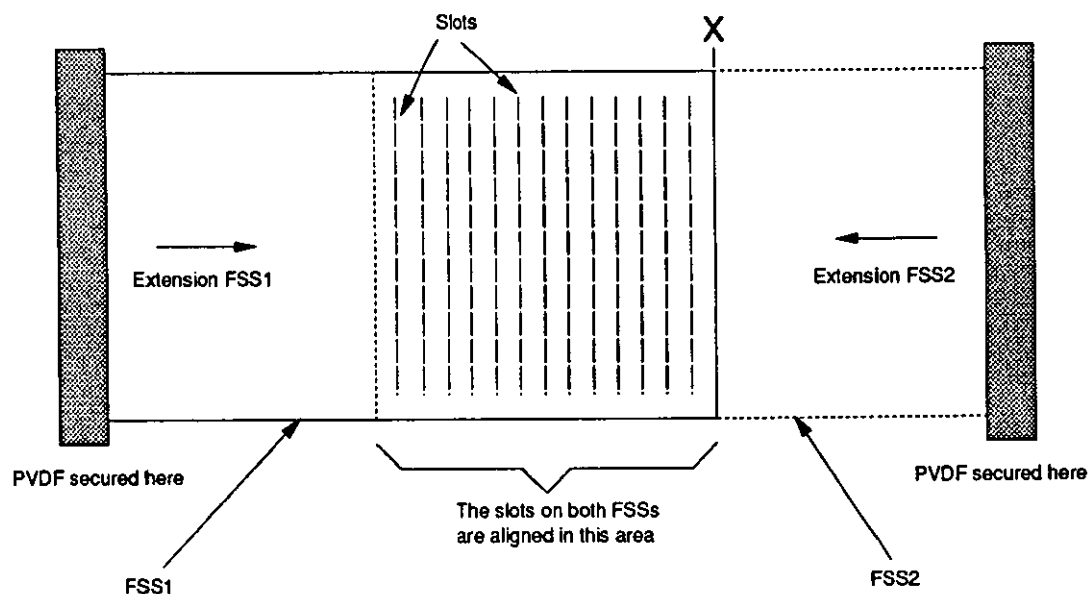


Fig. 5.25: Maximising the relative movement of the RPFSS by only overlapping the PFSSs at their ends

The total *relative* movement of the PFSS in the overlapped area when the maximum electric field ($E=30\text{V}/\mu\text{m}$) is applied was calculated at the position marked X in Figure 5.25 using Equation 5.4.

$$\begin{aligned}
\delta_{FSS1_x} &= E \times l \times d_{31} \\
&= 30.10^6 \times 300.10^{-3} \times 23.10^{-12} \\
&= 0.207 \text{ mm}
\end{aligned}$$

$$\begin{aligned}
\delta_{FSS2_x} &= E \times l \times d_{31} \\
&= 30.10^6 \times 150.10^{-3} \times 23.10^{-12} \\
&= 0.1035 \text{ mm}
\end{aligned}$$

Note: When calculating δ_{FSS1_x} a length, l , of 300mm was used because the extension is occurring at the end of FSS1. When the extension at X of FSS2 was calculated, δ_{FSS2_x} , the length, l , used was only 150mm because point X is only halfway along the length of this PFSS. The total relative movement at X is the sum of these two extensions because they occur in opposite directions.

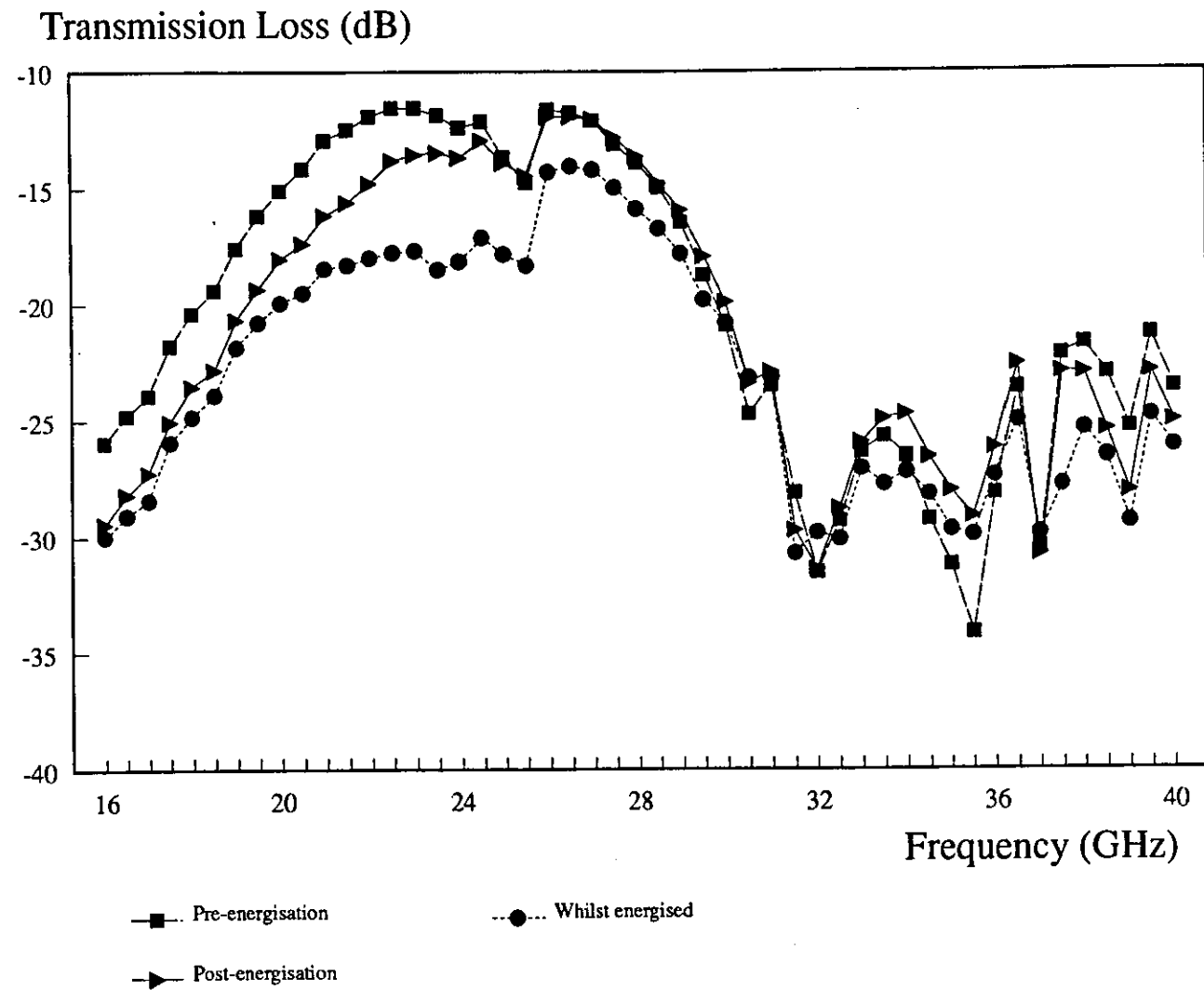
$$\delta_x = \delta_{FSS1_x} + \delta_{FSS2_x} = 0.3105 \text{ mm}$$

This movement is the same at any position within the overlapped area because the sum of the lengths causing the movement/extension is always 450mm. This theoretical movement is greater than the slot widths on the two PFSSs and so should allow complete shuttering if the PFSSs are accurately aligned.

The PFSSs were positioned, as described above, between two 6mm thick perspex sheets. A frequency scan of the structure over the Q-band was made. The PFSSs were then energised with a 5.1kV voltage source. The transmission loss of the structure was seen to increase. When this increase stopped a second frequency scan of the structure was made. The energisation voltage was now removed and the PFSSs were allowed to contract. The transmission loss reduced. When this contraction stopped a final frequency scan of the structure was made.

The frequency scans made in the Q-band exhibited multiple peaks due to standing waves in the supporting perspex structure. Three frequency scans, before, during, and after energisation were made in the K-band using the same procedure as for the Q-band scans described above. The frequency scans in both the K- and Q-bands are plotted in Graph 5.33.

Graph 5.33: Frequency scans of the RPFSS in the K- and Q-bands



At the resonant frequency of 23.0GHz a reduction in transmitted power of -6dB occurred when the PFSSs were energised. When the energisation voltage was removed the PFSSs did not return to their original positions. Graph 5.33 shows an increased transmission loss of 1.5 dB at the resonant frequency compared with the loss before the PFSSs were energised.

The transmission power differences at the K- and Q-band transition frequency (25.5GHz) can be partially attributed to the criticality of the alignment of the slots in the two PFSSs. Between the K- and Q-band frequency scans the PFSSs were realigned between the perspex, if the realignment was not exact the structure would produce a different frequency response. This will not significantly affect the shape of the transmission response at frequencies away from this transition frequency but does mean comparisons cannot be made between power levels in the K-band and power levels in the Q-band.

The frequency response of the double layer PFSS-perspex structure was scanned again following realignment of the slots. Only the K-band was scanned because the previous experiment had shown the resonant frequency to be in this band. Graph 5.34 shows the transmission response. A reduction in transmitted power of greater than 6dB was obtained at the resonant frequency when the PFSSs were energised. A difference in resonant frequency also occurred during energisation. This resonant frequency shift could be accounted for if the PFSSs did not both extend in exactly the same direction. This would cause the length of the slots to reduce slightly when the PFSSs were energised. The slightly shorter slots would have a higher resonant frequency. This is shown in Figure 5.26.

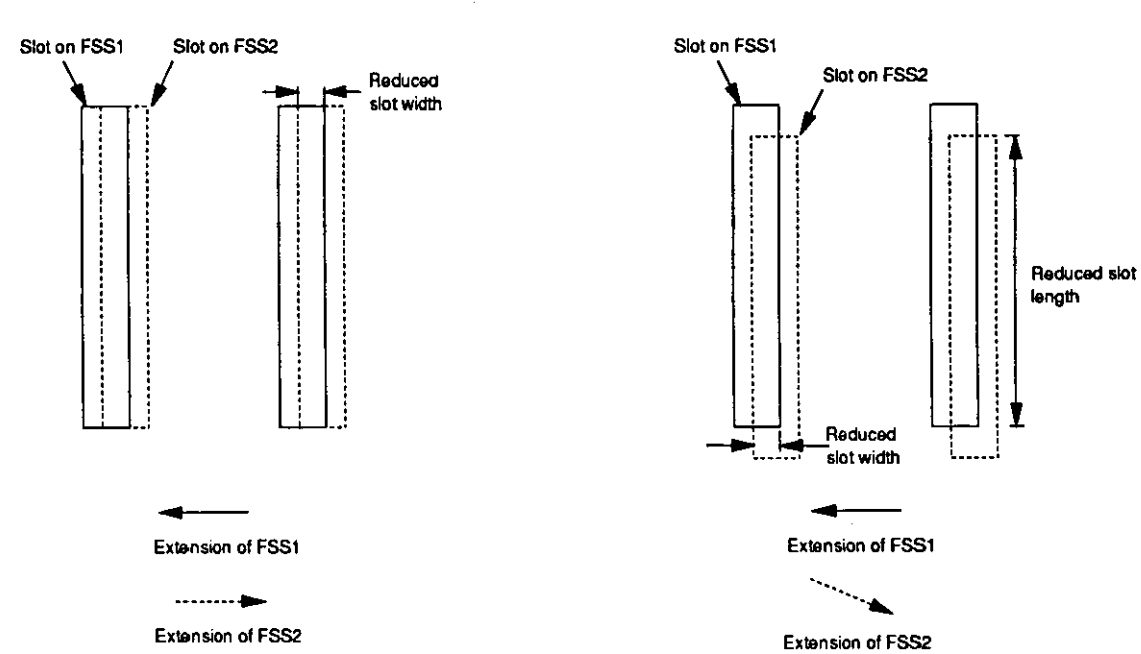
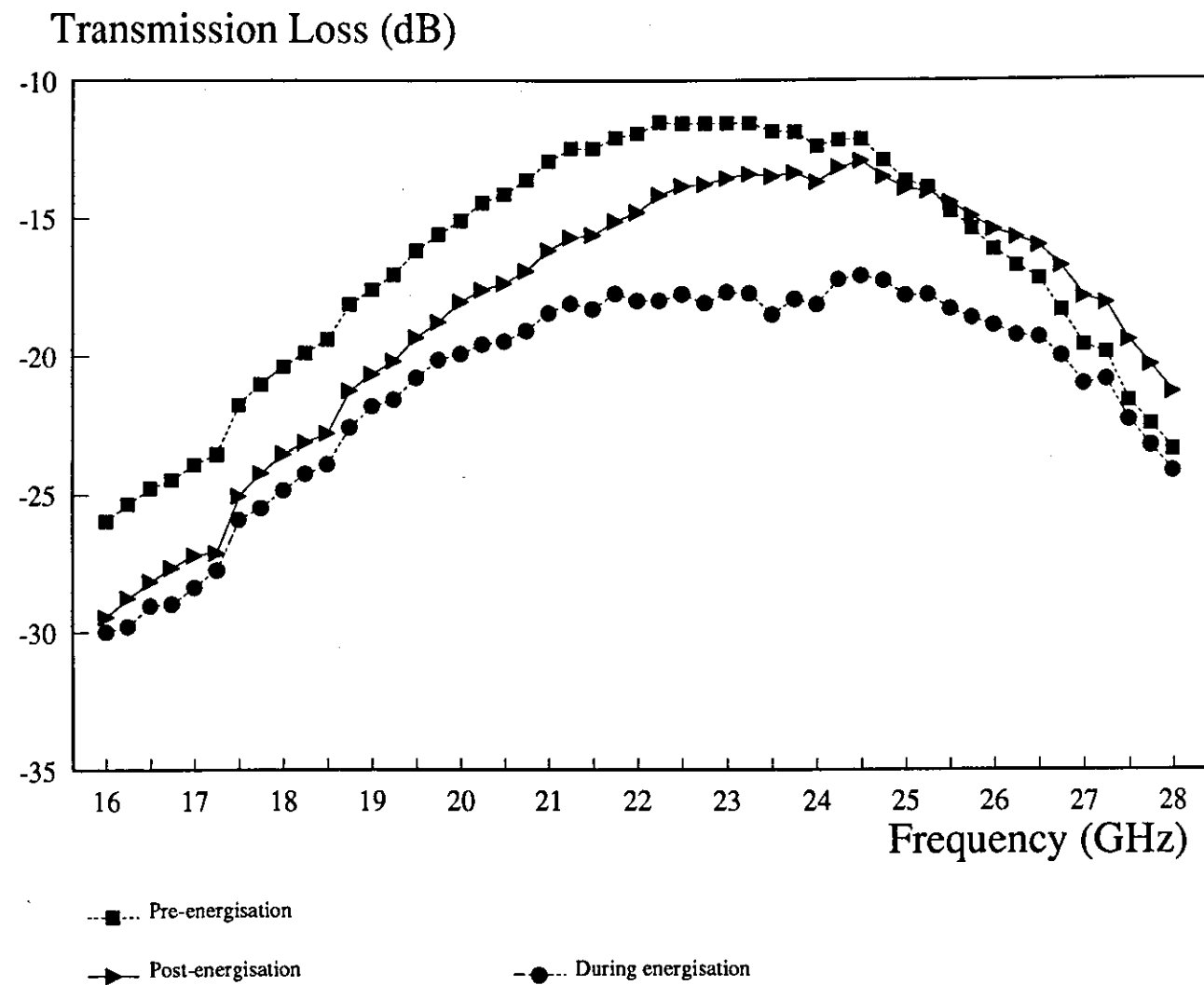


Fig. 5.26: The reduction in slot length

Graph 5.34: A frequency scan of the RPFSS in the K-band



5.12.1 The effect of varying the energisation voltage

Frequency scans of the longer (300mm) PFSSs, positioned between the perspex sheets with half of the PFSSs overlapping, as described above and shown in Figure 5.25, were made at energisation voltages ranging between 1kV and 5kV.

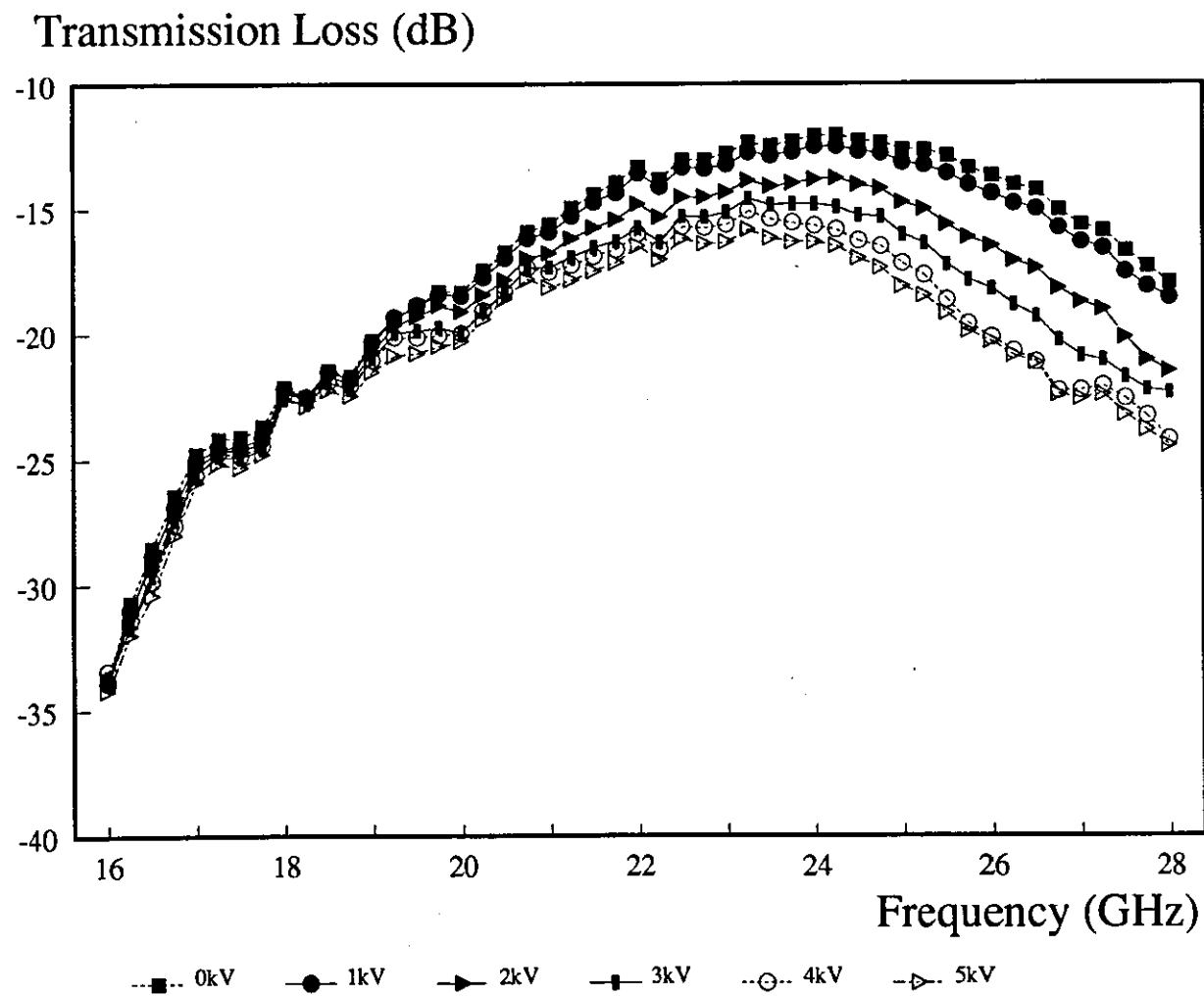
The maximum electric field which can be applied to the PVDF is 30V/ μ m (Table 3.3, Chapter 3). The PVDF substrate is 110 μ m thick, hence the maximum electric field which can be applied is:

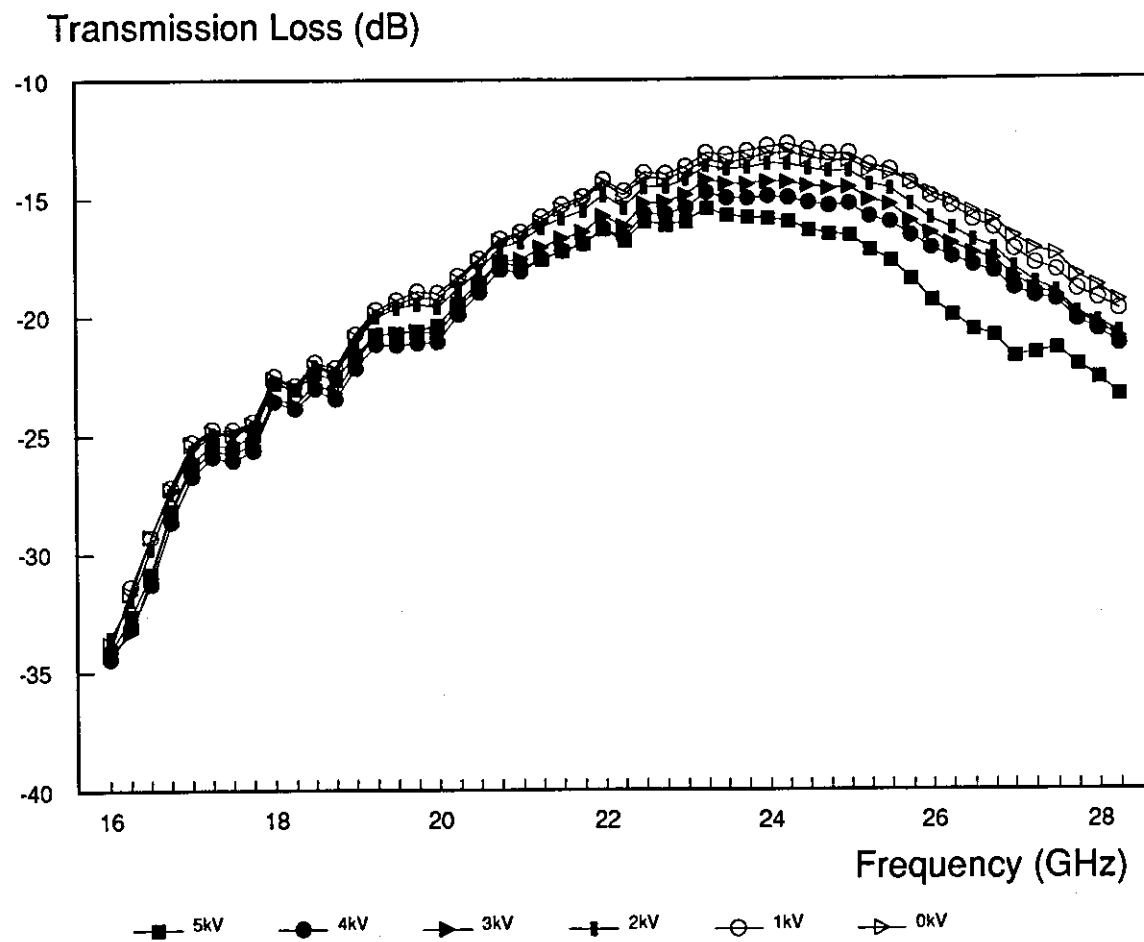
$$V = E \times t = 30 \times 110^{-6} = 3.3kV$$

Frequency scans were made at 5kV because the material was still extending as the energisation voltage was increased beyond 3.3kV (the calculated maximum).

Frequency scans were made in the K-band where the resonant frequency was found in the previous experiment. The un-energised RPFSS had a resonant frequency at 24.2GHz and a loss at this resonance of -12dB. When an energisation voltage of 1kV was applied to the PFSSs the loss increased to -12.5dB. The six plots of the frequency response at energisation voltages from 0 to 5kV, in 1kV increments are plotted in Graph 5.35. A second set of frequency response curves were produced when the energisation voltage was reduced from 5kV back down to 0kV. These curves are plotted in Graph 5.36. The two graphs are summarised in Table 5.4.

Graph 5.35: The effect of varying the energisation voltage from 0kV to 5kV





Graph 5.36: The effect of varying the energisation voltage from 5kV to 0kV

Increasing Voltage (kV)	Resonant Frequency (GHz)	Loss At Resonance (dB)	Decreasing Voltage (kV)	Resonant Frequency (GHz)	Loss At Resonance (dB)
0	24.25	-12.0	0	24.25	-13.1
1	24.25	-12.5	1	24.25	-12.75
2	24.25	-13.8	2	24.0	-13.6
3	24	-14.8	3	23.25	-14.2
4	23.25	-15.1	4	23.25	-14.8
5	23.25	-15.6	5	23.25	-15.6

Table 5.3: Summary of the effect of varying the energisation voltage

When the energisation voltage was reduced to 1kV the structure had a loss at the resonant frequency of -12.75dB. Removing the energisation voltage completely caused this loss to increase to -13.1dB. This indicates the alignment of the slots on the two PFSSs was better when energised to 1kV than at 0kV. The two graphs, 5.35 and 5.36, and Table 5.3 also confirm the observation made earlier that the PFSSs do not return exactly to their original positions when the energisation voltage is removed. The large loss experienced from the 110 μ m thick PFSS with 3.55mm long and 0.1mm wide slots in Section 5.11 was attributed to the narrow slot width. This can now be confirmed by the findings of the above experiment: when the energisation voltage is increased the width of the slots reducing has the effect of reducing the transmitted power. The greatest change in transmitted power occurred when the energisation voltage was increased from 1kV to 2kV.

At energisation voltages above 5kV arcing started to occur within the perspex-PVDF structure. It was not clear whether this arcing was occurring through the PVDF substrate or across the perspex.

This chapter has described experimental results and computer models of conventional (copper-polyester) and reconfigurable (piezoelectric) FSSs.

Where possible the transmission response of each FSS was both computer modelled and measured in the anechoic chamber. Comparisons were made between the measured and modelled responses and reasons for discrepancies between the two were suggested.

The resonant frequency shift of piezoelectric and copper-polyester FSSs as a function of DS and S were analysed. The results of this analysis were used to establish the design criteria of the RFSS.

Booker's extension to Babinet's Principle was proven experimentally and used to allow slotted FSSs to be computer modelled.

The effect of dipole and slot length and width, element shape, and substrate material and thickness were studied. Different methods of mounting the RFSS were investigated. This included stretching the PFSSs in a frame and mounting them between dielectric materials.

The Chapter is concluded by demonstrating the microwave shuttering effect which can be created by energising an RPFSS. The effect of varying the energisation voltage of this RPFSS was also studied.

6 CONCLUSIONS

This research was conducted to establish the practical feasibility of the Reconfigurable FSS described in the Patent^[2].

Piezoelectric materials and methods of implementing these in an RFSS were studied and described in chapters 3 and 4 respectively. Initial experiments with PVDF were also described in Chapter 4. Chapter 5 detailed the results of extensive FSS transmission response measurements and models. The results from these experiments and computer models have enabled the conclusions listed in this chapter to be made.

The research concentrated on using the planar movement of one FSS with respect to another to change the frequency response of the RFSS structure. Originally it was intended to alter the resonant frequency of the RFSS by increasing, or reducing, the effective length of the dipoles, or slots. The amount of movement, DS , required to obtain a significant frequency shift was modelled (graphs 5.1 and 5.2).

The models consisted of two single layer FSSs, positioned as shown in Figure 4.1, to form a double layer FSS. By moving one of these FSSs with respect to the other the frequency response of the double layer FSS could be altered. The amount of movement, DS , required to provide the desired resonant frequency shift, increased when the gap, S , between the FSSs was increased. When the gap between the FSSs was small, 0.062mm in the model, the increase in movement, DS , required to produce a shift in resonant frequency was not *significantly* greater than when there was no gap between the FSSs.

The movement, DS , was achieved by operating PVDF in its length extension mode. The two PFSSs were secured at opposite ends, as shown in Figure 5.25, so the relative displacement between them, DS , was proportional to the total length of the PVDF (Section 5.12).

The largest PFSSs which were used in this investigation were 300mm x 150mm; this limitation was imposed by the raw material cost of the PVDF. The movement required to produce a significant resonant frequency shift in the 12-40GHz range over which experiments were conducted could not be achieved from these relatively small PFSSs. This instigated the development of slotted RFSSs which cause complete "blocking" of the incident microwaves as opposed to just altering their resonant frequency. This "blocking"

or "shuttering" of the microwaves was achieved by extending the PFSSs in the direction of the width of the slots. The slots only have to be moved a small distance, DS , for the RFSS to completely block all of the incident microwaves (Figure 4.17). This enabled the RFSS to be switched between its "open" mode, where it was transparent to microwaves at its resonant frequency, to its "closed" mode where it blocked the incident microwaves at all frequencies. Section 5.12 described the successful action of a reconfigurable piezoelectric FSS. The shuttering concept was also demonstrated in the manual (vacuum) frame prior to being implemented on piezoelectric FSSs. This was described in Section 5.3.1.

The method employed to achieve the shuttering could be used in larger RPFSSs to obtain a resonant frequency shift. This would be possible because the relative displacement, DS , obtainable from PFSSs is proportional to their length (the longer the PFSS, the greater the extension). By positioning the slots so their length is in the direction of this larger extension a significant change in slot length and hence shift in resonant frequency could be obtained.

In the RFSS "shutter" PFSSs with arrays of slots, as opposed to dipoles, were necessary for the shuttering to occur. When the RFSS is used to shift the resonant frequency total blocking is not required and dipoles or slots could be used as the elements on the FSSs. (The length of the slots would reduce whereas the length of the dipoles would increase when the RFSS was energised.) However other factors dictate the use of slots in PFSSs. These include the need to maximise the electroded area of the PFSSs and to provide a continuous electrode across the entire PFSS surfaces, criteria which are not met by arrays of dipoles. These criteria are necessary to ensure the maximum electric field is applied to the PVDF substrate and to enable easy electrical connections to be made to the electrodes.

Graph 5.1 was used to establish the fundamental design criteria of the RFSS; this was to maximise the displacement, DS , and minimise the gap, S , between the two FSSs. This graph showed the gap can have a significant effect on the resonant frequency. When the displacement, DS , is kept constant at 2.5mm, the resonant frequency can be shifted from 16GHz to 24GHz by varying S between 0.062mm and 0.262mm. The synthetic piezoelectric materials investigated (PZT and PVDF) both have larger piezoelectric strain constants when operated in their thickness expansion mode than they do in their length extension mode (Table 3.2). An alternative to utilising the piezoelectric material to obtain

a planar displacement, DS , would be to operate the material in its thickness expansion mode and alter the gap, S , between two FSSs. This method would require careful design because the resonant frequency shift obtained by altering S is also dependent on the relative positions of the dipoles (slots) on the two FSSs. e.g. When DS was 2.0mm, (Graph 5.1) the resonant frequency only shifted from 23 to 27GHz when S was increased from 0.062 to 0.262mm, this compares with the 8GHz frequency shift described above when DS was 2.5mm.

Altering the gap, S , to achieve a resonant frequency shift, as opposed to altering DS , has the advantage of not requiring the piezoelectric material across the entire FSS area. It only needs to be positioned at strategic sites to hold the RFSS structure together; these sites could be behind the copper elements, thus eliminating the problems caused by lossy piezoelectric materials.

An alternative to maximising the displacement DS , or S , is to develop an FSS with elements with a resonant frequency which alters significantly when there is a small change in DS (or S).

FSSs with two different elements were considered, square loops and arrays of alternately long and short slots. Square loops enable orthogonally polarised microwaves to be transmitted through the RPFSS. When the RPFSS is energised two opposite sides of the loops are blocked, "shuttering" microwaves of one polarisation but still allowing transmission of the orthogonally polarised microwaves. The resonant frequency of these transmitted microwaves is not significantly altered.

FSSs with alternately long and short slots exhibit two transmission response peaks; these were attributed to the resonances of the two slots (Graph 5.17). A null is also produced between these peaks. This RFSS operates on the same principle as the microwave shutter described above except instead of the RPFSS switching between an open and closed state it switches between two resonant frequencies. The shift in resonant frequency is theoretically unlimited but is restricted to a predetermined value which is controlled by the lengths of the slots.

Booker's extension to Babinet's principle^[37 p.496] states that the transmission response of a slotted FSS is the same as the reflection response of the complementary FSS with arrays

of dipoles. This principle was experimentally proven (Section 5.2.1) and then used to enable modelling of slotted FSSs with the modal analysis software. (Without the application of Booker's extension this software could only model FSSs with arrays of dipoles.)

The results of this experiment showed the FSS with arrays of slots has a slightly narrower passband bandwidth than the complementary FSS with arrays of dipoles. This effect could be caused by the two FSSs not being truly complementary. (In a pair of truly complementary FSSs the values of permittivity ($\epsilon_r\epsilon_0$) and permeability ($\mu_r\mu_0$) on the two FSSs are interchanged.)

The modelled and measured frequency response curves for copper-polyester FSSs agreed well (Section 5.4.1.1 and 5.4.1.2). The measured transmission response curves of PVDF FSSs had a lower resonant frequency, greater loss at the resonance and a larger passband bandwidth than the models predicted. This was attributed to unrealistic values of ϵ_r and $\tan\delta$ being used in the models. The values used were quoted for a frequency of 10^4 Hz. No values were available for frequencies in the gigahertz range where experiments were conducted.

The values of ϵ_r and $\tan\delta$ in the PVDF are larger than those in the polyester substrate. This may mean the inaccuracy introduced to the model by not modelling the true Babinet's complement, (the values of permittivity and permeability were not interchanged as described above), may have a significant effect on the results of the PVDF models.

Comparisons between measured copper-polyester and PVDF FSSs showed the PVDF FSSs have a broader -3dB passband bandwidth, a lower resonant frequency, and a greater loss at this resonance than copper-polyester FSSs with identical elements.

Experiments with different thicknesses of PVDF substrate showed further increases in passband bandwidth and transmission loss at resonance, and further reductions in resonant frequency, occur as the PVDF substrate thickness is increased (Section 5.10).

Reducing the width of the slots on an FSS, below approximately 0.4mm (0.05λ), also causes an increase in the transmission loss of the FSS (Section 5.11, Graph 5.31).

In the RFSS shuttering experiments two PFSSs were used, this has the effect of doubling the PVDF substrate thickness. Also the slots in these PFSSs were narrow to enable the complete shuttering action to occur. These properties will cause a high passband loss as explained above and seen in Graph 5.35 (-12.0dB).

The transmission loss increases further, as expected, when the energisation voltage applied to the electrodes on the PFSSs was increased. The loss reached a maximum of -15.6dB when the voltage applied to the electrodes was 5kV.

The perspex sheets which the RPFSS was sandwiched between also reduce the resonant frequency and introduce interference into the frequency response. The perspex is necessary to provide a supporting structure for the RPFSS. The interference is caused by standing waves in the perspex sheets. Graph 5.15 shows one of these standing waves coincides with the resonant frequency of the RPFSS resulting in a gain in the transmission response (sections 5.6.1.2, 5.7.2.2, and 5.9.1). The thickness and relative permittivity of the perspex sheets control the frequency of the standing waves. By considering the operating frequencies of the RPFSS when selecting the perspex it should be possible to produce constructive interference which maximises the resonant frequency gain at the required frequency.

In summary RFSSs manufactured from PVDF must:

- consist of arrays of slots, as opposed to dipoles;
- be large to enable a significant resonant frequency shift to be achieved;
- have a slot width greater than 0.4mm to minimise passband attenuation.

Also the resonant frequencies the RFSS is to be operated at must be considered when the supporting frame is designed to ensure standing waves in the frame provide constructive interference.

APPENDIX A: REFERENCES

1. Kraus, J.D.: *Antennas*, McGrawhill Incorporated, New York, 1988, pp600-603.
2. Vardaxoglou, J.C.: "Reconfigurable Frequency Selective Surfaces"
UK Patent Pending, Patent Application Number 9119039.7; Sept. 1991.
3. Otoshi, T.Y.: "A Study of Microwave Leakage Through Perforated Flat Plates" *IEEE Trans. Microwave Theory Tech.*, March 1972, Short Papers, pp.235-6.
4. Claricots, P.J.B., Zhou, H.: "Design and performance of a reconfigurable mesh reflector antenna, Part 1: Antenna design" *IEEE Proceedings H, Microwave Ant. Propagat.*, December 1991, Vol.138, Part 6, pp.485-492.
5. Claricots, P.J.B., Zhou, H.: "Design and performance of a reconfigurable mesh reflector antenna, Part 2: Antenna performance" *IEEE Proceedings H, Microwave Ant. Propagat.*, December 1991, Vol.138, Part 6, pp.493-496.
6. Agrawal, V.D., Imbriale, W.A.: "Design of a Dichroic Cassegrain Subreflector" *IEEE Trans. Antennas Propagat.*, July 1979, Vol.AP-27, No.4, pp.466-473.
7. Chen, C.C.: "Transmission Through a Conducting Screen Perforated Periodically with Apertures" *IEEE Trans. Microwave Theory Tech.*, September 1970, Vol.MTT-18, No.9, pp.627-632.
8. Chen, C.C.: "Transmission of Microwaves through Perforated Flat Plates of Finite Thickness" *IEEE Trans. Microwave Theory Tech.*, January 1973, Vol.MTT-21, No.1, pp.1-6.
9. Andrasic, G., James, J.R.: "Microstrip Window Array" *Electron. Lett.*, January 1988, Vol.24, No.2, pp.96-97.
10. Andrasic, G., James, J.R.: "Superimposed Dichroic Microstrip Antenna Arrays" *IEE Proc.*, October 1988, Vol.135, Pt.H, No.5, pp.304-312.

11. Andrasic, G., James, J.R., Kinany, S.J.A., Peel, P.D.: "Leaky-Wave Multiple Dichroic Beamformers" *Electron. Lett.*, August 1989, Vol.25, No.18, pp.1209-1211.
12. Lee, S.W., Zarillo, G., Law, C.L.: "Simple formulas for transmission through periodic grids or plates" *IEEE Trans.*, 1982, AP-30, pp.904-909.
13. Chen, C.C.: "Scattering by a Two-Dimensional Periodic Array of Conducting Plates" *IEEE Trans. Antennas Propagat.*, September 1970, Vol.AP-18, No.5, pp.660-665.
14. Parker, E.A., Vardaxoglou, J.C.: "Plane-wave illumination of concentric-ring frequency-selective surfaces" *IEE Proc.*, June 1985, Vol.132, Pt.H, No.3, pp.176-180.
15. Parker, E.A., Hamdy, S.M.A.: "Rings as elements for frequency selective surfaces" *Electron. Lett.*, August 1981, Vol.17, No.17, pp.612-614.
16. Hamdy, S.M.A., Parker, E.A.: "Current distribution on the elements of a square loop frequency selective surface" *Electron. Lett.*, July 1982, Vol.18, No.14, pp.624-626.
17. Langley, R.J., Parker, E.A.: "Equivalent circuit model for arrays of square loops" *Electron. Lett.*, April 1982, Vol.18, No.7, pp.294-296.
18. Vardaxoglou, J.C., Parker, E.A.: "Performance of two tripole arrays as frequency-selective surfaces" *Electron. Lett.*, September 1983, Vol.19, No.18, pp.709-710.
19. Comtesse, L.E., Langley, R.J., Parker, E.A., Vardaxoglou, J.C.: "Frequency Selective Surfaces in Dual and Triple Band Offset Reflector Antennas" *Proc. 17th European Microwave Conference*, 1987, pp.208-213.
20. Anderson, I.: "On the Theory of Self-Resonant Grids" *Bell System Tech. Jour.*, December 1975, Vol.54, No.10, pp.1725-1731.
21. Vardaxoglou, J.C., Parker, E.A.: "Modal analysis of scattering from two-layer frequency-selective surfaces" *Int. J. Elect.*, 1985, Vol.58, No.5, pp.827-830.

22. Simpkin, R., Vardaxoglou, J.C.: "The Analysis of Cascaded Frequency Selective Surfaces using a Scattering Matrix and a Coupled Integral Equation method"
23. Stylianou, A., Vardaxoglou, J.C.: "Improved Convergence of Iterative Scheme for Analysing Arrays of Finite Size" *Electron. Lett.*, May 1990, Vol.26, No.10, pp.641-643.
24. Atochem Sensors Ltd., Kynar Piezo Film Product Data.
25. Pennwalt Corporation, Kynar Piezo Film Technical Manual: 1983.
26. King, T.G., Preston, M.E., Murphy, B. J. M., Canell, D.S.: "Piezoelectric Ceramic Actuators: A Review of Machinery Applications" *Prec. Eng.*, Vol.12, No.3, pp.131-136, July 1990.
27. Sessler, G.M.: "Piezoelectricity in Polyvinylidenefluoride" *J. Acoust. Soc. Am.*, Vol.70, No.6, pp.1596-1608: Dec. 1981.
28. The Piezo Book, Burleigh Instruments Inc., USA.
29. Timoshenko, S., Young, D.H.: *Elements of Strength of Materials*, 5th Ed., D. Van Nostrand Coy., London, 1968.
30. Vernitron Ltd., Piezoelectric Ceramics Sales Information Brochure.
31. Brush Clevite, Piezoelectricity - A Data Book for Designers.
32. Brown, C.S., Kell R.C., Taylor, R., Thomas, L.A.: "Piezoelectric Materials" *Proc. Inst. Elec. Eng.*, Vol.109 pt.B, No.43, pp.99-114: 1962.
33. Kawai, H.:
Japan. J. Appl. Phys., 8, 975: 1969.
34. Manufacturer's Data, GTS Flexible Materials Ltd.
35. Vardaxoglou, J.C., Stylianou, A.: "An Iterative Method of Analysing Double Layer Frequency Selective Surfaces"
Proc. JINA'90 International Symposium on Antennas: 1990.

36. Private Communication, Mr Richard Brown, Atochem Sensors Ltd.
37. Balanis, C.A.: *Antenna Theory*, John Wiley and Sons Inc., New York, 1982.
38. Balanis, C.A.: *Advanced Engineering Electromagnetics*, John Wiley and Sons Inc., New York, 1989.
39. Birks, J. B. Ed.: *Modern Dielectric Materials*, Heywood and Company Ltd., London, 1960.

